The Philosophical Magazine

FIRST PUBLISHED IN 1798

A Journal of Theoretical Experimental and Applied Physics

Vol. 3 January 1958 No. 25
Eighth Series

UNIVERSITY OF HAWAII
LIBRARY
APR 9 '58

£1 5s. 0d., plus postage
Annual Subscription £13 10s. 0d., payable in advance

Printed and Published by
TAYLOR & FRANCIS LTD
RED LION COURT, FLEET STREET, LONDON, E.C.4

THE PHILOSOPHICAL MAGAZINE

Editor

Professor N. F. Mott, M.A., D.Sc., F.R.S.

Editorial Board

Sir Lawrence Bragg, O.B.E., M.C., M.A., D.Sc., F.R.S.
Sir George Thomson, M.A., D.Sc., F.R.S.
Professor A. M. Tyndall, C.B.E., D.Sc., F.R.S.

Authors wishing to submit papers for publication in the Journal should send manuscripts directly to the Publishers.

Manuscripts should be typed in *double* spacing on one side of quarto (8×10 in.) paper, and authors are urged to aim at absolute clarity of meaning and an attractive presentation of their texts.

References should be listed at the end in alphabetical order of authors and should be cited in the text in terms of author's name and date. Diagrams should normally be in Indian ink on white card, with lettering in soft pencil, the captions being typed on a separate sheet.

A leaflet giving detailed instructions to authors on the preparation of papers is available on request from the Publishers.

Authors are entitled to receive 25 offprints of a paper in the Journal free of charge, and additional offprints can be obtained from the Publishers.

The *Philosophical Magazine* and its companion journal, *Advances in Physics*, will accept papers for publication in experimental and theoretical physics. The *Philosophical Magazine* publishes contributions describing new results, letters to the editor and book reviews. *Advances in Physics* publishes articles surveying the present state of knowledge in any branch of the science in which recent progress has been made. The editors welcome contributions from overseas as well as from the United Kingdom, and papers may be published in English, French and German.

THE

PHILOSOPHICAL MAGAZINE

A JOURNAL OF THEORETICAL, EXPERIMENTAL AND APPLIED PHYSICS

First Published in 1798

[EIGHTH SERIES—VOL. 3]

Observations on Helical Dislocations in Crystals of Silver Chloride†

By D. A. Jones and J. W. Mitchell
H. H. Wills Physical Laboratory, University of Bristol

[Received November 12, 1957]

Abstract

Prismatic and concentric helical prismatic dislocations are generated by the stress field which appears around a spherical glass inclusion in a silver chloride crystal when the crystal is cooled from a temperature of 370°c to room temperature. The properties of these dislocations are described and their origin is discussed.

§ 1. Introduction

During the course of experimental work on chemical sensitization (Evans *et al.* 1955), it was noticed that the chemical and photochemical reactivity of silver halide crystals was enhanced in the neighbourhood of glass particles. Chemical development was often spontaneously initiated near the particles and this source of fog was eliminated when they were removed by filtering the molten silver halide through fine glass capillary tubes.

At the time, it was suspected that the particles increased the average local density of dislocations and that this was responsible for the increased reactivity. We have now deliberately incorporated particles of hysil glass in silver chloride crystals and studied the distribution of dislocations around them by etching (Jones and Mitchell 1957) and by the separation of silver along the dislocation lines during exposure (Hedges and Mitchell 1953). Prismatic (Seitz 1950) and helical prismatic dislocations with ⟨110⟩ directions as axes are generated by the stress field which arises on cooling from the differential contraction between the silver chloride and

† Communicated by the Authors.

the glass. Spherical particles have also been made and introduced into the crystals ; the symmetry of the resulting stress field has greatly facilitated the interpretation of the observations.

§ 2. Experimental Methods

The silver chloride was prepared and purified as described by Clark and Mitchell (1956). Glass spheres were made by the method of Sollner (1939). Glass particles were introduced into the oxygen stream of an oxy-coal gas blowpipe and passed through the jet where they fused into spheres. These were collected in a dish containing distilled water and separated into size classes by sedimentation. The most useful particles were of almost perfect spherical form with diameters between 0·5 and 5 microns.

Single crystals of silver chloride were made in the form of thin sheets by the method described by Clark and Mitchell (1956). A drop of a suspension of the glass spheres in distilled water was placed on the surface of the upper glass plate which was to be in contact with the silver halide. After the evaporation of the water, a reasonably uniform distribution of the spheres remained. Their surface density could be controlled conveniently by varying the concentration of the suspension so that isolated or interacting prismatic dislocations could be produced as desired. The spheres became imbedded in the crystals but usually remained within 20 microns of the surfaces ; this was convenient for etching, for the separation of silver along the dislocation lines during exposure and for microscopic examination. After cooling to room temperature, the crystals were separated from the glass plates, between which they were grown, and cut into sections. These were annealed in an atmosphere of chlorine for 8 hours at 370°c. The chlorine was then condensed by immersing a side arm in liquid air and the specimens were cooled to room temperature. This treatment reduces the density of dislocations in many crystals with (001) surfaces to a negligible value. The properties of the prismatic dislocations which are generated around spherical inclusions during the cooling of the annealed crystals can therefore be studied without complications arising from their interactions with other dislocations.

In the early stages of the work, the crystals were etched and then exposed to render visible the dislocation lines below the surface. It was found, however, that etching, which removed the upper half of the loop systems by dissolving away the surface, destroyed information which was essential for the interpretation of the observations. The crystals have since been simply exposed to a 250 watt medium pressure mercury vapour lamp with a frosted envelope at a distance of 10 cm for 2 to 3 minutes. During this time, very little silver separates on (001) surfaces to obscure the dislocations which are decorated down to a depth of 20 to 30 microns depending on the duration of the exposure. The distribution of silver along the dislocation lines is almost continuous and the individual particles can scarcely be resolved. Screw dislocations are always more lightly

decorated than edge dislocations. The paper is illustrated with photographs of wire models of the dislocation systems. The illustrations are effectively projections of the systems on an (001) plane from a point above the plane.

§ 3. Experimental Observations

Dislocation loops are formed around any glass inclusion in a crystal of silver chloride which has been grown from the fused substance. The observations which are described in this section have, however, all been made with spherical particles.

The thin single crystal sheets of silver chloride usually have (001) surfaces. The systems of prismatic and helical prismatic dislocations which are formed around a sphere have as possible axes the four ⟨110⟩ directions which lie in a plane passing through the centre of the sphere parallel to the surface of the crystal. One, two, three and four systems have been observed around individual spheres. Sometimes a few loops of systems along the ⟨110⟩ axes which are inclined downwards from the surface have been observed. In crystals with (111) surfaces, systems of prismatic dislocations are formed with any of the six possible ⟨110⟩ directions which are parallel to the surface as axes. The systems formed at different particles along particular ⟨110⟩ directions in a plane parallel to the surface will be illustrated and discussed in the remainder of this section.

The majority of the systems consist of sequences of loops and figures of eight as shown in figs. 4 and 7, together with more complicated closed dislocation loops such as those illustrated in figs. 5 and 6. The diameter of the sphere in fig. 4 is 3·5 microns. The diameter of the loops is 2·4 microns and the overall length of the system 15 microns. The loops have a nearly constant diameter over the whole length of a system and this is usually slightly smaller than the diameter of the spherical inclusion. When they are far from other inclusions and systems of prismatic dislocations, they usually lie in planes normal to the axes of the systems along which they are spaced at remarkably regular intervals.

In figures of eight and more complicated configurations (fig. 6), the dislocations cross at an angle of approximately 90°. Although the diameters of the spherical particles were usually about 5 microns and the diameters of the loop systems slightly less than this, the quality of the decoration allows the details of the configurations to be clearly resolved. It has been found that the complex configurations are formed from two concentric helical dislocations of opposite twist. At all the cross-over points, one helical dislocation is outside the other, showing that they must have been generated as concentric helices, and not as two independent helices which were subsequently combined by lateral displacement.

In the many hundreds of systems which were examined in detail, it proved possible to find configurations which appeared to be in every possible stage of development. Figures 1 and 2 show configurations which were frequently observed. It was deduced that a narrow loop was

first formed in the silver chloride at its interface with the sphere by glide in a plane containing a ⟨110⟩ direction and that it expanded around a cylindrical surface with the ⟨110⟩ direction as axis to generate single loops, figures of eight and more complex configurations. These units were randomly distributed along the ⟨110⟩ directions but a concentric helical dislocation was often observed in contact with the sphere as in fig. 3. Here the diameter of the spherical particle was 4·1 microns and the diameter of the prismatic dislocation 4·1 microns near the surface of the sphere, decreasing to 3·3 microns at the other end of the system.

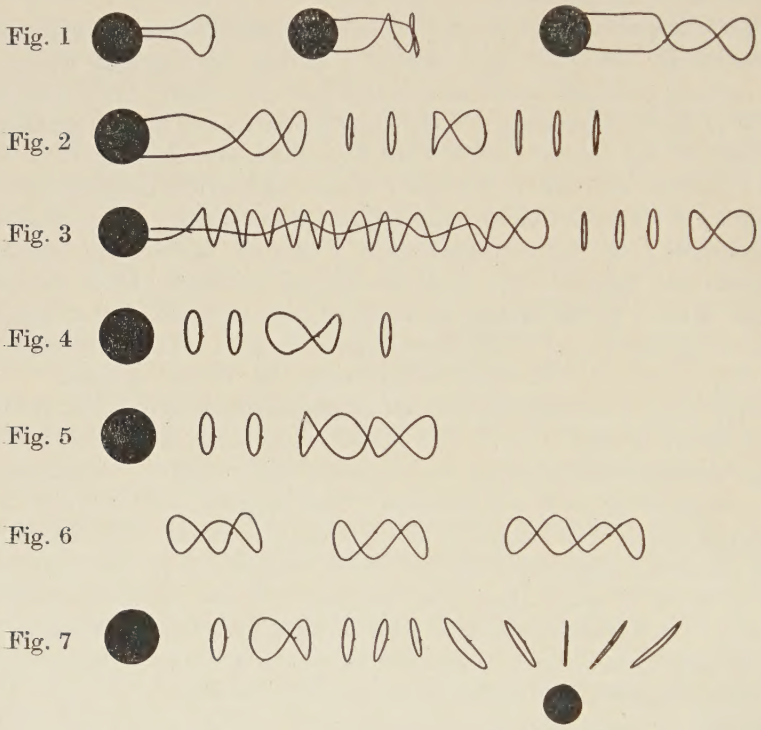

Many single helical dislocations with axes along ⟨110⟩ directions were observed. The diameter and pitch usually varied with distance from the sphere and the dislocations could often be followed to the point where they made contact with the surface of the crystal. Single prismatic loops around single helical dislocations, around the inner helical dislocation of a concentric pair, and around both dislocations of a concentric pair have been observed. Such isolated prismatic dislocations have never been observed to surround only the outer dislocation of a concentric pair.

A number of specimens were prepared with a high density of particles so that the interactions between the prismatic dislocations could be studied. In these specimens, loop systems generated by one sphere were sometimes observed to pass by a smaller particle which had not generated any dislocations. The individual loops were then displaced as shown in

fig. 7. A similar displacement was produced if a loop system passed by another loop system with an axis at right angles and it became evident that the inclination of the prismatic dislocations provided a sensitive indicator of the presence of local shearing stresses in the crystals.

§ 4. Interpretation of the Observations

The interpretation of the observations is based upon an extension of a mechanism proposed by Seitz (1950) in his discussion of prismatic punching and prismatic dislocations in thallous halide crystals. He pointed out that two prismatic dislocations of opposite sign could be generated by the expansion of a dislocation loop around the glide prism. Nye (1949) has established that silver chloride deforms by pencil glide with a $\langle 110 \rangle$ slip vector so that prismatic punching is a possible mode of deformation.

To interpret our own observations, we have to explain the generation of prismatic and helical prismatic dislocations on the surfaces of cylinders with axes along the possible $\langle 110 \rangle$ slip vectors and diameters slightly less than that of the spherical inclusion. The motion of such prismatic dislocations along the slip cylinder transports material away from the spherical inclusion to reduce the strain arising from the differential contraction on cooling. It may reasonably be assumed that there is no coherence between the silver halide and the glass at the interface and that the silver chloride there is redistributed by subsidiary slip and diffusion processes. The prismatic dislocations move outwards without any appreciable change in their projected area upon a plane at right angles to the axis of the glide cylinder ; diffusion processes leading to climb are not important for these phenomena. The experimental observations show that the strains are transmitted over distances large compared with the diameters of the glass spheres.

The stress field produced by differential contraction between the silver chloride and the glass sphere has, ideally, spherical symmetry. The shearing stress is zero in radial directions. With respect to any $\langle 110 \rangle$ slip vector, it has a maximum value at the surface of the sphere upon a cylindrical surface which has the slip vector as axis and a diameter $\sqrt{2}$ times the radius of the sphere. Small dislocation loops are therefore formed on the surface of this glide cylinder. The forward edge component then glides outward under the influence of the steadily decreasing stress field. The screw components of the loop, which are parallel to the axis of the glide cylinder, experience a tangential force which causes them to glide in opposite directions around its surface. This force is greater near the interface than further away so that, although the dislocation must retain the screw orientation at the interface, it will elsewhere become inclined to the axis as it glides round the cylinder. The introduction of the edge components as a result of this inclination stabilizes the dislocation on a particular glide cylinder because any radial displacement would involve climb. If these two dislocations remain upon the same cylindrical surface during their rotation round the axis under the action of the

shearing stress, their meeting will produce a prismatic dislocation corresponding to the introduction of additional material into the lattice. It is convenient to describe this as a positive prismatic dislocation. An equivalent amount of material is removed from the incoherent interface between the silver chloride and the glass sphere. A succession of such dislocations may be generated by independent events in which small loops are formed by slip and expand round glide cylinders. The remarkably uniform diameter of the loops in many systems is probably determined by the diameter of the glide cylinder upon which the shearing stress at the interface has the maximum value. The regular spacing arises from their mutual repulsion which is also responsible for the transmission of stresses along the cylinder. This is essentially one of the mechanisms proposed by Seitz (1950) for the generation of prismatic dislocations and for the interpretation of prismatic punching.

The observations illustrated in fig. 7 confirm that positive prismatic dislocations are formed. The prismatic dislocations pass another spherical inclusion which is surrounded by a stress field. The strain energy is lowered by the overlapping of the region of dilatation around the edge of the positive prismatic dislocation and the region of compression around the spherical inclusion. This interaction, together with an analysis of the forces acting on the dislocations, establishes that they are of a positive type.

The most striking feature of the observed phenomena, the occurrence of figures of eight, of more complex closed dislocation loops (fig. 6) and of concentric helical dislocations (fig. 3), requires an extension of the above mechanism for its interpretation. If the dislocations are displaced radially during their rotation round the glide cylinder, they may not meet to generate prismatic dislocations, but may continue their rotation with the production of concentric helical dislocations. This is illustrated by the loops in contact with the spheres in figs. 1, 2 and 3. If the dislocations meet after each has made a complete rotation around the glide cylinder, figures of eight will be formed. The more complex systems result from a larger number of rotations before intersection. The radial displacements which lead to the formation of helical prismatic dislocations and to their subsequent intersection are most likely to occur where the dislocations involved are in the screw orientation, that is to say, at the interface with the spherical inclusion. As already pointed out, when climb is not permitted, the edge components of composite dislocations stabilize them against radial displacements with respect to the axis of the glide cylinder. This also explains why the dislocations do not attract each other when they are rotating on their respective glide cylinders in the same way as two screw dislocations of opposite hand. The dislocation lines cross at an angle of nearly 90°. The attractions of the screw components may then, in a sense, be balanced by the mutual repulsions of the edge components although a displacement of the edge components could only result from climb.

In the majority of the concentric helical prismatic dislocations, the outer and the inner helices were of very nearly the same diameter but in some (as, for example, in fig. 3), the outer helix was of constant diameter while the diameter of the inner helix decreased as the surface of the sphere was approached. In these cases, the screw element of the inner dislocation at its intersection with the interface has moved inwards during its rotation round the axis of the glide cylinder.

The single helical dislocations are formed when the primary loop expands so that one of the screw dislocations meets the surface of the crystal. The rotation of the screw element of the other dislocation at its contact with the interface between the silver halide and the spherical particle around the axis of the glide cylinder will generate a single helical dislocation.

The single prismatic dislocation loops which surround the helical dislocations are produced by the expansion of loops, formed by slip, around cylindrical surfaces with greater or smaller radii than the outer dislocation of the helical system.

§ 5. Conclusion

A stress operated mechanism for the generation of helical prismatic dislocations has not previously been described. The method of incorporating glass spheres into silver halide crystals, which has been introduced for the first time in this investigation, provides a powerful means for generating helical prismatic dislocations and for studying their properties.

Acknowledgments

This work has been carried out during the tenure of a University of Bristol Graduate Scholarship by D. A. Jones. It has also been supported by a grant from Kodak, Ltd., which is gratefully acknowledged.

References

Clark, P. V. Mc.D., and Mitchell, J. W., 1956, *J. photogr. Sci.*, **4**, 1.
Evans, T., Hedges, J. M., and Mitchell, J. W., 1955, *J. photogr. Sci.*, **3**, 73.
Hedges, J. M., and Mitchell, J. W., 1953, *Phil. Mag.*, **44**, 223.
Jones, D. A., and Mitchell, J. W., 1957, *Phil. Mag.*, **2**, 1047.
Nye, J. F., 1949, *Proc. roy. Soc.* A, **198**, 191.
Seitz, F., 1950, *Phys. Rev.*, **79**, 723.
Sollner, K., 1939, *Industr. Engng Chem.*, **11**, 48.

The Centre of a Dislocation: II—The Dilated Slit†

By Elizabeth H. Yoffe
Cavendish Laboratory, Cambridge

[Received October 14, 1957]

Abstract

This paper describes the second part of some investigations of the elastic field near the centre of an edge dislocation. It is concerned with the local expansion due to atomic misfit, causing a singularity similar to a particular type of centre of pressure. The corresponding stress field is added to that of Part I to give the complete elastic field of a dislocation in a crystal.

The solution is also applicable to the dilation of a slit by a solid inclusion, and therefore gives an indication of the stress field of a tapered precipitate in a crystal matrix.

§ 1. Introduction

At the centre of an edge dislocation in a crystal lattice the atoms next the slip plane are so far out of position that they are necessarily displaced normal to the slip plane as well as parallel to it. The atoms as it were ride up over those on the opposite side of the slip plane in the limited region where the relative transverse displacement is large (cf. Read 1953). This has the effect of introducing a discontinuity in the elastic field, as though additional elastic material had been inserted in a finite slit along the slip plane.

Fig. 1

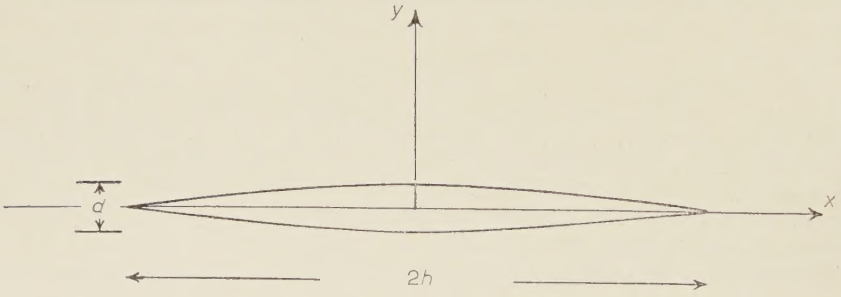

The dilated slit and Cartesian axes.

The problem considered in this paper is that of determining the stress field due to such dilation of a slit, for various distributions of the additional material. Similar boundary value problems have been solved by Muskhelisvili (1953) using the conformal transformation of an ellipse to

† Communicated by the Author. Part I appeared in *Phil. Mag.*, **2**, 1197.

a circle. The slit is treated as the limit of a narrow ellipse and a solution is given for the straight slit dilated by uniform internal pressure to an elliptical aperture.

Since the final form of the slit in the present problem is not necessarily elliptical, it is found more convenient to use Cartesian coordinates, and a different method based on higher order dislocations, as described in a recent paper by the author (Yoffe 1957).

§ 2. Dilation Due to Misfit

For purposes of calculation the metal crystal containing a dislocation is replaced by an isotropic elastic body in a state of plane strain, and Cartesian axes are so chosen that the z axis represents the dislocation line and the (xz) plane corresponds to the slip plane. The problem is to determine the components of displacement u, v, in the x, y directions respectively, and the stress components $\widehat{xx}$, $\widehat{yy}$, $\widehat{xy}$ due to various dilations of a slit between the points $(h, 0)$ and $(-h, 0)$.

Fig. 2

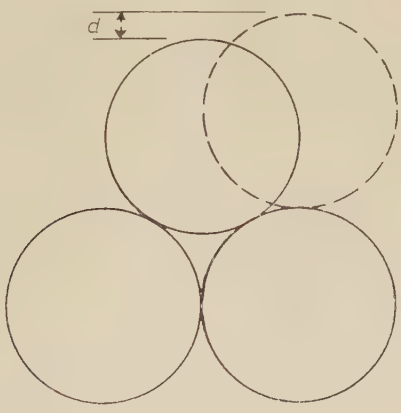

The quantity d in a two dimensional lattice.

The amount of dilation, or relative displacement v' of the two sides of the slit, is defined as a function of x on the slip plane :

$$v'(x) = \lim_{\epsilon \to 0} v(x, \epsilon) - v(x, -\epsilon)$$

and is assumed zero for $|x| > h$, increasing symmetrically to a maximum value d at $x=0$. This is because v' is due to atomic misfit caused by an edge dislocation of relative displacement u', where u' increases from zero at $x=h$ to one atomic spacing a at $x=-h$.

In the simple two dimensional array sketched in fig. 2 the maximum value d is given by :

$$d = a(1 - \cos 30^\circ) = 0{\cdot}134a.$$

In more general three dimensional lattices

$$d = ca$$

where c is a constant to be calculated in each case and is of the order 0·1.

If the atoms are regarded as spheres rolling up over one another as in fig. 2, the following simple relation between u' and v' may be obtained :

$$v' = a\left[\frac{1}{2}\sqrt{\left(3+4\frac{u'}{a}-4\left(\frac{u'}{a}\right)^2\right)}-\cos\frac{\pi}{6}\right]$$

but u' must still be determined as a function of x by choosing a particular Law of Force (Yoffe *loc. cit.*).

Fig. 3

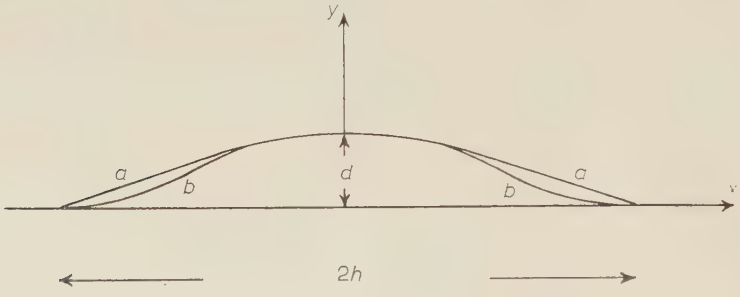

Alternative forms assumed for $v'(x)$.

It is assumed that $v'(x)$ resembles one of the following curves, represented for simplicity in terms of straight lines and parabolas (see fig. 3) :

(*a*) Straight line of arbitrary initial gradient merging into a parabola $(A-Bx^2)$ near $x=0$.

(*b*) Parabolas at $x=0$, $x=\pm h$, joined by straight line segments.

When v' is assumed to take one of these forms the stress field is readily derived from second order dislocations.

The final displacements of the atom centres are not assumed but calculated. The quantity v' represents the width of imaginary additional material inserted in the slit. It may be considered as the non-elastic part of the relative displacement of the atoms nearest the slip plane. The final displacement ∇v contains both elastic and non-elastic terms.

§ 3. Dislocations of the First Three Orders

All the dislocations used in this paper are plane dislocations of the second type, requiring imaginary additional material along the negative x axis. The order of a dislocation depends on the variation of v' with x.

The zero order dislocation of this type has $v'=$constant on $x<0$. It has the stress function

$$U_0 = Ax \log r \ldots (r^2=x^2+y^2) \qquad \ldots \quad (1)$$

for some constant A, from which may be deduced the components of stress and displacement :

$$\left.\begin{aligned} \widehat{yy}_0 &= (Ax/r^2)(3-(2x^2/r^2)) \\ 2\mu v_0 &= A[2(1-\sigma)\theta - (xy/r^2)] \end{aligned}\right\} \quad . \quad . \quad . \quad . \quad (2)$$

where $\tan\theta = y/x$. This is a Volterra dislocation, and corresponds to a Burgers edge dislocation on the (yz) plane.

$$v_0' = 2\pi(1-\sigma)A/\mu.$$

The first order dislocation is also a Volterra dislocation, since it has relative displacement as a rigid body :

$$v' \propto r \text{ on } x<0.$$

A stress function having the required properties is

$$U_1 = -\tfrac{1}{4}A(2r^2 \log r - r^2) \quad . \quad . \quad . \quad . \quad . \quad (3)$$

with components of stress and displacement such as :

$$\left.\begin{aligned} \widehat{yy}_1 &= -A(\log r + \cos^2\theta), \\ 2\mu v_1 &= -A[(1-2\sigma)y \log r + 2(1-\sigma)x\theta - 2(1-\sigma)y], \\ v_1' &= 2\pi(1-\sigma)Ar/\mu. \end{aligned}\right\} \quad (4)$$

This dislocation corresponds to a linear distribution of zero order dislocations along the negative x axis (cf. Mann 1949). The zero order stress function may therefore be obtained by differentiating U_1 with respect to $-x$:

$$-\frac{\partial U_1}{\partial x} = U_0$$

and the same is true of the various components

$$-\frac{\partial \widehat{yy}}{\partial x} = \widehat{yy}_0 \text{ etc.}$$

(cf. Yoffe 1957).

The second order dislocation is not a Volterra dislocation since it has relative displacement proportional to the square of the distance from the origin. A suitable stress function is

$$U_2 = \frac{1}{4}A\left[\left(\frac{2x^3}{3} + 2xy^2\right)\log r - \frac{4}{3}y^3\theta - \frac{5}{9}x^3 - \frac{7}{3}xy^2\right] \quad . \quad . \quad (5)$$

with components :

$$\left.\begin{aligned} \widehat{xx}_2 &= A(x \log r - 2y\theta - x), \\ \widehat{yy}_2 &= Ax \log r, \\ \widehat{xy}_2 &= -Ay \log r, \\ 2\mu u_2 &= \tfrac{1}{4}A\{2 \log r[(1-2\sigma)x^2 - (3-2\sigma)y^2] - 8(1-\sigma)xy\theta \\ &\quad -(3-4\sigma)x^2 + (5-4\sigma)y^2\}, \\ 2\mu v_2 &= A[(1-2\sigma)xy \log r + (1-\sigma)x^2\theta + \sigma y^2\theta - (1-2\sigma)xy], \\ v_2' &= \pi(1-\sigma)Ar^2/\mu. \end{aligned}\right\} \quad (6)$$

It is readily verified that

$$\frac{\partial^2 U_2}{\partial x^2} = -\frac{\partial U_1}{\partial x} = U_0 \quad . \quad . \quad . \quad . \quad . \quad . \quad . \quad (7)$$

with similar relations for each set of components.

It may be noted that all terms of (6) are finite at the origin, so that a continuous stress field may be built up by combining second order dislocations. Such a field would however have singularities at infinity unless the dislocations are so chosen that their fields cancel at large distances.

By an argument developed in the previous paper (Yoffe *loc. cit.*) this cancelling is achieved by finite difference approximation to the derivative. Let each term of eqn. (7) be differentiated once more with respect to $(-x)$:

$$-\frac{\partial^3 U_2}{\partial x^3} = \frac{\partial^2 U_1}{\partial x^2} = -\frac{\partial U_0}{\partial x} = U_{-1}, \quad . \quad . \quad . \quad . \quad . \quad (8)$$

then the stress function U_{-1} gives a suitable stress field at infinity:

$$U_{-1} = -A(\log r + \cos^2\theta), \quad . \quad . \quad . \quad . \quad . \quad . \quad . \quad . \quad (9)$$

$$\left.\begin{aligned}
\widehat{xx}_{-1} &= \frac{A}{r^2}\left(1 - \frac{8x^2y^2}{r^4}\right), \\
\widehat{yy}_{-1} &= -\frac{A}{r^2}\left(3 - \frac{12x^2}{r^4} + \frac{8x^4}{r^4}\right), \\
\widehat{xy}_{-1} &= -\frac{Axy}{r^4}\left(6 - \frac{8x^2}{r^2}\right), \\
2\mu u_{-1} &= -\frac{Ax}{2r^2}\left[(1-4\sigma) + \frac{x^2-3y^2}{r^2}\right], \\
2\mu v_{-1} &= \frac{Ay}{2r^2}\left[5 - 4\sigma + \frac{y^2-3x^2}{r^2}\right].
\end{aligned}\right\} \quad . \quad . \quad . \quad (10)$$

U_{-1} is the stress function of a centre of pressure at the origin, causing compression in the y direction and tension in the x direction. All components of U_{-1} tend to zero at infinity.

Fig. 4

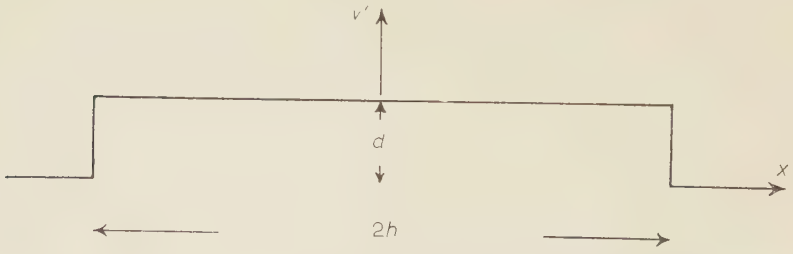

The relative displacement $v'(x)$ obtained from two zero order dislocations.

If therefore dislocations of zero, first or second order are combined in such a way as to represent one of the terms of eqn. (8), then there will be no singularity at infinity.

For example it is readily verified that a zero order dislocation at $(h, 0)$ and an equal but negative one at $(-h, 0)$ may cause the slit to be dilated by a constant amount as in fig. 4. Let suffixes h, $-h$ relate coordinates to these points as new origins so that

$$\theta_h = \tan^{-1}(y/x-h),$$

$$r_h = \sqrt{[(x+h)^2+y^2]} \quad \text{etc.}$$

Then the stress field of the two dislocations may be calculated from the stress function

$$U = A[(x-h)\log r_h - (x+h)\log r_h] \qquad . \; . \; . \quad (11)$$

with $A = \mu d/2\pi(1-\sigma)$. At points a large but finite distance from the origin this function U may be expanded in a rapidly converging Taylor series :

$$U = U_0(x-h) - U_0(x+h)$$

$$= -2h\frac{\partial U_0}{\partial x} - \frac{h^3}{3}\frac{\partial^3 U_0}{\partial x^3} \cdots$$

so that $U/2h \to -\partial U_0/\partial x = U_{-1}$ as in (8), or

$$U \to -\frac{\mu d h}{\pi(1-\sigma)}(\log r + \cos^2\theta) \qquad . \; . \; . \; . \; . \quad (12)$$

and the field is regular at infinity.

Fig. 5

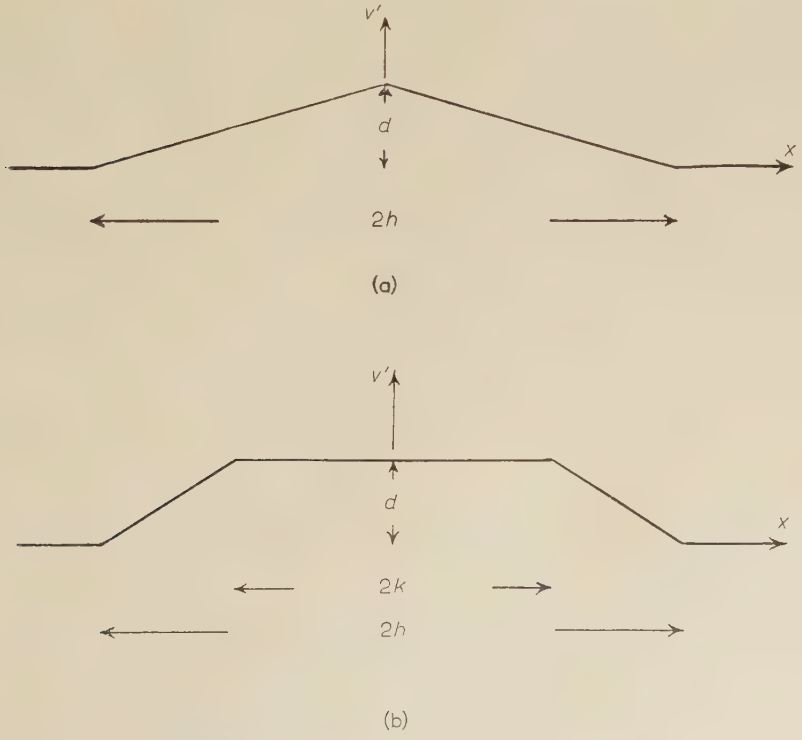

(*a*) Relative displacement corresponding to eqn. (13).
(*b*) Relative displacement corresponding to eqn. (14).

Similarly the stress fields of first order dislocations may be combined in any manner which approximates to their second derivative. For example

$$U_1(x-h)-2U_1(x)+U_1(x+h)\to h^2\frac{\partial^2 U_1}{\partial x^2}=h^2U_{-1}. \qquad (13)$$

So all components are finite at large distances if first order dislocations are placed at $(h, 0)$ $(-h, 0)$ and two negative ones at 0. The resulting dilation of the slit is shown in fig. 5 (a), when the constant A in each U_1 is chosen as $A=\mu d/2\pi(1-\sigma)h$.

A more general form is given by the stress function

$$U=U_1(x-h)-U_1(x-k)-U_1(x+k)+U_1(x+h)\to(h^2-k^2)U_{-1} \qquad (14)$$

as shown in fig. 5 (b), where $0\leqslant k<h$. Equation (14) is readily verified by expansion in Taylor series. The constant A in each U_1 is here $\mu d/2\pi(1-\sigma)(h-k)$ so that at large distances

$$U\to-\frac{\mu d(h+k)}{2\pi(1-\sigma)}\cdot(\log r+\cos^2\theta). \qquad (15)$$

§ 4. Stress Field of the Dilated Slit

To dilate a slit along the smooth curves shown in fig. 3, second order dislocations are distributed between $\pm h$ to give systems equivalent to the first term of eqn. (8). They may be distributed in any manner representing an approximation to the third derivative, so that at large distances the stress function still reduces to CU_{-1} where C is a constant.

A curve of the type (b) of fig. 3 may be specified by two parameters k and k' which determine the radii of curvature at 0, h and $-h$ as follows:

$$v'=\begin{cases} 0\ldots(|x|\geqslant h) \\ \dfrac{d}{(2h-k-k')}\cdot\dfrac{(h-x)^2}{k}\ldots(h-k\leqslant x\leqslant h) \\ \dfrac{d}{(2h-k-k')}\cdot\dfrac{(h-x)^2-(h-k-x)^2}{k}\ldots(k'\leqslant x\leqslant h-k) \\ \dfrac{d}{(2h-k-k')}\left[\dfrac{(h-x)^2-(h-k-x)^2}{k}-\dfrac{(k'-x)^2}{k'}\right]\ldots(|x|\leqslant k') \end{cases} \qquad (16)$$

with $v'(x)=v'(-x)$. The dislocations are all of second order, situated at the points $x=\pm h, \pm(h-k), \pm k'$. The stress function of the whole system is given by:

$$U=\frac{U_2(x-h)-U_2(x-h+k)}{k}-\frac{U_2(x-k')-U_2(x+k')}{k'}+\frac{U_2(x+h-k)-U_2(x+h)}{k} \qquad (17)$$

with U_2 defined by eqn. (5) in which $A=\mu d/\pi(1-\sigma)(2h-k-k')$ and at large distances

$$\begin{aligned} U &\to \tfrac{1}{3}(3h^2-3hk+k^2-k'^2)U_{-1} \\ &= -\frac{\mu d(3h^2-3hk+k^2-k'^2)}{3\pi(1-\sigma)(2h-k-k')}\cdot(\log r+\cos^2\theta) \quad . \quad . \quad (17\,a) \\ &= CU_{-1} \end{aligned}$$

as required.

A curve of the type (a) of fig. 3 may be regarded as the limit of type (b) as $k \to 0$, the first and last terms of U in (17) reducing to the stress functions of first order dislocations :

$$U_{k\to 0}=U_1(x-h)-\frac{U_2(x-k')-U_2(x+k')}{k'}+U_1(x+h)\to\frac{3h^2-k'^2}{3}U_{-1}. \quad . \quad . \quad . \quad (18)$$

This relation may also be obtained directly, since the curve (a) may be specified by one parameter k' as follows :

$$v'=\begin{cases} 0 \quad (|x|\geqslant h) \\ d(h-x)/(h-\tfrac{1}{2}k') \quad (k'\leqslant x\leqslant h) \\ d(h-x-(k'-x)^2/2k')/(h-\tfrac{1}{2}k') \quad (-k'\leqslant x\leqslant k') \\ d(h-x)/(h-\tfrac{1}{2}k') \quad (-h\leqslant x\leqslant -k'). \end{cases} \qquad (19)$$

From consideration of eqns. (4) and (6) it is found that such a v' may be composed of first order dislocations at $\pm h$ and second order ones at $\pm k'$, so the result (18) follows, with $A=\mu d/2\pi(1-\sigma)(h-\frac{1}{2}k')$.

If k' also tends to zero in eqn. (18) the stress system is that of fig. 5 (a) and eqn. (14).

The stress field is completely determined from the stress function, so that the problem is now solved. From any given curve of the types in fig. 3 the constants k and k' are determined, substituted in (17) and the required components calculated in the usual way.

For example, the normal stress $\widehat{yy}$ at points along the slip plane is calculated from

$$\widehat{yy}=\frac{\partial^2 U}{\partial x^2}.$$

In the case of equally spaced dislocations, $k=2h/3$, $k'=\frac{1}{3}h$ in (17), and the stress is given by :

$$\begin{aligned} \widehat{yy}=\frac{3\mu d}{2\pi(1-\sigma)h^2}&[(x-h)\log r_h-3(x-\tfrac{1}{3}h)\log r_{\frac{1}{3}h} \\ &+3(x+\tfrac{1}{3}h)\log r_{-\frac{1}{3}h}-(x+h)\log r_{-h}]. \quad . \quad . \quad . \quad . \quad (20) \end{aligned}$$

This has the maximum value $3{\cdot}3\mu d/\pi(1-\sigma)h$ compression at $x=0$ and changes to tension at about $x=0{\cdot}47h$.

If both parameters are smaller as for $k=0{\cdot}2h$, $k'=0{\cdot}1h$ the maximum compressive stress increases slightly to $3{\cdot}8\mu d/\pi(1-\sigma)h$ and $\widehat{yy}$ changes sign at about $x=0{\cdot}6h$.

If k is zero as in (18) the stress $\widehat{yy}$ becomes infinite at $\pm h$, but remains finite at $x=0$ with the value $3{\cdot}4\mu d/\pi(1-\sigma)h$ and changes sign at about $0{\cdot}7h$.

If k is zero and $k' \to h$ in (18) the graph of v' becomes a smooth curve with no straight segments. The dislocations are situated only at $x=\pm h$, with infinite tensile stress at these points. The compressive stress at $x=0$ is $2\mu d/\pi(1-\sigma)h$, and $\widehat{yy}$ changes sign at $x=0{\cdot}75h$.

If the relative displacement of atom centres is required, then elastic terms must be added to $v'(x)$. If the inter-atomic distance normal to the slip plane is a, then the relative displacement Δv is calculated from the equation

$$\nabla v = v(x, \tfrac{1}{2}a) - v(x, -\tfrac{1}{2}a)$$

and differs from $v'(x)$ by a term depending on a.

§ 5. Strain Energy and Density Change

The strain energy per unit length in the z direction of a large elastic body containing the dilated slit is calculated from the surface integral in the usual way. But the field of each slit considered is that of the stress function $C(\log r + \cos^2\theta)$ at large distances. Such stresses and displacements decrease so rapidly for increasing r that their contribution is negligible if the radius R of the outer surface is sufficiently large. The remaining term of the strain energy is given by:

$$E = -\tfrac{1}{2}\int_{-h}^{h} \widehat{yy} \,.\, v'\,dx$$

$$= -\int_{0}^{h} \widehat{yy} \,.\, v'dx \quad . \quad . \quad . \quad . \quad . \quad . \quad . \quad (21)$$

where v' is given by a chosen form of (16), and $\widehat{yy}$ is deduced from (6) and (17).

This quantity E may be calculated for any chosen values of k and k'. It may even be calculated for zero k since the product $v' \,.\, \widehat{yy}$ remains finite as $\widehat{yy}$ approaches an infinite value at $x=\pm h$. For k zero, the strain energy is found to have the value $0{\cdot}74\mu d^2/\pi(1-\sigma)$ for $k'=0{\cdot}1h$, and the larger value $\mu d^2/\pi(1-\sigma)$ if $k'=h$. For evenly spaced dislocations with $k=\frac{2}{3}h$, $k'=\frac{1}{3}h$, the strain energy is $0{\cdot}8\mu d^2/\pi(1-\sigma)$, while for smaller parameters $k=0{\cdot}2h$, $k'=0{\cdot}1h$, the strain energy is slightly smaller, $E=0{\cdot}77\mu d^2/\pi(1-\sigma)$.

When the field of the dilated slit is used to represent local expansion at an edge dislocation it is found that the strain energies of slit and dislocation may be simply added. This is because there are no cross terms in the strain energy of the combined system, one having relative displacement u' and zero $\widehat{yy}$ on the x axis, the other a non zero v' but vanishing $\widehat{xy}$.

The change in density of an elastic body due to the presence of an edge dislocation is zero according to first order elasticity theory. But if the lattice is dilated at the centre by atomic misfit, even first order elasticity admits a change of volume, and therefore of density.

The increase in volume ∇V per unit length in the z direction of all the elastic material initially bounded by a cylinder of radius R is found by integrating the radial displacement round the outer surface :

$$\nabla V = \int_{-\pi}^{\pi} u_r R \, d\theta \quad . \quad . \quad . \quad . \quad . \quad . \quad . \quad (22)$$

where $u_r = u \cos\theta + v \sin\theta$

$$= \frac{C}{2\mu R}[1-2(1-\sigma)\cos 2\theta] \quad . \quad . \quad . \quad . \quad . \quad (23)$$

by eqn. (10). This gives

$$\nabla V = \pi C/\mu$$

where the constant C is determined by the form of the dilation as shown in § 4 :

$$C = \frac{\mu d(3h^2-3hk+k^2-k'^2)}{3\pi(1-\sigma)(2h-k'-k)}.$$

But the u_r of eqn. (10) applies to a body which extends to infinity, so that certain stresses act at the surface of radius R. If this surface is supposed free, it is necessary to add a stress function U_R as follows :

$$U_R = \frac{C}{R^2}\left(r^2 \cos 2\theta + \tfrac{1}{2}r^2 - \frac{r^4}{2R^2}\cos 2\theta\right)$$

which contributes a further radial displacement

$$u_r = \frac{C}{\mu R}\left(\frac{1-2\sigma}{2} - (1-\sigma)\cos 2\theta\right).$$

On adding this to (23) the change in volume is found to be

$$\nabla V = 2\pi C(1-\sigma)/\mu. \quad . \quad . \quad . \quad . \quad . \quad . \quad (24)$$

This ∇V, as might be expected, is equal to the volume of imaginary material added within the slit.

If the average density of the body is ρ, the change in density is given approximately by

$$\nabla\rho = -\rho\frac{\nabla V}{V}$$

$$= -2\rho C(1-\sigma)/\mu R^2.$$

§ 6. Conclusion

It has been shown how to calculate the elastic stress field surrounding a slit dilated by an arbitrary distribution of enclosed material. At a distance the field is that of a particular type of centre of pressure, the

actual values of the stresses depending on the contours of the inclusion. For a smoothly tapered inclusion the stresses remain finite everywhere, but an angular form causes singularities at isolated points.

The strain energy of a large body containing such a slit may be calculated with accuracy, but the density change, as calculated in § 5, is less reliable. As pointed out by Stehle and Seeger (1956) the second order terms of the elastic dilation are no longer negligible when integrated over a large volume, and their total may even exceed those of first order theory. This effect makes the displacements of the present paper unreliable at large distances, but does not affect the components of stress or strain.

It seems clear that the stress field of an edge dislocation in a crystal lattice must include terms of the type discussed here. At large distances such terms may often be negligible, but they may have considerable influence on the migration of solute atoms and the formation of precipitates on the slip planes.

Acknowledgments

I wish to thank Dr. P. B. Hirsch for very helpful criticism and advice, Dr. J. D. Eshelby for reading the manuscript and the Atomic Energy Research Establishment, Harwell, for a grant.

References

Mann, E. H., 1949, *Proc. roy. Soc.* A, **199**, 376.
Muskhelisvili, N. I., 1953. *Mathematical Theory of Elasticity* (Holland : Noordhoff), p. 340.
Read, W. T., 1953, *Dislocations in Crystals* (New York : McGraw-Hill), p. 26.
Stehle, H., and Seeger, A., 1956, *Z. Phys*, **146**, 217.
Yoffe, E. H., 1957, *Phil. Mag.*, **2**, 1197.

Further Interactions of the Heavy Nuclei of the Cosmic Radiation†

By V. Y. Rajopadhye‡ and C. J. Waddington
H. H. Wills Physical Laboratory, Bristol

[Received September 10, 1957]

Abstract

Earlier results obtained at Bristol from a study of nuclear interactions produced by heavy nuclei of the primary cosmic radiation passing through nuclear emulsions have been amplified and confirmed. Revised values are given for the fragmentation probabilities and mean free paths which are of greater statistical weight and in good agreement with those reported previously. Values are derived from the fragmentation probabilities in air and in hydrogen which probably represent upper limits to the true values. The implications of the results are discussed.

§ 1. Introduction

The experiment reported here is a continuation of a previous paper by Fowler, Hillier and Waddington (1957), which will be referred to as Paper I. In that paper the results were given of an analysis of 317 nuclear interactions produced by heavy cosmic ray nuclei passing through nuclear emulsions exposed at high altitude. The present paper reports the result of a similar analysis made on a further 470 interactions.

As before, the incoming nuclei have been separated into charge groups distinguished in the following manner : If Z is the charge of a nucleus, then L nuclei have $3 \leqslant Z \leqslant 5$; M nuclei $6 \leqslant Z \leqslant 9$; H' nuclei $10 \leqslant Z \leqslant 19$; VH nuclei $Z \geqslant 20$ and H nuclei $Z \geqslant 10$; so that H nuclei include H' nuclei and VH nuclei. Thus, in order to determine the fragmentation probabilities, i.e. the probability that a nucleus of a given charge group should produce, in a nuclear interaction, a secondary nucleus of the same or lighter charge groups, it is necessary to determine only the charge groups to which these nuclei belong. In practice it is generally possible to measure the charge of a nucleus to within one charge and thus the errors introduced by incorrect charge identification are usually small. For example, since the completion of Paper I further charge measurements have been made on many of the L and M nuclei observed in that experiment (Waddington 1957 a), which show that less than 19% of the carbon and boron nuclei were assigned to the incorrect charge groups and that the error in the

† Communicated by the Authors.
‡ On leave of absence from S. P. College, Poona, India.

relative numbers of L and M nuclei was less than 4%. The charge determinations on the L and M nuclei in the present experiment should be more accurate than those in Paper I, since they were made by an observer with greater experience of making these rather subjective measurements.

Fig. 1

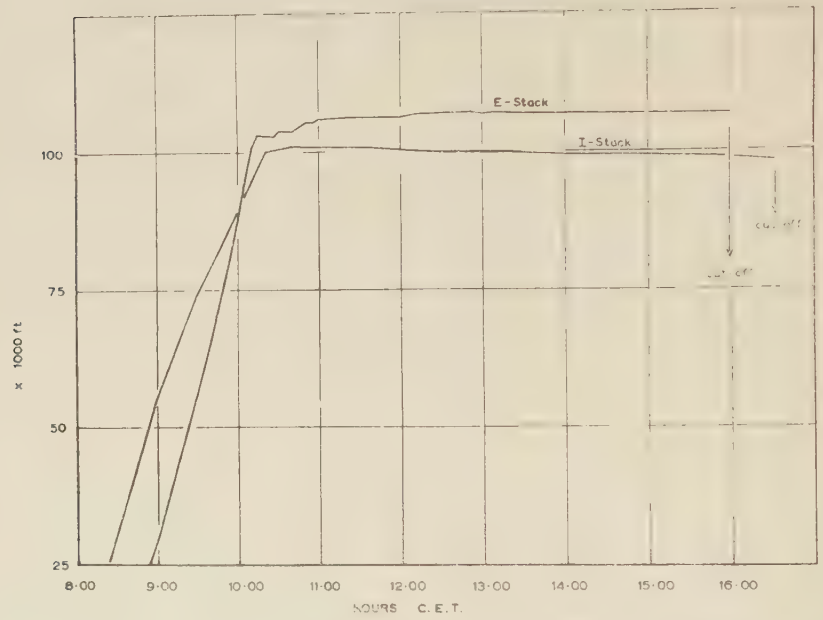

Flight curves of E and I stacks. Altitudes expressed in thousands of feet.

From the combined data of the two experiments an attempt has been made to determine upper limits to the fragmentation probabilities in air and in hydrogen. The values obtained strongly support the view that the observation of a ratio of L to M nuclei greater than about 0·25 at 10 to 15 g cm^{-2} of residual atmosphere is incompatible with the assumption that there are no L nuclei incident at the top of the atmosphere. Furthermore, it appears that these values of the fragmentation probabilities in air can only be raised by reducing those in hydrogen and thus increasing the significance of any observed primary L nuclei.

§ 2. Experimental Procedure

Of the 470 interactions found in the present investigation, 84 were observed in the same stack of nuclear emulsions as those analysed in Paper I, the E stack, while the remaining 386 were observed in another stack, the I stack, exposed under closely similar conditions. Details of the exposures and physical dimensions of these stacks are given in table 1, while the flight curves are shown in fig. 1. Both these exposures were

Table 1. Exposure Details and Physical Dimensions of Emulsion Stacks

	No. of emulsions	Dimensions (cm)	Date	Mean altitude (feet)	Duration (hours)	Rate of ascent (ft/min)
E stack	80	$20\times15\times0{\cdot}06$	14.9.54	106 000	5·75	1000
I stack	60	$38\times25\times0{\cdot}06$	20.9.55	100 000	6·67	570

Table 3. Relative Proportions of Interactions and Stars

	L nuclei (%)	*M* nuclei (%)	*H* nuclei (%)		*L* nuclei no.	*L* nuclei %	*M* nuclei no.	*M* nuclei %	*H* nuclei no.	*H* nuclei %
p-interactions	8·7	10·1	13·5	*X*-stars	31	17·8	61	15·3	38	19·4
l-interactions	29·5	30·6	32·0	*R*-stars	72	41·1	193	48·5	76	38·8
h-interactions	61·8	59·3	54·5	*T*-stars	72	41·1	144	36·2	82	41·8
Mean free path in emulsion ($g\ cm^2$)	59·4	50·9	36·4							

made over Northern Italy, where the geomagnetic cut-off energy is about 1·5 Bev per nucleon (Fowler and Waddington 1956), and as a result the great majority of the nuclei entering the emulsions were moving with relativistic velocities.

Fig. 2

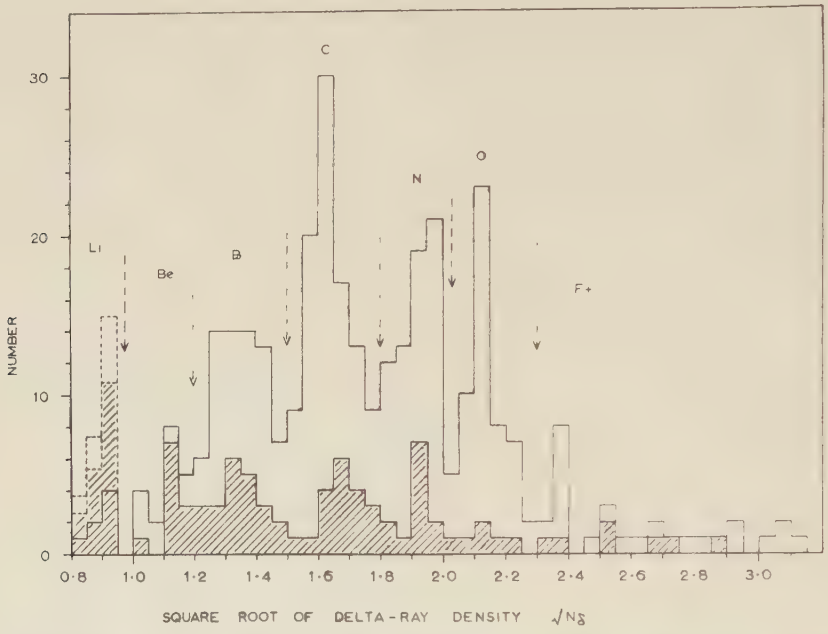

Charge spectrum of M and L nuclei observed in I stack. Secondary fragments are shown shaded.

Emulsions of the I stack were scanned, along a line parallel to the top edge, for the tracks of multiply charged nuclei. These tracks were then followed through the emulsions until the particle interacted or left the stack. Any fast secondary fragments heavier than α-particles emitted from these interactions were also followed until they in turn interacted or left the stack. In the E stack, where the interactions produced by nuclei entering the top edges had already been analysed in Paper I, a scan was made parallel to the side edges and of the end plates. These scans were made principally for H nuclei. Throughout, tracks were only accepted if they had a projected length of greater than 4 mm per emulsion and a zenith angle of less than 60°.

The charges of the L and M nuclei were determined by δ-ray counting with similar procedures to those employed previously (Waddington 1957a). The results of these measurements in the I stack are shown in fig. 2. The charge assignments shown in this figure were based on the observation of charge-indicating interactions. Similar measurements were made on the

appropriate tracks in the *E* stack and the results are shown in fig. 3. In this case the charge assignments have been calculated from the following relation determined previously for this stack (Waddington 1957 a): $Z=3{\cdot}76\ (N_\delta - 0{\cdot}46)^{1/2}$, where N_δ was the δ-ray density per $100\,\mu$.

The charges of the majority of the *H* and *VH* nuclei have been determined with a photo-densitometer, and details of the procedures employed will be published in a forthcoming paper by Hillier and Rajopadhye. It is estimated that these determinations have a probable error of half a charge, if it is assumed that the highest charge peak with an appreciable abundance observed in their charge spectrum is due to iron nuclei. In a number of cases it proved impracticable to make these densitometer measurements and the charges have been estimated from a δ-ray count. These latter determinations are not claimed to be very accurate, but do generally enable the separation of the nuclei into different charge groups. Particles identified in this manner are indicated in the table of interactions (table 2) by asterisks.

Fig. 3

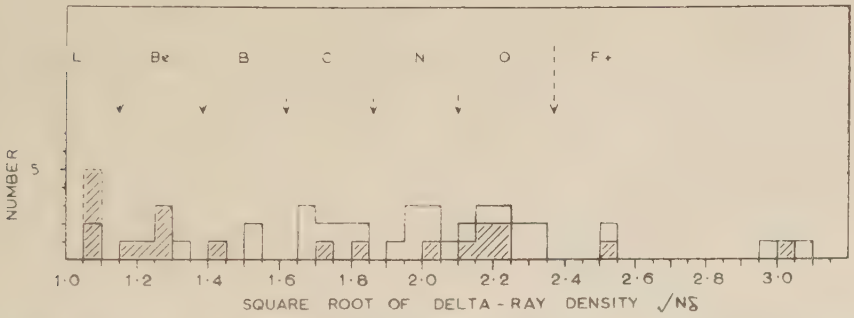

Charge spectrum of *M* and *L* nuclei observed in *E* stack. Secondary fragments are shown shaded.

All the charge determinations made in primary nuclei were made near the point at which they were detected, while all those on the secondary nuclei were made near their parent interactions. In a few cases, less than ten, this procedure resulted in an obvious anomaly between the measured charge and that apparent near the interaction. These anomalies, when confirmed, were found to be due to the presence of undetected interactions, which were generally either of the type in which only particles with minimum ionization were produced together with the heavy fragment of reduced charge, or to interactions which occurred very near to an interface of the emulsions. The occurrence of these events indicated that not all interactions of these types can have been observed. However, it appears very unlikely that an appreciable proportion were missed, because of the small number found in this manner. This conclusion is supported by the close agreement of the observed mean free paths with those found by other workers (Noon and Kaplon 1955). While no attempt has been made

Table 2. Characteristics of each one of the 470 nuclear interactions observed in emulsion; Δ indicates the nature of the heavy fragment, n_α, N_h and n_s the number of the α, slow and shower particles emitted. p and not p signify whether it is an interaction with a proton or not.

Lithium

N_h	Δ	n_α	n_s	
0		1	6	p
0		1	1	not p
0		1	?	p
0		1	?	p
0			4	p
0			3	not p
0			3	not p
1		1	2	p
1			5	p
3			8	
3			7	
5		1	4	
5		1	3	
5		1	3	
5			10	
5			9	
5			6	
9		1	2	
14			8	
16			13	
21		1	15	
21			5	
27			14	
29			4	
33			4	

Beryllium

N_h	Δ	n_α	n_s	
1	Li		2	not p
1		2	0	not p
1		1	4	p
1		1	2	p
2		1	6	
2			3	
3		1	5	
5		1	3	
5		1	2	
5			8	
7		1	4	
8			8	
13			14	
15			?	
16	Li		1	
16			17	
27			3	
31			18	
?		1	?	

Boron

N_h	Δ	n_α	n_s	
0	Li	1	0	not p
0		2	1	not p
0		2	?	p
0		1	7	p
0		1	6	p
0		1	6	p
0		1	5	p
0		1	4	p
0		1	4	p
0		1	4	p
0		1	3	not p
0		1	3	not p
0		1	3	not p
0			6	p
0			?	p
1	Li	1	0	p
1		2	4	p
1		2	2	p
1		2	1	p
1		1	8	p
2		1	15	
2		1	9	
2		1	2	
3		1	11	
3		1	?	
4	Be		2	
4	Be		1	
4		2	1	
4		1	11	
4		1	5	
4			8	
4			8	
4			?	
5		1	10	
5		1	10	
5		1	8	
5		1	3	
5			14	
6		2	12	
6		2	3	
7	Li	1	1	
7		1	8	
8		2	5	
8		1	7	
8			12	
8			7	
8			?	
9			9	
11			4	
12		1	21	
12			8	
13	Li		5	
15		1	9	
15			12	
17			14	
18			20	
19			11	
21			10	
26			15	
27			8	
28			8	
29			?	
30			17	

Carbon

N_h	Δ	n_α	n_s	
0	Be	1	?	p
0	Be		5	p
0	Li	1	5	p
0	Li		5	p
0	Li		5	p
0		3	?	p
0		2	3	p
0		2	3	p
0		2	2	not p
0		2	2	not p
0		2	?	p
0		2	?	p
0		1	7	p
0		1	5	p
0			9	p
1	Be	1	1	p
1	Be	1	0	p
1	Li		3	p
1		3	0	p
1		2	6	p
1		2	6	p
1		1	10	p
1		1	7	p
1		1	5	not p
1		1	4	p
1			5	p
2		2	2	
2		2	2	
2		2	?	
2			35	
2			20	
2			16	
2			15	
3		3	2	
3		2	4	
3		1	6	
3			22	
3			11	
3			7	
3			7	
3			?	
3			?	
4		2	2	
4		1	?	
4			10	
4			8	
5	Be	1	0	
5		1	5	
5			10	
5			7	
6		2	2	
6		2	?	
6		1	8	
6		1	5	
6			6	
7		2	3	
7		1	23	
7			9	
8	Li		7	
8		2	5	
8		1	8	
8		1	6	
8		1	?	
8			9	
9	Be		?	
9		1	5	
9			12	
10		2	2	
10		2	2	
10			50	
11			19	
12		1	?	
13			12	
14		1	10	
14		1	7	
14		1	5	
15		1	8	
15			10	
16		1	7	
17			44	
18			16	
20			14	
21		1	7	
23		1	18	
23		1	17	
25			30	
26			23	
30			22	
32			8	
32			?	
34			9	
39			7	
?		2	?	
?		2	?	
?		1	?	

Nitrogen

N_h	Δ	n_α	n_s	
0	C		2	p
0	C		2	p
0	B	1	0	not p
0	B		6	p
0	Li		7	p
0		3	5	p
0		3	1	not p
0		3	1	not p
0		2	13	p
0		1	8	p
0			10	p
1	B		2	not p
1	Li	1	2	p
1		3	3	not p
1		3	2	p
1		1	9	p
2	N		2	
2	B	1	?	
2	Be		14	
2		1	5	
2			24	
2			24	
2			11	
2			11	
3	C		3	
3	B		3	
3			17	
3			?	
4	Be		7	
4	Li		10	
4		2	?	
4		1	5	
4		1	?	
4			15	
4			?	
5	B		3	
5	B		1	
5	Li	1	4	
5		2	7	
5		2	4	
5		2	?	
5		1	14	
5		1	9	
5			13	
5			10	
6	C		2	
6		2	5	
6		1	11	
6			6	
8	N		1	
8			?	
9	C		5	
9	B		8	
10	Li	1	?	
12		1	10	
12			33	
13			38	
14	Li		14	
14			18	
16		2	7	
16			?	
17		1	11	
18		1	6	
18			?	
19		1	4	
20			16	
21			?	
24			35	
25			6	
30		1	3	
33			19	
?		2	?	

Oxygen

$N_\hbar$	Δ	n_α	n_β	
0	B	1	5	p
0		3	8	p
0		3	6	p
0		3	5	p
0		3	2	not p
0		3	?	p
0		2	5	p
0		2	5	p
0		1	8	p
1	C	1	0	not p
1	B	1	1	p
1		2	5	not p
2		2	?	
2	N		2	
3	B	1	5	
3	Li	3	17	
3	Li	1	?	
3	Li		5	
3		2	?	
3		1	8	
3		1	6	
3			10	
4		2	6	
4		2	3	
4		1	15	
4		1	7	
5		1	11	
5		1	9	
5		1	?	
6	O		1	
6	N		5	
6	C		4	
6		2	6	
6		1	30	
6		1	6	
6			10	
6			8	
7	Li		7	
7		2	3	
8			14	
9	N		3	
12			17	
13			55	
13			19	
16		2	24	
16		1	6	
16		1	5	
17			18	
17			16	

Oxygen

$N_\hbar$	Δ	n_α	n_β
20			14
20			10
20			?
21		2	5
21			23
21			15
22			12
24	C		13
24			14
28			18
30			8
?		1	?

Fluorine

$N_\hbar$	Δ	n_α	n_β	
1	N		1	not p
1	Li	1	4	not p
2			14	
3		3	3	
3		1	10	
4	B	1	3	
4		1	6	
4		1	?	
4			16	
14	Li		8	
15	B		11	
15		1	5	
19			12	
24			25	
34			16	

Neon

$N_\hbar$	Δ	n_α	n_β	
0	N	1	9	p
0	Be	1	6	p
0*		3	4	p
1*	N	1	0	not p
1		1	23	p
2	O	1	0	
2	F		3	
2		2	?	
2*			17	
3	C	1	3	
3	B	1	11	
3		1	11	
4*	Ne		10	
4	Ne		1	
4*	F		4	
4*	B	1	6	
4*	Be	1	10	
4			18	
5*	O		5	
5		2	8	
7	B	1	4	
7			?	
9	Be	2	5	
10		3	5	
11	O	1	?	
14		1	27	
15	Li		26	
30			26	
?		2	?	

Sodium

$N_\hbar$	Δ	n_α	n_β	
0	O	1	2	p
0	C	2	3	p
0	C	1	8	p
0*	Li	2	8	p
0		5	5	p
0		3	8	p
0		3	7	p
1			31	p
2		1	22	
4	O		9	
4	C		11	
12			?	
13*		2	7	
19	B	2	5	
30			28	

Magnesium

$N_\hbar$	Δ	n_α	n_β	
0	Ne	1	0	not p
0	B	1	5	p
0	N		7	p
0*		4	5	p
0		3	9	p
0			22	p
1		5	?	p
2*	N	2	4	
2*	C		13	
3	F		5	
3*	Li	3	17	
3*	Li		17	
5	C	2	11	
5	C		5	
5		1	18	
6*	C	3	5	
7		3	10	
11	Ne		6	
14*	Li	1	?	
17			17	
18			23	
24			1	
27		1	30	
28			50	
?	N, Be		?	

Aluminium

$N_\hbar$	Δ	n_α	n_β
2	B	1	10
7	O, B		4
9*		4	8
17		2	?
18*		1	13
21*			70
21		2	20
27			32

Silicon

$N_\hbar$	Δ	n_α	n_β	
1*	Si*		1	p
3	F	1	?	
5		2	19	
6	N	2	6	
11	Na		4	
26*	Ne		?	
26			20	
?	C	4	?	

Phosphorus

$N_\hbar$	Δ	n_α	n_β	
0	B	4	4	p
1*	O	1	7	p
1	Ne	1	8	p
2*	P*		1	
4	Al		0	
4		3	15	
9	Ne	1	7	
10			?	
18	C	1	18	

Sulphur

$N_\hbar$	Δ	n_α	n_β	
0*	F	2	8	p
5*		2	19	

Chlorine

$N_\hbar$	Δ	n_α	n_β
10	C	2	10

Argon

$N_\hbar$	Δ	n_α	n_β
3	Mg	3	9
5	F	1	12
5	B, Be	1	?
15	Si		9

Potassium

$N_\hbar$	Δ	n_α	n_β
—	—	—	—

Calcium

$N_\hbar$	Δ	n_α	n_β	
1	Ca*		5	not p
1	Ne*, B		7	p
10	Be	3	11	

Scandium

$N_\hbar$	Δ	n_α	n_β
—	—	—	—

Titanium

$N_\hbar$	Δ	n_α	n_β	
0	8*	1	6	p
4	Mg	1	18	
19	F	3	13	
27			15	

Vanadium

$N_\hbar$	Δ	n_α	n_β
—	—	—	—

Chromium

$N_\hbar$	Δ	n_α	n_β	
0	P	3	3	p
4	Al	1	?	
9	O	4	11	
17		2	40	
18	O, Li	1	?	
18	F	1	25	

Manganese

$N_\hbar$	Δ	n_α	n_β
-	-	-	-

Iron

$N_\hbar$	Δ	n_α	n_β	
1	Cr*	1	?	p
4	P*	2	4	
8	Ca*	2	3	
15			128	
16	B, Be	2	15	
40		2	20	

to improve the values quoted in Paper I for the mean free paths of L and M nuclei, new values of $39{\cdot}6 \pm 5{\cdot}4$ g/cm^2 and $26{\cdot}8 \pm 5{\cdot}5$ g/cm^2 have been obtained for the H' and VH nuclei. These values, taken in conjunction with those quoted in Paper I†, give $38{\cdot}7 \pm 3{\cdot}7$ g/cm^2 and $31{\cdot}2 \pm 4{\cdot}4$ g/cm^2 respectively for the mean free paths.

Every interaction observed was classified in terms of the number of black and grey prong emitted, N_h, the type of secondary fragment, if any, the number of secondary α-particles, n_α, and the number of fast singly charged particles, n_s. In Paper I it was shown that for interactions of the type observed in this experiment none of the secondary fragments, $Z \geq 2$, were ejected with angles of greater than 10° to the line of flight of the incoming nucleus. For this reason all the tracks of heavily ionizing particles emitted within this angle were closely studied, and if necessary traced through the stack, to determine whether they were due to secondary fragments or to slow evaporation particles from the target nucleus. It is, therefore, very unlikely that any secondary fragments can have been missed in this work.

§ 3. Results and Analysis

The detailed features of all the interactions observed in this experiment are shown in table 2, with the exception of those of the type where one black prong is the only product. These interactions have been neglected in this work, as they were in Paper I, because of their low efficiency of detection. An examination of the data presented in this table showed that these results were consistent with those of Paper I. For this reason, in what follows, all the data have been combined.

While a knowledge of the fragmentation probabilities in emulsion, $P_{m\,n}$, enables the observed flux values to be extrapolated to the top of the detecting emulsions, these are not the correct values to use for an extrapolation to the top of the atmosphere. At present there appear to be no experimental results on the appropriate fragmentation probabilities in air and very few on those in hydrogen. Previously the values in air have either been obtained from those in emulsions by calculation from a geometrical model of the nucleus (Noon and Kaplon 1955), or from the fragmentations produced in glass (Bradt and Peters 1950). In this paper an attempt has been made to separate the interactions with the light elements in emulsion —carbon, nitrogen and oxygen—from those with the free hydrogen and from those with the heavy elements silver and bromine. This separation has been made on a statistical basis and depends on the number of slow particles emitted from the target nucleus, N_h.

The observed interactions were divided into three classes :

(i) X-stars. These stars will be characterized by having $N_h = 0$ or 1. If there is a black or grey prong then for the star to be included in this class the prong must not be at an angle of greater than 90° to the line of flight

† The mean free path for VH nuclei was erroneously quoted in this paper, and should have been $35{\cdot}1 \pm 6{\cdot}8$ g/cm^2.

of the incoming nucleus. If $N_h = 0$ then the sum of the charges of the particles produced in the star must be at least one charge greater than that of the primary nucleus and at least one of these particles must be singly charged. Stars of this class may be due either to interactions with free protons in emulsion, *p*-interactions, or to collisions with complex nuclei in which at most one slow charged particle is emitted from the target nucleus.

(ii) *R*-stars. These are characterized by having $N_h \leq 7$ but do not include *X*-stars. They may be due either to interactions with light nuclei in emulsion, *l*-interactions, or to interactions with heavy nuclei which do not seriously disrupt the target nucleus.

(iii) *T*-stars. These are characterized by having $N_h > 7$ and are due to interactions with the heavy nuclei in emulsion, *h*-interactions.

Before it is possible to attempt a separation of the stars in these empirical groups into those due to *p*-, *l*- and *h*-interactions, it is necessary to determine the true proportions of such stars which will be produced by a given incoming nucleus. To do this for collisions betwene complex nuclei the interaction cross sections, σ, have to be calculated for the different constituents of the emulsion. A model which permits this calculation has been proposed by Bradt and Peters (1950) to fit the observed mean free paths of different nuclei in glass and brass. These authors proposed an ' overlap ' model such that σ of a nucleus with a radius R_t when approached by a nucleus with radius R_i was given by :

$$\sigma = \pi (R_t + R_i - 2\Delta R)^2 \quad . \quad . \quad . \quad . \quad . \quad . \quad . \quad (1)$$

and ΔR had the empirical value of $0{\cdot}85 \times 10^{-13}$ cm. Now $R = r_0 A^{1/3}$ where A is the atomic weight, and in 1950 r_0 was assumed to be about $1{\cdot}45 \times 10^{-13}$ cm. This relation has now been checked and found to be applicable over a wide range of media and incident nuclei, ranging from α-particles in air (McDonald 1956) to *H* nuclei in lead (Eisenberg 1954). If the presently accepted value of r_0 ($1{\cdot}20 \times 10^{-13}$ cm) is used instead, then ΔR must be varied to fit all the data, decreasing with increasingly heavy incident nuclei, as might be expected from such a model. Thus the general applicability of eqn. (1) must be regarded as fortuitous.

While eqn. (1) appears to be valid for all incident nuclei between helium and iron and all target media between air and lead, it is not valid for incident protons, nor presumably for a hydrogen medium. However, values of σ for 860 Mev protons in various elements have been measured by Chen *et al.* (1955) using an attenuation method, while σ for proton–proton interactions at the same energy is known from the work of Shapiro *et al.* (1954). These results are shown in fig. 4, which shows that the experimental values lie on a smooth curve. This curve has been used to obtain the cross sections of the various constituents of emulsion, and a mean free path for protons in emulsion of 37 cm calculated. This value is in close agreement with that found experimentally and may be contrasted with the value of 28 cm found from eqn. (1).

Thus, when calculating the partial cross sections in emulsion for p-, l- and h-interactions, eqn. (1) was used for the complex target nuclei, while the data of fig. 4 were used for the proton component. Due to the small proportion of hydrogen in emulsion this procedure hardly affects the total cross section in emulsion. These proportions for different incident nuclei, and the total mean free paths, are shown in table 3, together with the observed proportions of X- R- and T-stars.

From the data shown in these tables it is possible to determine the number of l- and h-interactions in the X- and R-stars —all the T-stars being due to h-interactions —provided that it is assumed that those X-stars which are not p-interactions have the same proportion of l- and h-interactions as the entire sample. Fragmentation probabilities, P^{i}_{mn}, were then calculated for the T-stars and the further assumption made that these values were those for h-interactions, P^{h}_{mn}.

Fig. 4

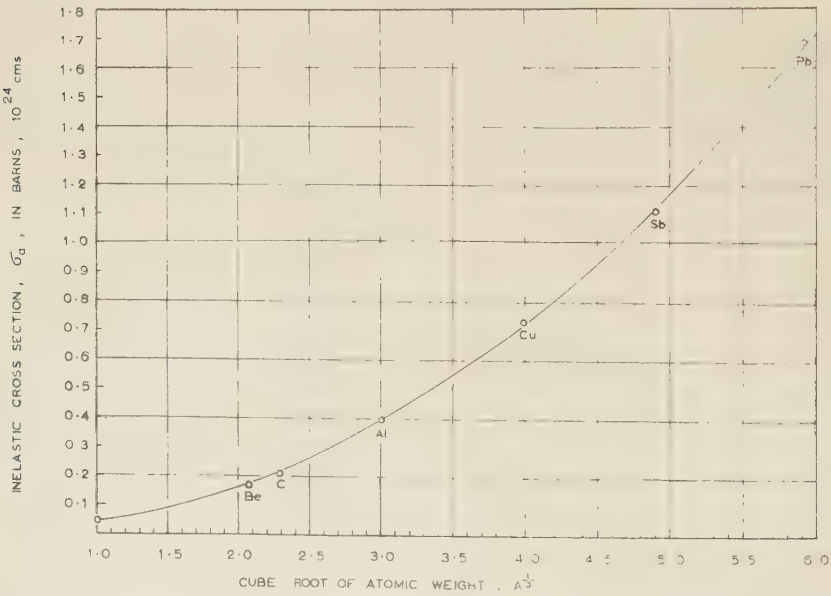

The inelastic cross section, σ, as a function of the cube root of the atomic weight for protons on various elements (from data of Chen *et al.* (1955) and Shapiro *et al.* (1954)).

Since the T-stars are all interactions in which the heavy target nucleus has been considerably broken up, and must, therefore, be generally due to moderately central collisions having small impact parameters, the incoming nucleus must also generally have been severely broken up. As a result, the probability of the incoming nucleus leaving a residual nucleus, or secondary fragment, should be less for these T-stars than for those h-interactions, with their larger impact parameter, included among the R- and X-stars. Thus, the values for P^{h}_{mn} calculated from the T-stars would

appear to be underestimates of the true probability that a secondary fragment will be produced in a h-interaction.

Fragmentation probabilities, assumed to be those for l interactions, P^l_{mn}, were then obtained from the R-stars by making a correction for that proportion of them which were due to h-interactions by using the values of P^h_{mn} found above. A similar procedure for the X-stars, correcting both for the l- and h-interactions, then gave the fragmentation probabilities for p-interactions, P^p_{mn}. These values of P^l_{mn} and P^p_{mn} will be upper limits to the true values. This is true for P^l_{mn} because the values of P^h_{mn} used to correct the data were lower limits to the true values, and for P^p_{mn} because the main correction is also due to P^h_{mn}, although in this case there is admittedly also a correction due to P^l_{mn} which is itself an upper limit.

This derivation is dependent upon the assumption that the fragmentation probabilities derived from the T-stars are always less or equal to those of the other h-interactions among the R- and X-stars. It is not possible to prove that this assumption is correct, although it is very plausible. However, for the most important fragmentation probabilities, those into M and L nuclei, the correction introduced by using P^h_{mn} is small. For example, P^h_{mn} has its greatest value for $P^h_{HL}=0{\cdot}15$, yet even if it were assumed that $P^h_{HL}=0$ for R-stars, P^l_{HL} would only be raised from 0·21 to 0·25, an increase much less than the statistical uncertainty. The implicit assumption has also been made that the fragmentation probabilities for l-interactions among the X-stars will not be very much greater than for those among the R-stars. Since the proportion of l-interactions among the X-stars is, in every case, less than 10% of those among the R-stars, unless this assumption is very seriously in error the values of P^l_{mn} should not be affected. Moreover, it should be noted that any variaion in P^l_{mn} must affect P^p_{mn} in the reverse manner. For example, the results of bombarding carbon with 90 Mev neutrons (Kellogg 1953) suggests that $P^p_{CL}\sim 1$, implying that the quoted values of P^h_{ML} might be too small. If this is correct then the quoted values of P^l_{ML} must be too high.

The values obtained for P^l_{mn} and P^p_{mn} are upper limits to the fragmentation probabilities in air and in hydrogen, and can be used to extrapolate observed flux values through these media. The majority of expriments on the relative abundances of L and M nuclei have used detectors exposed between 5 and 20 g/cm^2 of air below the top of the atmosphere. Hence the effect of passage through air on the ratio of L and M nuclei has been calculated for two cases: (*a*) when the flux of L nuclei at the top of the atmosphere, J_{L^0}, is zero, and (*b*) when J_{L^0} is 0·4 of the flux of M nuclei, J_{M^0}. This calculation was made using the simplified diffusion equations reported previously (Waddington 1957 b), which neglect the effect of consecutive interactions, and using the interaction mean free paths shown in table 3. The results of these calculations are shown in fig. 5, together with the experimental point found by (Waddington 1957 a) under 12 g/cm^2 of residual atmosphere. It can be seen that while the statistical errors are such that at depths greater than 20 g/cm^2 it is difficult to distinguish between cases (*a*) and (*b*), for lesser depths there is a marked divergence.

Table 4 (*a*). Fragmentation Probabilities in Emulsions

$P_{LL}=0{\cdot}08\pm0{\cdot}02$	$P_{MM}=0{\cdot}08\pm0{\cdot}02$	$P_{HH}=0{\cdot}20\pm0{\cdot}03$	$P_{H'H'}=0{\cdot}12\pm0{\cdot}03$	$P_{VHVH}=0{\cdot}21\pm0{\cdot}08$
$P_{L\alpha}=0{\cdot}56\pm0{\cdot}07$	$P_{ML}=0{\cdot}14\pm0{\cdot}02$	$P_{HM}=0{\cdot}27\pm0{\cdot}04$	$P_{H'M}=0{\cdot}29\pm0{\cdot}05$	$P_{VHH'}=0{\cdot}21\pm0{\cdot}08$
	$P_{M\alpha}=0{\cdot}77\pm0{\cdot}06$	$P_{HL}=0{\cdot}17\pm0{\cdot}03$	$P_{H'L}=0{\cdot}16\pm0{\cdot}04$	$P_{VHM}=0{\cdot}24\pm0{\cdot}08$
		$P_{H\alpha}\quad 1{\cdot}27\pm0{\cdot}12$	$P_{H'\alpha}\quad 1{\cdot}13\pm0{\cdot}12$	$P_{VHL}=0{\cdot}18\pm0{\cdot}08$
				$P_{VH\alpha}=1{\cdot}68\pm0{\cdot}35$

Table 4 (*b*). Fragmentation Probabilities for *p*-, *l*- and *h*-interactions

$P^h_{LL}=0{\cdot}06\pm0{\cdot}03$	$P^l_{LL}=0{\cdot}12\pm0{\cdot}07$	$P^p_{LL}=0{\cdot}11\pm0{\cdot}11$
$P^h_{L\alpha}\quad 0{\cdot}28\pm0{\cdot}7$	$P^l_{L\alpha}\quad 0{\cdot}79\pm0{\cdot}26$	$P^p_{L\alpha}=1{\cdot}57\pm0{\cdot}40$
$P^h_{MM}\quad 0{\cdot}04\pm0{\cdot}02$	$P^l_{MM}\quad 0{\cdot}17\pm0{\cdot}06$	$P^p_{MM}=0{\cdot}06\pm0{\cdot}06$
$P^h_{ML}=0{\cdot}06\pm0{\cdot}02$	$P^l_{ML}=0{\cdot}23\pm0{\cdot}07$	$P^p_{ML}=0{\cdot}38\pm0{\cdot}11$
$P^h_{M\alpha}=0{\cdot}36\pm0{\cdot}06$	$P^l_{M\alpha}\quad 1{\cdot}27\pm0{\cdot}28$	$P^p_{M\alpha}=1{\cdot}57\pm0{\cdot}25$
$P^h_{HH}\quad 0{\cdot}12\pm0{\cdot}04$	$P^l_{HH}=0{\cdot}29\pm0{\cdot}11$	$P^p_{HH}=0{\cdot}30\pm0{\cdot}12$
$P^h_{HM}\quad 0{\cdot}12\pm0{\cdot}04$	$P^l_{HM}=0{\cdot}46\pm0{\cdot}15$	$P^p_{HM}=0{\cdot}35\pm0{\cdot}15$
$P^h_{HL}=0{\cdot}15\pm0{\cdot}05$	$P^l_{HL}=0{\cdot}21\pm0{\cdot}09$	$P^p_{HL}=0{\cdot}11\pm0{\cdot}09$
$P^h_{H\alpha}\quad 1{\cdot}15\pm0{\cdot}17$	$P^l_{H\alpha}=1{\cdot}23\pm0{\cdot}40$	$P^p_{H\alpha}=1{\cdot}90\pm0{\cdot}38$

It is clear that the experimental point shown is not consistent with $J_{L^0}/J_{M^0}=0$, particularly when it is remembered that this extrapolation probably represents an overestimate of the correction for secondary production.

Fig. 5

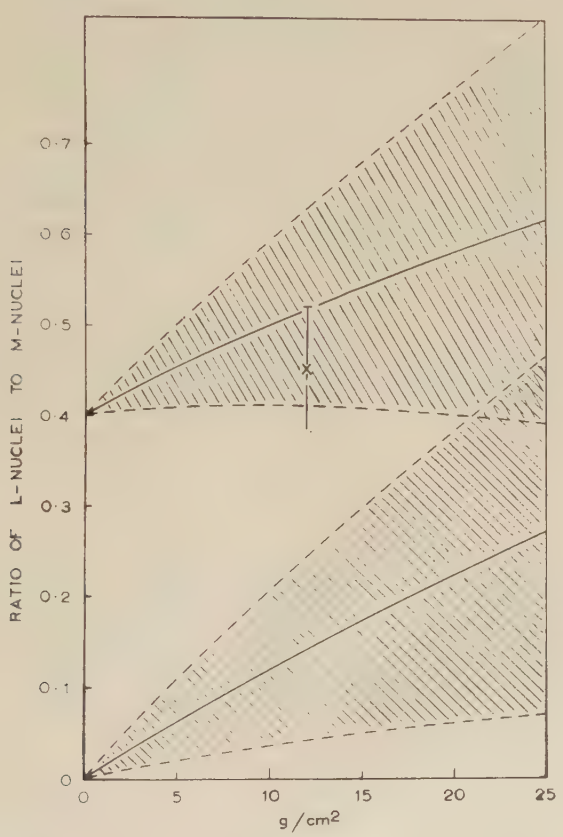

The ratio of L to M nuclei as a function of the depth of residual atmosphere in g/cm², with the limits due to the statistical errors of the derived values of the fragmentation probabilities.

When extrapolating the fluxes at the top of the atmosphere through interstellar hydrogen it is necessary to consider the effects of consecutive interactions and to use the diffusion equations published by Kaplon *et al.* (1954). Unfortunately the statistical weights of the P^p_{mn} values are so low that only tentative conclusions can be drawn regarding the propagation of these nuclei. However, it does appear that, assuming $J_{L^0}/J_{M^0}=0{\cdot}4$, the observed charge spectrum is consistent either with a pure H nuclei source after passing through about 20 g/cm² of hydrogen, or a source with no L nuclei after passing through about 8 g/cm² of hydrogen. If a density

of 10^{-24} g/cm^3 is assumed for the interstellar hydrogen, i.e. the cosmic rays are at least confined to the galactic disc, then these two cases correspond to lifetimes of 20 million and 8 million years respectively, which are considerably longer than the values currently accepted (Rossi 1955). If cosmic ray particles are confined within the galactic halo then these lifetimes will be as much as two orders of magnitude greater. It should be noticed that if J_L/J_M is in fact less than 0·40 because the values of P'_{mm} obtained in this paper are too low, then the quoted values of P^p_{mm} must be too high and a smaller J_L/J_M ratio will still imply an appreciable lifetime.

Detailed values of the fragmentation probabilities in hydrogen are of considerable importance in our understanding of the significance of the observed cosmic ray charge spectrum. It is to be hoped that the theoretically quite simple, though experimentally difficult, experiments to find these parameters will soon be undertaken.

§ 4. Conclusion

The most important conclusion that we reach from this work is that the several recent experiments, reported at the Varenna Conference, which give $J_L/J_M \geqslant 0{\cdot}4$ at 8–15 g/cm^2 of residual atmosphere are not compatible with absence of L nuclei at the top of the atmosphere.

Acknowledgments

The authors are grateful to Professor C. F. Powell, F.R.S., for the hospitality and facilities of his laboratory. We wish to thank the observers Miss B. Bolt, Mrs. A. Boult, Mrs. H. Burrows, Miss P. Curry and Miss C. Rothwell for careful and consistent scanning. One of us (C. J. W.) thanks the Royal Society for the award of a Mackinnon Research Studentship, while V. Y. R. thanks the Government of India for a scholarship under the Colombo Plan.

References

Bradt, H. L., and Peters, B., 1950, *Phys. Rev.*, **77**, 54.
Chen, F. F., Leavitt, C. P., and Shapiro, A. M., 1955, *Phys. Rev.*, **99**, 857.
Eisenberg, Y., 1954, *Phys. Rev.*, **96**, 1378.
Fowler, P. H., Hillier, R. R., and Waddington, C. J., 1957, *Phil. Mag.*, **2**, 293.
Fowler, P. H., and Waddington, C. J., 1956, *Phil. Mag.*, **1**, 637.
Kaplon, M. F., Noon, J. H., and Racette, C. W., 1954, *Phys. Rev.*, **96**, 1408.
Kellogg, D. A., 1953, *Phys. Rev.*, **90**, 224.
McDonald, F. B., 1956, *Phys. Rev.*, **104**, 1723.
Noon, J. H., and Kaplon, M. F., 1955, *Phys. Rev.*, **97**, 769.
Rossi, B., 1955, *Nuovo Cim. Suppl.*, **2**, 275.
Shapiro, A. M., Leavitt, C. P., and Chen, F. F., 1954, *Phys. Rev.*, **95**, 663.
Waddington, C. J., 1957 a, *Phil. Mag.*, **2**, 1059; 1957 b, *Nuovo Cim.*, **6**, 748.

Absorption of Negative K-Mesons and the Neutron and Proton Distributions in Heavy Nuclei†

By P. B. Jones
Cavendish Laboratory, Cambridge

[Received August 23, 1957]

Abstract

Negative K-mesons captured by the heavy nuclei in nuclear emulsion form K-mesic atoms. It is shown that absorption occurs in the nuclear surface and takes place when the K^--meson is in a 5g state. Observations on capture events producing a visible Σ^--hyperon, and on the ratio of π^+ to π^--mesons created can give information on the relative neutron and proton densities in the part of the nuclear surface where the total density is less than 10% of the density at the centre of the nucleus. Experimental evidence suggests that in this region of the nucleus the density of neutrons is approximately equal to the density of protons.

§ 1. Introduction

Johnson and Teller (1954) have suggested that as a result of the modification of the proton charge independent potential by the Coulomb potential, the density of neutrons is considerably greater than the density of protons at the surface of a heavy nucleus. The radial density distributions of neutrons and protons in heavy nuclei have been compared experimentally by Hess and Moyer (1956) who studied the deuterons produced in (p, d) and (n, d) reactions at large angles to the incident beam. Using 300 Mev nucleons they found evidence for a possible excess of neutrons in the surface regions of heavy nuclei. For lead this excess could take the form of a surface layer of neutrons $0{\cdot}8 \times 10^{-13}$ cm thick. On the other hand, Abashian *et al.* (1956), by measurements on the absorption cross sections of 700 Mev π^+ and π^--mesons in lead find no evidence for a neutron excess in the nuclear surface. These methods however, are not sensitive to the relative numbers of neutrons and protons in the extreme part of the nuclear surface where the total density is less than 10% of the density at the centre of the nucleus. The purpose of this note is to point out that this part of the nuclear surface can be investigated by observations on the absorption in heavy nuclei of slow negative K-mesons.

The K^--meson is captured in a Bohr orbit of very high principal quantum number and then makes electromagnetic transitions to states of lower energy. The theory of Wightman (Bethe and de Hoffmann 1955)

† Communicated by the Author.

shows that absorption by the nucleus takes place from a state with the highest possible angular momentum. In § 3 it is shown for a nucleus with $A=94$ and $Z=41$, that this is the 5g state. In the Schrodinger equation for the bound K^--meson the nucleus is represented by a complex potential $V=U+iW$. Unless U is attractive and $|U| \geqslant |W|$, the K^--meson wave function for a 5g state must have extremely small values inside the nucleus and the absorption must take place on the surface. In § 2 the range of values that U can have is investigated semi-quantitatively.

In almost all cases the K^--meson is absorbed by a single nucleon producing a hyperon and a π-meson (Dilworth 1957). If the interaction is charge independent, the amplitudes a_0 and a_1 for the production of a Σ-hyperon in states with isotopic spin $T=0$ or 1 are related by $a_1=a_0(0{\cdot}8e^{i70^\circ})$ for the absorption of slow K^--mesons by free protons (Alvarez 1957). The $T=1$ amplitude, b_1, for production of a Λ^0-hyperon satisfies $|b_1|^2=0{\cdot}07\ |a_0|^2$. The normalized transition probabilities for possible reactions, calculated using these relations, are given in table 1.

Table 1. The normalized transition probabilities for the different modes of absorption of a slow K^--meson by a single free proton or neutron, calculated from the experimental relations found by Alvarez (1957), are shown

Reaction	Normalized transition probability
$K^-+p \rightarrow \Sigma^+ + \pi^-$	0·14
$\Sigma^- + \pi^+$	0·28
$\Sigma^0 + \pi^0$	0·11
$\Lambda^0 + \pi^0$	0·02
$K^-+n \rightarrow \Sigma^0 + \pi^-$	0·20
$\Sigma^- + \pi^0$	0·20
$\Lambda^0 + \pi^-$	0·05

The transition probabilities for absorption in nuclear matter may be different because the relations between the amplitudes a_0, a_1 and b_1 depend on the relative momentum and angular momentum of the K^--meson and the nucleon. This dependence is unknown but is assumed to be weak. In support of this it should be mentioned that the relative transition probabilities observed for the absorption of fast K^--mesons by free protons (Rosenfeld 1957) agree with the results of table 1 within the present large experimental errors. Final state interactions, other than Coulomb, should not affect the transition probabilities if the absorption takes place on the surface of the nucleus where the nucleon density is low.

Using the results of table 1, the expected ratio of the number of π^- to the number of π^+-mesons produced for absorption in a heavy nucleus with $A=94$ and $Z=41$ and neutron and proton radial density distributions equal, is $R=0{\cdot}61$. In addition, the ratio of the number of Σ^--hyperons produced by the reaction

$$K^- + n \rightarrow \Sigma^- + \pi^0 \qquad \ldots\ldots\ldots \quad (1.1)$$

to the number produced by the reaction

$$K^- + p \rightarrow \Sigma^- + \pi^+ \qquad \ldots\ldots\ldots \quad (1.2)$$

should be $S=0{\cdot}94$. Experimental values exist for both ratios (Dilworth 1957). In § 3 they are shown to depend strongly on the relative numbers of neutrons and protons in the nuclear surface. In § 4 the values of R and S calculated as a function of the neutron excess in the nuclear surface are compared with the experimental values.

§ 2. The K⁻-Nucleus Potential

In this section an estimate is made of U, the real part of the K$^-$-nucleus potential. As an approximation to this we consider the energy level shift of a K$^-$-meson interacting with an infinite nucleus. Coulomb interactions are neglected. The absorption of a K$^-$-meson by two correlated nucleons is experimentally observed to have low probability. One reason for this is that in the centre of mass system of the two nucleons, each nucleon would need to have a momentum of 460 Mev/c to produce a real final state of a nucleon and a hyperon. The probability of such high momentum is small. However, elastic scattering through an intermediate state of a nucleon and a hyperon can still make an important contribution to U. It will be shown that this contribution is always positive in sign. The approximations to be used here are almost identical with those used by Deser *et al.* (1954) and by Brueckner (1955) to estimate the energy level shift of the s-state in π-mesic atoms.

The energy level shift of a single meson interacting with a system of nucleons has been calculated by Riesenfeld and Watson (1956) and Watson (1957). A first approximation to their result is

$$U=U_1+U_2$$

$$U_1=N_1 P\int \frac{d^3q}{(2\pi)^3}\frac{\langle\beta|R|q\rangle\langle q|R|\beta\rangle}{w_0+2E_0-E_y(q)-E(q)}$$

$$U_2=N_2\mathrm{Re}\langle\beta\,|\,t(0)\,|\,\beta\rangle. \qquad \hbar=c=1.$$

Here P denotes the principal value of the integral. R is an operator which destroys a K$^-$-meson and two nucleons and creates a nucleon and a hyperon. The $|q\rangle$ are a complete set of states of one nucleon and one hyperon, and $|\beta\rangle$ is the nuclear ground state. In the calculation of U_1, the momentum transform of the two-nucleon wave function $\psi(q)$ used is the Gaussian form proposed by Brueckner (1955). In the present

case this term gives a negative contribution to U_1 only for values of $\psi(q)$ for which q is greater than 460 Mev/c, and so the sign of U_1 is not affected by the momentum dependence of R and $\psi(q)$. We reasonably assume R to be a constant. w, E and E_y are the energies of the K^--meson, nucleon and hyperon respectively. N_1 is the effective density of correlated pairs of nucleons. The mean free path in nuclear matter for absorption of a K^--meson by two nucleons is $\lambda=(N_1\sigma)^{-1}$, where σ is the cross section. Two-nucleon processes involving the production of virtual K^+-K^- pairs should be unimportant and will not be included. In this case $U_1=4500v(\lambda)^{-1}$ Mev, for small values of v, the K^--meson velocity in the centre of mass system of the two nucleons. λ is in units of 10^{-13} cm. If absorption by a pair of nucleons occurs in 5% of all cases, $\lambda=10^{-12}$ cm and setting $v=0{\cdot}1$, $U_1=45$ Mev.

To estimate U_2, we relate the K^--nucleon scattering matrix at zero energy, $t(0)$, to the zero-energy s-state cross section for K^--p elastic scattering using for this an extrapolated value of 40 mb (Alles *et al.* 1957, Rosenfeld 1957). Assuming that the real parts of the K^-–p and K^-–n zero-energy s-state scattering lengths are both positive and equal in magnitude, we find $U_2=-70$ Mev for a K^--meson in nuclear matter of density $N_2=0{\cdot}17\times10^{39}$ nucleons per cm^3. This is the extreme negative value that can be contributed to U, unless the K^-–n cross section happens to be greater than 40 mb.

The actual value of U is not important for present purposes. However, these results combined suggest that U cannot be large and attractive, and therefore that absorption occurs in the nuclear surface only. In addition there is some experimental evidence that the real part of the optical model potential for K^--mesons is attractive and has about the value estimated here for U (Alles *et al.* 1957).

§ 3. Calculation of R and S

The ratio R of π^+ to π^--mesons produced in the surface of the nucleus, and S, the ratio of Σ^+-hyperons produced by reaction (1.1) to Σ^--hyperons produced by reaction (1.2) are calculated in this section as functions of the neutron excess in the nuclear surface. All calculations are for a heavy nucleus with $A=94$ and $Z=41$, which represents the elements Ag, Br and I in nuclear emulsion. The light nuclei are represented by a nucleus with $A=13{\cdot}8$ and $Z=6{\cdot}9$.

In first order perturbation theory the mean life τ, for nuclear absorption of the K^--meson from a state with unperturbed wave function ϕ is given by $(\tau)^{-1}=\langle\phi\,|\,W\,|\,\phi\rangle$. W is the imaginary part of the complex K^--nucleus potential and is taken to be $+100$ Mev. This is obtained from the mean life in nuclear matter which is $0{\cdot}6\times10^{-23}$ seconds estimated using the measured absorption cross section, in hydrogen, for K^--mesons of momentum 10–170 Mev/c (Rosenfeld 1957). It has been assumed here that the free particle absorption cross section is unaltered in nuclear

matter of normal density†. In table 2 the approximate mean lives of several states are given both for transitions ($\Delta l=\pm 1$) to a state of lower energy with the emission of a γ-ray (Dirac 1947) and for nuclear absorption. It is seen that absorption takes place from the 5g state. It is worth mentioning that some absorption from the 4f or 6h states would in no way alter the results to be obtained here.

Table 2. The approximate mean lives of bound states of captured K$^-$-mesons are given both for $\Delta l=\pm 1$ γ-ray transitions to states of lower energy and for nuclear absorption. The mean lives for nuclear absorption are calculated using a K$^-$-meson mean life in nuclear matter of $0{\cdot}6\times 10^{-23}$ seconds. The charge distribution found by Hofstadter (1956) is assumed equivalent to the nucleon density distribution

State	Mean life for electromagnetic transitions	Mean life for nuclear absorption
6h	$1{\cdot}0\times 10^{-16}$ sec	10^{-15} sec
5g	$3{\cdot}9\times 10^{-17}$ sec	$0{\cdot}4\times 10^{-17}$ sec
4f	$1{\cdot}3\times 10^{-17}$ sec	$0{\cdot}25\times 10^{-19}$ sec

$u(r)=r\Psi(r)$ has been found numerically for $U+iW=0+100i$. $\Psi(r)$ is the K$^-$-meson radial wave function for the 5g state. The nuclear potential has been taken as

$$V=(U+iW)[\exp\{(r-a)/z_1\}+1]^{-1}$$

where $a=5{\cdot}5\times 10^{-13}$ cm. $z_1=0{\cdot}55\times 10^{-13}$ cm, the value found by Hofstadter (1956) from measurements on the nuclear charge distribution. The form of $u(r)$ is not sensitive to the exact values of the parameters a, U and W. The behaviour of $u(r)$ depends mainly on the high angular momentum.

The probability of the absorption taking place at a distance r from the centre of the nucleus is

$$P(r)=\text{const.}\mid u(r)\mid^2\{\rho_{\mathrm{n}}F_{\mathrm{n}}(r)+(\omega_{\mathrm{p}}/\omega_{\mathrm{n}})\rho_{\mathrm{p}}F_{\mathrm{p}}(r)\}.$$

ρ_{n} and ρ_{p} are the neutron and proton densities at $r=0$. ω_{n} and ω_{p} are the transition probabilities for absorption of the K$^-$-meson by neutrons or protons (see table 1). The proton form factor (Hofstadter 1956) is

$$\begin{aligned} F_{\mathrm{p}}(r)&=1 && \text{for} && 0<r<(c-z_3)\\ &\quad (c+z_3-r)/2z_3 && && (c-z_3)<r<(c+z_3)\\ &\quad 0 && && (c+z_3)<r \end{aligned}$$

† For the optical model of the nucleus this approximation is good (Lane 1957). Watson (1957) points out that the potential V is essentially the optical model potential.

Two neutron form factors have been used. The first has the same form as $F_p(r)$ except that the parameter c is replaced by $c+\Delta c$. Δc is then a measure of the neutron excess. For the second neutron form factor, $F_n(r)=F_p(r)$ for $r<(c+z_3)$. However for $(c+z_3+\Delta h)>r>(c+z_3)$, $F_n(r)=0{\cdot}05F_p(0)$. This represents an outer shell, Δh in depth. of neutrons with extremely low density which would not be detectable by other methods.

For the light nuclei the suggestion of Johnson and Teller. if correct, would lead to $\Delta c \simeq 10^{-14}$ cm only. for a neutron potential of 35 Mev and the charge distribution found by Hofstadter. It is therefore assumed that for the light nuclei $F_n=F_p$. The ratio of the number of K$^-$-mesons captured by light and heavy nuclei is taken to be 3/7.

In the case of the ratio R, it is necessary to consider the interaction of the pions with the nucleus. The hypothesis of charge symmetry implies that π^+ and π^--mesons are scattered and absorbed equally in self-conjugate nuclei. For the heavy nuclei this is not true. To estimate the correction we use the pion absorption model of Brueckner *et al.* (1951). and the phenomenological theory of pion production by two nucleons of Rosenfeld (1954). The correction arises from absorption of the pion by two protons or two neutrons which are assumed to be in a singlet s-state. The difference of the mean absorption cross sections per nucleon for π^+ and π^--mesons is $\sigma(+)-\sigma(-)=0{\cdot}15\Gamma\eta^2(1+\eta^2)^{1/2}$ mb. η is the momentum of the pion in the centre of mass system of the two nucleons in units of μc (μ is the pion mass). For the correction we have used $\Gamma=4$†, which results in a change of less than 4% in R. Geometrical corrections to R and S, present only if there is a neutron excess at the nuclear surface, are at the most a few per cent.

The transition probabilities of table 1 can now be used to calculate R and S. In figs. 1 to 4, R and S are shown as functions of Δc and Δh. In all figures the curves (*a*) show the values of R and S for capture by the heavy nuclei alone. The curves (*b*) show the values of R and S resulting when K$^-$-mesons are captured by both light and heavy nuclei in the ratio 3/7.

§ 4. Discussion

The calculated values of R and S are seen to depend strongly on the relative numbers of neutrons and protons in the nuclear surface. The dependence is of course greater for the case of absorption of K$^-$-mesons by the heavy nuclei alone.

The value of S (Dilworth 1957) found from observations on K$^-$-meson capture events in nuclear emulsion which produce a visible Σ^--hyperon, is 0·6. With neutron and proton density distributions equal. the predicted

† Γ is defined (Francis and Watson 1953) as the ratio P/P_d, where P is the probability. in nuclear matter, of a neutron and a proton being separated by a distance d, and P_d is the corresponding probability for the ground state of the deuteron. $d=\hbar/p$, where p is the relative momentum that the two nucleons need to be able to absorb a pion.

value is $S=0{\cdot}87$. Figure 3 indicates that Δc, for the absorption model used here, is probably less than $0{\cdot}2\times10^{-13}$ cm. For the second neutron form factor the corresponding limit is $\Delta h<0{\cdot}5\times10^{-13}$ cm.

Fig. 1

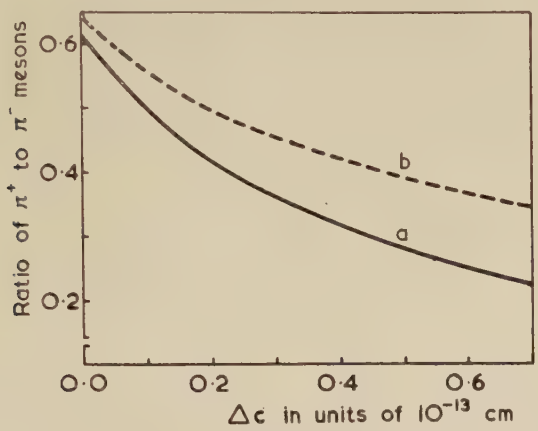

The ratio R, of π^+ to π^--mesons produced in the nuclear surface is shown as a function of Δc, the neutron excess for the first neutron form factor. The curve (*a*) is for capture by the heavy nuclei alone, and curve (*b*) is for capture of the K^--meson by both light and heavy nuclei in the ratio 3/7.

Fig. 2

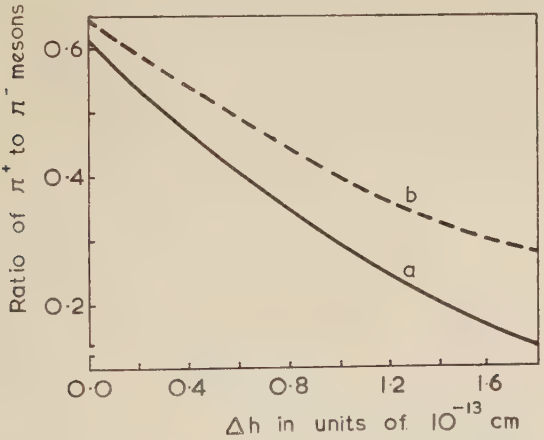

R is shown as a function of Δh, the neutron excess for the second neutron form factor.

$R=0{\cdot}64$ is predicted when $\Delta c=\Delta h=0$. The true experimental value of R is unknown. The existing value of $R=0{\cdot}20$ has been obtained from the low energy end of the pion spectrum only, and so is very heavily biassed in favour of the π^--meson (Dilworth 1957).

Fig. 3

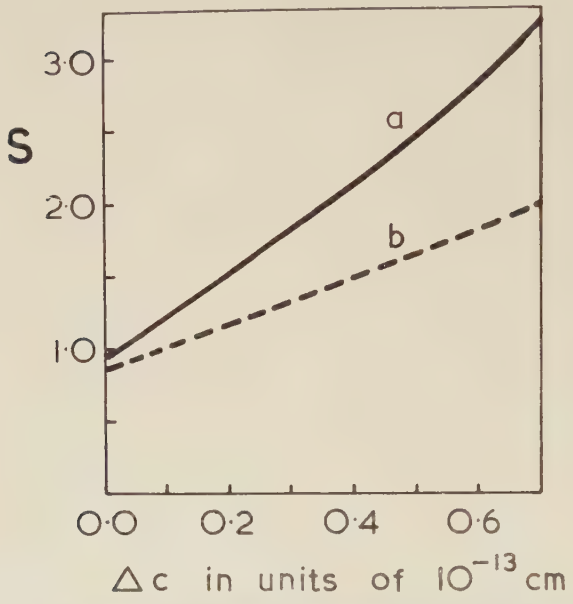

The ratio S, of Σ^--hyperons produced by reaction (1.1) to Σ^--hyperons produced by reaction (1.2) is shown as a function of Δc.

Fig. 4

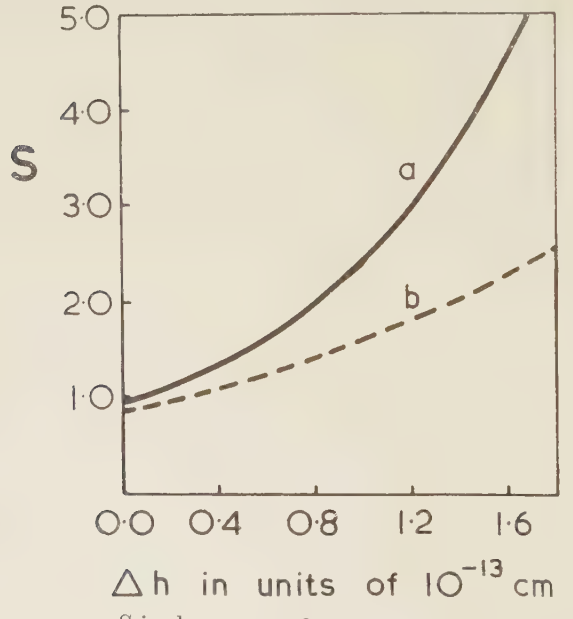

S is shown as a function of Δh.

An optical model may be used for the pion–nucleus interaction. The value of the ratio Γ is very poorly known and so we do not take into account refraction and pion–nucleon scattering. The importance of scattering for pions of these energies is in any case much reduced by the exclusion principle. Using $\Gamma=4$, we find for the K^--meson absorption model considered here, that the probability of escape of a charged pion is 0·66. Considering the large uncertainties in Γ this compares well with the value of 0·53 found by Dilworth (1957).

Finally, the results of table 1 deserve some comment. Alvarez (1957) has pointed out that the relation between a_0 and a_1 is based on the assumption that the absorption of a slow K^--meson by a free proton all takes place from one atomic state. Observations on absorption in deuterium should decide whether or not this assumption is good. In this case, absorption of the K^--meson by both nucleons should not, for the reasons mentioned in § 2, be important.

Acknowledgments

The writer wishes to thank Dr. R. J. Eden, Dr. R. M. Eisberg and Professor D. H. Wilkinson for criticism of this work, and Professors C. Dilworth, L. Alvarez and A. H. Rosenfeld for permission to use unpublished results, and also the Department of Scientific and Industrial Research for a grant.

References

Abashian, A., Cool, R., and Cronin, J. W., 1956, *Phys. Rev.*, **104**, 855.
Alles, W., Biswas, N. N., Ceccarelli, M., and Crussard, J., 1957, *Preprint*.
Alvarez, L., 1957, *7th Rochester Conference*.
Bethe, H. A., and de Hoffmann, F., 1955, *Mesons and Fields* (Evanston, Illinois: Row, Peterson and Company), p. 103.
Brueckner, K. A., 1955, *Phys. Rev.*, **98**, 769.
Brueckner, K. A., Serber, R., and Watson, K. M., 1951, *Phys. Rev.*, **84**, 258.
Deser, S., Goldberger, M. L., Baumann, K., and Thirring, W., 1954, *Phys. Rev.*, **96**, 774.
Dilworth, C., 1957, *7th Rochester Conference*.
Dirac, P. A. M., 1947, *Quantum Mechanics*, 3rd edition (Oxford: University Press), p. 245.
Francis, N. C., and Watson, K. M., 1953, *Amer. J. Phys.*, **21**, 659.
Hess, W. N., and Moyer, B. J., 1956, *Phys. Rev.*, **101**, 337.
Hofstadter, R., 1956, *Rev. mod. Phys.*, **28**, 214.
Johnson, M. H., and Teller, E., 1954, *Phys. Rev.*, **93**, 357.
Lane, A. M., 1957, *Rev. mod. Phys.*, **29**, 191.
Riesenfeld, W. B., and Watson, K. M., 1956, *Phys. Rev.*, **104**, 492.
Rosenfeld, A. H., 1954, *Phys. Rev.*, **96**, 139; 1957, *7th Rochester Conference*.
Watson, K. M., 1957, *Phys. Rev.*, **105**, 1388.

The Heat Capacity of Diamond between 12·8° and 277°K†

By J. E. Desnoyers‡ and J. A. Morrison
Division of Pure Chemistry, National Research Laboratories, Ottawa, Canada

[Received September 23, 1957]

Abstract

The heat capacity of 160 g of diamonds has been measured in the temperature range 12·8° to 277°K with estimated accuracies of ±20% at 13°K, ±6% at 20°K, ±0·8% at 100°K and ±0·2% for $T>200$°K. Fitting of the results in the region $T<\Theta_D/20$ to the low temperature expansion for the heat capacity gives $\Theta_0=2219\pm20$°K; this agrees excellently with Θ (elastic) $=2240\pm5$°K, derived from elastic constants determined by McSkimin and Bond. Down to 75°K the results are in reasonable agreement with earlier measurements of DeSorbo, but at lower temperatures an anomaly reported by DeSorbo has not been confirmed.

§1. Introduction

Although thermal, elastic and optical properties of diamond have been studied extensively for a number of years, rather large discrepancies in existing data are apparent. For example, the heat capacity of diamond has been measured below 300°K by Pitzer (1938) and by DeSorbo (1953), but the two sets of results differ systematically by up to 15%. Large differences also appear in elastic constant data. A lattice frequency spectrum has been derived by Smith (1948), but its reliability can hardly be judged with the present experimental information. It was therefore thought desirable to make the new heat capacity measurements which are described in this paper. Since the first draft of the paper was completed, Burk and Friedberg (1957) have made a preliminary report on similar measurements in the region $T<200$°K.

At temperatures less than about $\Theta_D/20$ the heat capacity of a solid is given by

$$C_v=aT^3+bT^5+cT^7+\ldots \quad . \quad . \quad . \quad . \quad . \quad . \quad (1)$$

The coefficients a, b and c may be determined most conveniently from a plot of C_v/T^3 against T^2. The coefficient a may also be deduced from the elastic constants of the crystal, and this provides a useful correlation between thermal and elastic properties. Theory and a number of experiments suggest that the coefficients b and c are usually positive for simple crystals (Blackman 1937, Barron and Morrison 1957), but DeSorbo's (1953) low temperature results show Θ_D increasing with

† Communicated by the Authors.
‡ Summer student, University of Ottawa.

temperature just above $T=0$°K, thus indicating a negative value of b for diamond. This result, if correct, would be of considerable interest, especially as existing heat capacity data for other diamond structures (silicon, germanium and grey tin) suggest that b is small and positive for these elements.

The present results show no maximum in Θ_D at low temperatures and indicate that both b and c are positive. The derived value of Θ_0 agrees well with the value of Θ(elastic) computed from elastic constants recently reported by McSkimin and Bond (1957).

§2. Experimental

The calorimetric sample was approximately 160 g of clear industrial diamonds; their average dimension was about 3 mm. Most of the diamonds were lightly coloured either yellow, brown or green, but none contained occlusions. Whether they were of type I or type II is not known; this was not thought to be important because Robertson *et al.* (1936) had not detected a significant difference between the heat capacities of the two types.

The measurements were made with a calorimeter assembly which had been used previously for experiments with alkali halide crystals. Details concerning the temperature scales, the handling of samples, etc., are given elsewhere (Berg and Morrison 1957). For the diamond experiments the calorimeter vessel contained $3{\cdot}5\times10^{-6}$ moles of helium to promote heat exchange. This amount of helium was such that its desorption during a single measurement would not significantly affect the heat capacity even at the lowest temperatures.

§3. Results

The original experimental results are recorded in the Appendix. The units of C_p are cal/g atm deg, where 1 calorie has been taken as 4·184 abs joules. The apparent Debye characteristic temperatures have been calculated directly from C_p, since the difference C_p–C_v is entirely negligible throughout the temperature region considered. A graph of apparent Θ_D against temperature is shown in fig. 1: the results obtained by Pitzer (1938) and DeSorbo (1953) are included for comparison.

An estimate of the accuracy of the measurements can be made from previous extensive measurements on alkali halide crystals with the same calorimeter assembly (Berg and Morrison 1957). There is every reason to expect that the accuracy of measuring the total heat capacity of the assembly has remained the same, so that it is only necessary to take account of the much smaller contribution of the diamonds to the total heat capacity at temperatures below 200°K. In this way we obtain estimated accuracies for the measured heat capacities of $\pm20\%$ at 13°, $\pm6\%$ at 20°, $\pm0{\cdot}8\%$ at 100° and $\pm0{\cdot}2\%$ for $T>200$°K. The results are consistent with a smooth Θ_D–T relation well within these estimated limits except for two points at the very lowest temperatures which are just outside them (fig. 1).

Fig. 1

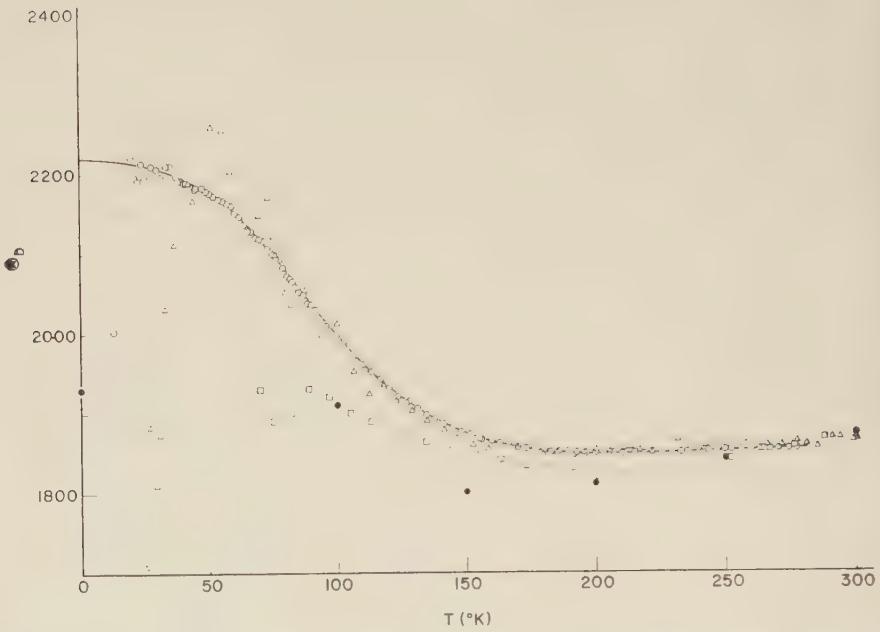

The apparent Debye characteristic temperature of diamond as a function of the absolute temperature.

○—present results.
□—Pitzer (1938).
△—DeSorbo (1953).
●—Smith (1948).

§4. Discussion of Results

4.1. *Comparison with Earlier Measurements*

The present results agree rather well with DeSorbo's down to 75°K. Their greater internal consistency is in part due to the larger specimen used—twice that used by DeSorbo (1953). Both sets of results show a consistently lower heat capacity than found by Pitzer (1938). The anomaly which appears in DeSorbo's results at lower temperatures has not been confirmed: below 75°K, Θ_D increases regularly and finally appears to level-off.

DeSorbo's anomaly may be due to his use of less perfect diamonds, but it could be explained more easily by a small systematic error in the heat capacity of the calorimeter vessel. The results would be very sensitive to such an error: for example, in the present experiments an uncertainty of 0·1% in the heat capacity of the calorimeter vessel corresponded to an uncertainty of 3·3% in the heat capacity of the diamond at 50°K. This is a more likely source of error than an undetermined effect of desorption of exchange gas, especially since DeSorbo obtained similar results with and without exchange gas.

4.2. *Thermodynamic Functions*

The thermodynamic functions of diamond at higher temperatures are not greatly affected by the differences in heat capacity between the present results and DeSorbo's. Values of S° and $H^\circ - H_0^\circ$ at 100°K for both sets of results are given in table 1. Higher temperature values may be obtained from DeSorbo's table II after correction for the differences shown here in table 1.

Table 1. Values of the Functions S° and $H^\circ - H_0^\circ$ for Diamond at 100°K

	S° (cal/g atm deg)	$H^\circ - H_0^\circ$ (cal/g atm)
De Sorbo (1953)	0·0192	1·3095
Present experiments	0·0172	1·3211

Fig. 2

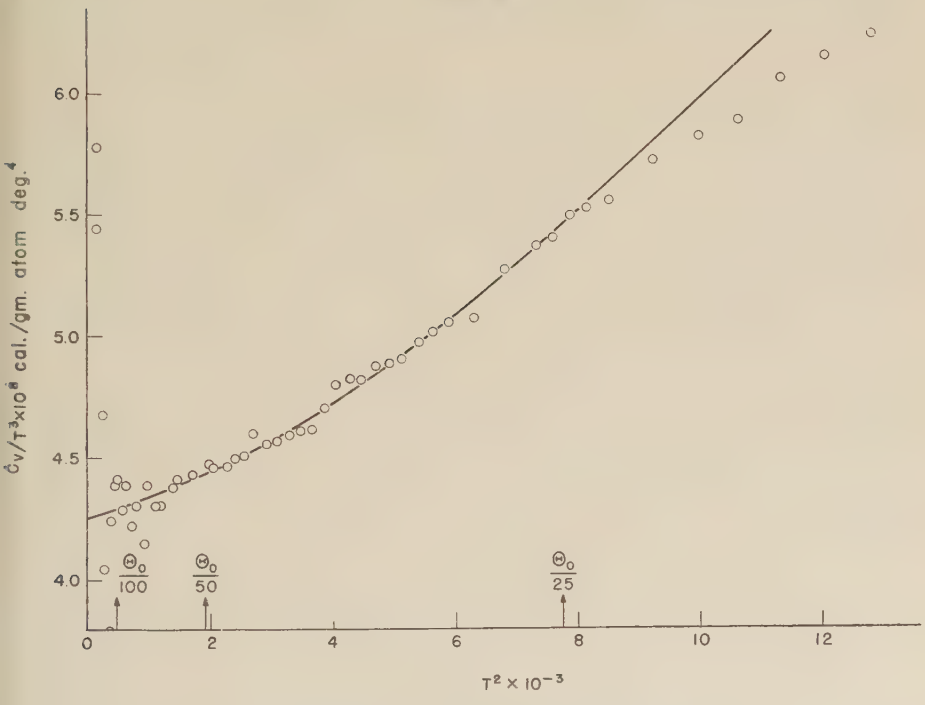

A graph of C_v/T^3 *vs* T^2 for diamond.

4.3. *The Low Temperature Expansion for* C_v

Θ_0, the Debye characteristic temperature at 0°K, can be deduced most accurately from a plot of C_v/T^3 against T^2 (Barron and Morrison 1957). Such a plot for the diamond results is shown in fig. 2. The solid curve represents the best fit to the low temperature expansion for the heat

capacity (eqn. (1)). The derived values of a, b and c are given in the middle line of table 2. The other two lines of the table contain maximum and minimum estimates of the coefficients. The values of b and c depend critically on the value chosen for Θ_0 so that their magnitudes cannot be obtained very accurately.

Table 2. Coefficients of the Low Temperature Expansion for the heat Capacity

$a\times10^8$ (cal/g atm deg^4)	$b\times10^{13}$ (cal/g atm deg^6)	$c\times10^{17}$ (cal/gm atm deg^8)	Θ_0 (°K)
4·35	5·5	11	2202
4·25	8·8	8	2219
4·15	13·0	4	2237

The form of fig. 2 proves to be much like that found for alkali halide crystals (Barron and Morrison 1957). Detectable changes in Θ_D occur down to temperatures well below $\Theta_D/50$. The dependence of C_v upon T up to $T=\Theta_D/50$ is given rather closely by the first two terms of eqn. (1).

4.4. *Comparison with Elastic Data*

The value of Θ_0 thus derived from the low temperature heat capacities (2219 ± 20°K) provides a partial criterion for judging the accuracy of existing elastic constant data: these should yield a characteristic temperature, Θ(elastic), in agreement with Θ_0. The most recent determinations of the elastic constants of diamond have been made by McSkimin and Bond (1957), and their results differ markedly from those of Bhagavantam and Bhimasenacher (1946) and of Prince and Wooster (1953), particularly for c_{12} and c_{44}. Θ(elastic) is sufficiently sensitive to the value of c_{44} to make it clear that the earlier results are not compatible with the present heat capacity measurements. The moduli given by McSkimin and Bond (1957) yield Θ(elastic)$=2240\pm5$°K when de Launay's (1956) tables are used for the calculation. This value agrees with Θ_0 within the assigned uncertainties. It may be noted here that Burk and Friedberg (1957) give $\Theta_0=2246$°K, which was obtained by linear extrapolation of results for the region $45°<T<100$°K plotted in the form of Θ_D against T^2. This would appear to correspond to a 'pseudo' aT^3+bT^5 region (Barron and Morrison 1957) and hence would be expected to yield slightly too large a value of Θ_0.

The good agreement between Θ_0 and Θ(elastic) suggests that McSkimin and Bond's elastic constants are the most reliable, but it should be stressed that Θ_0 is a direct check on the value of c_{44} only; the values of c_{11} and c_{22} need independent confirmation. In particular, new measurements of the compressibility of diamond would be valuable: the earlier measurements of Adams (1921) and of Williamson (1922) are inconsistent with the moduli given by McSkimin and Bond.

4.5. *Comparison with Models*

Smith (1948) has computed an approximate frequency spectrum for diamond and has derived values of Θ_D at selected temperatures. Her results for the region $T < 300$ °K are plotted in fig. 1; it is evident that they depart seriously from Θ_D as calculated from the measured heat capacities. The force constants for the model were based in part upon the elastic constants of Bhagavantam and Bhimasenacher (1946), which now appear to be less reliable: this will account for some of the discrepancy.

In addition, however, reservations may be held about the assumption of central forces for second neighbour interactions. It may prove useful to try in preference a five parameter theory assuming quite general forces between both first and second neighbours. This would neglect only interactions between pairs of atoms which have no common nearest neighbour. The force constants might be fixed by the elastic constants of McSkimin and Bond (1957), the first order Raman frequency shift (Robertson *et al.* 1934) and Θ_∞, the high temperature limiting value of Θ_D. Unfortunately, existing heat capacity results at high temperatures (Magnus and Hodler 1926) do not seem to be sufficiently accurate to give a good estimate of Θ_∞.

§5. Summary

The experimental results given here resolve some of the existing uncertainties about the thermal properties of diamond. In particular, they show that the form of the low frequency spectrum is not unlike that of other cubic crystals such as the alkali halides. The close agreement between Θ_0 and Θ(elastic) confirms the value of one of the elastic moduli (c_{44}) measured by McSkimin and Bond (1957).

Acknowledgments

We are grateful to Mr. Robert S. Parsons of J. K. Smit and Sons of Canada Limited for arranging the loan of the specimen of diamonds. We should also like to thank Dr. T. H. K. Barron for helpful discussion and for his criticism of this paper.

References

Adams, L. H., 1921, *J. Wash. Acad. Sci.*, **11**, 45.
Barron, T. H. K., and Morrison, J. A., 1957, *Canad. J. Phys.*, **35**, 799.
Berg, W. T., and Morrison, J. A., 1957, *Proc. roy. Soc.* (in the press).
Bhagavantam, S., and Bhimasenacher, J., 1946, *Proc. roy. Soc.* A, **187**, 381.
Blackman, M., 1937, *Proc. Camb. phil. Soc.*, **33**, 94.
Burk, D. L., and Friedberg, S. A., 1957, Abstracts for the Fifth International Conference on Low Temperature Physics and Chemistry, Madison, Wisconsin.
DeSorbo, W., 1953, *J. chem. Phys.*, **21**, 876.
deLaunay, J., 1956, *J. chem. Phys.*, **24**, 1071.
Magnus, A., and Hodler, A., 1926, *Ann. Phys., Lpz.*, **80**, 808.

McSkimin, H. J., and Bond, W. L., 1957, *Phys. Rev.*, **105**, 116.
Pitzer, K. S., 1938, *J. chem. Phys.*, **6**, 68.
Prince, E., and Wooster, W. A., 1953, *Acta cryst.*, **6**, 450.
Robertson, R., Fox, J. J., and Martin, A. E., 1934, *Phil. Trans.* A, **232**, 463 ; 1936, *Proc. roy. Soc.* A, **157**, 579.
Smith, H. M. J., 1948, *Phil. Trans.* A, **241**, 105.
Williamson, E. D., 1922, *J. Franklin Inst.*, **193**, 491.

APPENDIX

Measured Heat Capacities of Diamond

(units—cal/g atm deg)

T(°K)	C_p	T(°K)	C_p	T(°K)	C_p	T(°K)	C_p
12·833	0·000115	60·540	0·01035	120·283	0·1124	218·511	0·7146
12·968	0·000126	62·189	0·01131	123·697	0·1242	222·107	0·7449
16·015	0·000192	63·648	0·01237	126·975	0·1360	225·595	0·7761
16·745	0·000190	65·392	0·01349	127·870	0·1385	229·264	0·8068
18·631	0·000241	66·750	0·01433	131·154	0·1515	232·816	0·8404
19·757	0·000327	68·591	0·01573	134·485	0·1654	236·364	0·8711
21·304	0·000424	70·070	0·01681	137·805	0·1794	239·816	0·9033
22·464	0·000501	71·787	0·01814	141·116	0·1944	243·176	0·9341
24·100	0·000600	73·386	0·01965	144·495	0·2097	246·452	0·9644
25·276	0·000708	74·995	0·02116	147·945	0·2271	249·159	0·9887
26·994	0·000831	76·409	0·02220	151·444	0·2448	252·541	1·0220
28·299	0·000975	76·685	0·02279	154·989	0·2641	256·039	1·0553
29·992	0·00117	79·169	0·02546	156·186	0·2703	259·648	1·0926
31·332	0·00135	79·452	0·02555	159·510	0·2886	263·168	1·1232
33·407	0·00161	80·868	0·02762	162·867	0·3083	266·789	1·1614
34·606	0·00178	81·972	0·02895	166·298	0·3273	270·507	1·1967
37·316	0·00228	82·410	0·02954	169·777	0·3503	274·134	1·2332
38·046	0·00243	84·808	0·03258	173·316	0·3728	277·675	1·2686
41·319	0·00313	85·550	0·03364	176·730	0·3947		
41·325	0·00313	87·112	0·03574	180·042	0·4175		
44·491	0·00394	88·700	0·03838	182·415	0·4348		
45·228	0·00413	90·190	0·04058	185·742	0·4570		
47·570	0·00481	92·201	0·04360	189·157	0·4812		
48·985	0·00529	96·025	0·05077	192·641	0·5072		
50·450	0·00579	99·904	0·05812	196·182	0·5339		
52·045	0·00648	103·085	0·06462	199·611	0·5592		
53·980	0·00717	106·381	0·07311	203·157	0·5881		
55·597	0·00785	109·756	0·08149	206·809	0·6167		
57·333	0·00865	113·212	0·09073	210·341	0·6465		
58·957	0·00944	116·719	0·1009	215·014	0·6841		

The Use of a Model in Anharmonic Lattice Dynamics†

By D. J. Hooton
Department of Applied Mathematics, University of Liverpool

[Received October 10, 1957 ; in revised form November 20, 1957]

Abstract

Skyrme has recently discussed the use of a model in quantum mechanics. His method is applied to the case of the anharmonic vibrations of a crystal lattice, and compared with a previous treatment by the present author. Some remarks are added which give a new and more physical interpretation of the results of this earlier work.

§ 1. Introduction

The dynamics of a perfect crystal lattice has nowadays little interest except when the forces are strongly non-linear, or the lattice supposed to be in interaction with some internal perturbing system. The former case was treated some years ago by the present author (Hooton 1955 a) on the basis of a 'model' suggested originally by Born (1951). Recently, Skyrme (1957) has discussed the use of model systems in quantum mechanics in a wider context, and the philosophy of his approach is exactly that used in the papers quoted above. Indeed, Skyrme first illustrates his method by the academic example of a one-dimensional anharmonic oscillator. The physically interesting case of the *coupled* anharmonic oscillations of a lattice was developed by Hooton (1955 a) from precisely the same model and it is instructive to compare the two methods. Some generalization of Skyrme's formalism is of course required, since the lattice must be regarded as a system in thermal equilibrium. A simple way of doing this is indicated below, although it is not suggested that this approach should be followed in practice. For the anharmonic lattice, which is a system of great complexity, the methods used by Born (1951) and Hooton (1955 a) offer much greater hope of a simple solution. Indeed, we shall give here an alternative and more direct physical argument which yields the previous results immediately. In the present context Skyrme's terminology *can* be used to advantage to give a very clear statement of the method of approximation which the two approaches have, in fact, in common.

§ 2. The Dynamical Model

The method used by Hooton (1955 a) can be formulated briefly as follows. We introduce collective coordinates and momenta q, p (suffixes are omitted for simplicity) to describe the coupled vibrations of the lattice

† Communicated by the Author.

particles; they are obtained by a linear canonical transformation of matrix (e) from the displacements $X-X^0$ and momenta P of the individual atoms. The centres of vibration X^0 are parameters which must be determined by a method which takes full account of the non-linearity of the system—the only reasonable choice is to define them as the mean positions $\langle X \rangle$, the lattice being treated as a system in thermal equilibrium at temperature T. The transformation matrix (e) will also be determined if we can find an approximate form for the coupled motion in the lattice. Were the forces linear, this coupled motion would of course be a superposition of independent harmonic modes. Born (1951) has suggested that as a model of the non-linear motion we might again consider a set of 'normal modes' but now with frequencies ω (which appear as additional parameters) determined in a non-linear fashion. The chief problem is in fact to choose some characteristic of such a set of harmonic oscillations to impose on the actual motion, for which it must hold approximately if the model is to be at all realistic, thereby gaining equations which will determine the parameters introduced above.

We write† the actual Hamiltonian:

$$H=\tfrac{1}{2}\sum p^2+V(q), \qquad \ldots\ldots\ldots \quad (1)$$

where the potential $U(X) \equiv V(q)$ has arbitrary (polynomial) form. The model is written:

$$h=\tfrac{1}{2}\sum p^2+\tfrac{1}{2}\sum \omega^2 q^2. \qquad \ldots\ldots\ldots \quad (2)$$

The philosophy that this method has in common with Skyrme is to suppose that the level scheme of h is the same as that of H save for an approximately constant displacement ϵ, at least so far as the low levels are concerned. In fact in a lattice at normal temperature there will be comparatively little excitation above the ground state. For solid helium—to which the results of this method have already been applied (Hooton 1955 a)—we can deal practically with the zero-level alone; ϵ is then approximately ΔE_0, the difference in energy as $T \to 0$. It is also implied that the eigenfunctions $\psi_n(q)$ and $\phi_n(q)$ of (1) and (2) are similar—again an approximation which obviously fails for highly excited states. Skyrme's formal development depends on the approximate identification of these eigenfunctions, as we shall see below. It should be remembered that all these remarks can be expected to hold only when the parameters have been fixed so as to fit the model to the actual system, if this is indeed possible.

The preceding philosophy can be expressed by saying that the operator

$$H-h-\epsilon=\tilde{V}(q)-\epsilon, \quad \tilde{V}(q)=V(q)-\tfrac{1}{2}\sum \omega^2 q^2, \qquad \ldots \quad (3)$$

† The notation used differs from that of Born (1951) and Hooton (1955 a) in an obvious fashion, and is chosen to agree with Skyrme to facilitate comparison with his paper.

is very small, having approximately degenerate eigenstates of eigenvalue zero. This means that in forming any thermal average with the density matrix

$$\rho(H)=\exp(-H/kT)=\exp(-\epsilon/kT)\rho(h)\exp\{-(\tilde{V}-\epsilon)/kT\}. \quad . \quad (4)$$

we may approximately disregard the last factor—an approximation which effectively replaces the correct eigenfunctions ψ_n with the model functions ϕ_n in those states where this is most likely to be true.

Moreover, the free energy (from which all thermal lattice properties follow) can be written approximately

$$F=-kT\ln tr\rho(H)\simeq -kT\ln tr\rho(h)+\epsilon. \quad . \quad . \quad . \quad . \quad (5)$$

The eqn. (5) requires merely that the *average value* of the operator $\exp\{-(\tilde{V}-\epsilon)/kT\}$ should be unity; to first order in the operator $\tilde{V}-\epsilon$ this at the same time determines ϵ:

$$\epsilon=\langle\tilde{V}\rangle_h. \quad . \quad . \quad . \quad . \quad . \quad . \quad . \quad . \quad (6)$$

(Here $\langle f(q)\rangle_h=tr\{\rho(h)f(q)\}/tr\rho(h)$, the thermal average constructed according to the *model* Hamiltonian.)

Thus: $$F\simeq -kT\ln tr\rho(h)+\langle\tilde{V}\rangle_h, \quad . \quad . \quad . \quad . \quad . \quad (7)$$

which was in fact the form derived by Hooton (1955 a) by the use of perturbation theory. Once the various parameters have been specified to fit the model to the actual system, (7) can be completely worked out.

§ 3. Formal Use of the Model

In Skyrme's formulation, the model operator h is described in its own space of variables ξ, and a formal eigenvalue equation is derived for the operator $H-h-\epsilon$ in the combined q, ξ space. The (approximately degenerate) eigenfunctions, written $F(q,\xi)$, are defined by the relation

$$F(q,\xi)=\sum a_n\psi_n(q)\phi_n^*(\xi), \quad . \quad . \quad . \quad . \quad . \quad (8)$$

with arbitrary coefficients a_n. These eigenfunctions are to be determined so as to express the degree of correspondence between the states ψ_n and ϕ_n. The discussion of § 2 identifies q and ξ, which here implies writing

$$F(q,\xi)\simeq\Pi\delta(q-\xi); \quad . \quad . \quad . \quad . \quad . \quad (9)$$

in view of (8), this means putting $\psi_n\simeq\phi_n$ (with $a_n=1$) for all states. Before criticizing this procedure, it is worth noting that if (9) is inserted in Skyrme's variational principle:

$$\delta\int\int F^*(q,\xi)(H-h-\epsilon)^2F(q,\xi)\,dq\,d\xi=0 \quad . \quad . \quad . \quad (10)$$

one gets formally for ϵ the equation

$$tr(\tilde{V}(q)-\epsilon)=0. \quad . \quad . \quad . \quad . \quad . \quad . \quad . \quad (11)$$

This is just the eqn. (6) in the limit $T\to\infty$, since only the Boltzmann weighting factors are missing. Variation with respect to the other parameters contained in the operator is not easy to interpret even formally, since derivatives of the δ-functions are involved.

The fault in this use of Skyrme's formulation is clear. Whereas Skyrme dealt with the static energy problem, we wish to deal with a

thermodynamic problem. In § 2 a direct method of approximation was followed (in a single q-space) which used the thermal weighting factors of the model, $\exp\{-\epsilon_n/kT\}$, to cut off the excited states. In (9) and (11) all states have been given equal weight. Thus, if we wish to use Skyrme's very elegant formulation in terms of the combined q, ξ-space, the variables must be kept distinct and some weighting introduced to limit the approximation $\psi_n \simeq \phi_n$ to those states where it is likely to succeed. Obviously for a system in thermal equilibrium one should introduce the Boltzmann factors in a manner analogous to that of the direct method—an additional assumption which extends Skyrme's method to the more general problem.

The clue to this lies in the degeneracy of (8): *any* eigenfunction of $H-h$ should deliver us the same energy-difference ϵ. We might put $a_n=\delta_{nm}$ for each level ψ_m in turn; the function $F_m(q, \xi)\simeq\phi_m(q)\phi_m^*(\xi)$ is then itself an approximate eigenfunction of $H-h$, and if used in (10) would yield an estimate of ϵ (and the other parameters). Clearly this estimate is good only so long as the approximation $\psi_m\simeq\phi_m$ is justified. To cut off the excited states we might determine the parameters by forming the equation

$$\left\langle \delta\int\int F_m^*(q, \xi)(H-h-\epsilon)^2 F_m(q, \xi)\, dq\, d\xi \right\rangle_h = 0, \qquad (12)$$

which to a first approximation minimizes the *thermal average* of the mean-square deviation of H from the model value $h+\epsilon$ with respect to the states ϕ_n. For ϵ, (12) gives immediately the eqn. (6).

The preceding extension of Skyrme's arguments has been given to illustrate how the spirit of his method can be adapted to deal with a system in thermal equilibrium, which poses problems of a different character to those arising in his own examples. However, it is not suggested that in the present case this approach would provide any useful advantage over that described in § 2.

§ 4. Dynamical Definition of the Lattice

In the light of the preceding paragraphs, some remarks can usefully be added on the direct methods of fixing the parameters X^0, (e) and ω proposed in Born (1951) and Hooton (1955 a).

We wish the mathematical centres of vibration X^0 to take account of the fact that the mean positions of the atoms may differ considerably from the configuration of minimum potential energy. As remarked above, the only physically reasonable assumption is to define the X^0 as the mean positions $\langle X\rangle$ themselves. The system is then to be thought of as vibrating about its mean configuration, and we have to determine the coordinates q in a way which best describes the similarity of this motion to the harmonic vibrations of the model.

This definition of the X^0 was proposed by Born (1951) and is equivalent to writing

$$\langle q\rangle = 0; \qquad (13)$$

it in fact imposes on the actual system (1) a trivial characteristic of the model (2), viz., that the coordinates have zero mean values.

At the same time, the coordinates q were fully defined by imposing on the system a second characteristic of the model, viz., that different q should be uncorrelated and should have the appropriate mean-square deviations :

$$\langle qq' \rangle = \delta_{qq'} f(\omega, T). \quad . \quad . \quad . \quad . \quad . \quad . \quad (14)$$

Here $f(\omega, T) = \langle q^2 \rangle_h$ is a well-known thermal average for the harmonic oscillator.

According to a perturbation expansion of the density matrix (4) *in power of* q (Hooton, Edinburgh thesis) the eqns. (13), (14) lead piecemeal to the remarkably simple expressions :

$$\langle \partial V / \partial q \rangle_h = 0, \quad . \quad . \quad . \quad . \quad . \quad . \quad . \quad (15)$$

$$\langle \partial^2 V / \partial_q \partial_{q'} \rangle_h = \omega^2 \delta_{qq'}. \quad . \quad . \quad . \quad . \quad . \quad . \quad (16)$$

The immediate significance of these equations will appear directly.

In an attempt to get away from the small non-linearity implied in the expansion in powers of q a variational method was proposed in Hooton (1955 a), the free energy being minimized with respect to the parameters introduced above. It should perhaps be emphasized that this is a useful method only if the variation is applied to the *approximate* form of F as given in (7). The approximation is then that expressed in (3) and (4), which treats the operator $\tilde{V}(q) - \epsilon$ as small, regardless of what powers of q it contains. The variational method then gives just the eqns. (15), (16) in full. But although it is thus compatible with (13) and (14) within the approximation (and (13) at least must be insisted upon), this approach does not bring out clearly which characteristics of the non-linear system it is proposed to identify with those of the model.

A further point should be emphasized : all the preceding holds equally well for an arbitrary structure (say a single molecule) or a crystal lattice. The original intention of this work was to consider non-lattice solutions. This intention is no longer of interest, and we may take the mean configuration X^0 to be a regular lattice. In that case symmetry properties of the crystal should make the eqns. (15) redundant : the lattice (X^0) is *given*, its parameters being determined ultimately from the free energy in the usual way. Lattice symmetry certainly makes the first term of each eqn. (15) identically zero ; for the particular case of a one-dimensional chain the theory can be so developed that the next (cubic) term of (15) also vanishes identically (Hooton 1955 b). It seems reasonable to hope that this requirement can be satisfied in general, so that in effect only the eqns. (16) remain. It is, however, useful to treat both sets of eqns. (15), (16) together in what follows.

A direct interpretation of (15), (16) can readily be found. If the system were *harmonic* with potential $V'(q)$, equations of this type would express just the same characteristics of the normal modes as do (13) and (14) :

$$\langle \partial V' / \partial q \rangle = (\partial V' / \partial q)_{q=0} + \omega^2 \langle q \rangle - \omega^2 \langle q \rangle = 0 \quad . \quad . \quad . \quad (17)$$

(with the usual definition for the X^0), and

$$\langle \partial^2 V'/\partial q \partial q' \rangle = (\partial^2 V'/\partial q \partial q')_{q,\, q'=0} = \omega^2 \delta_{qq'} \quad . \quad . \quad . \quad (18)$$

(which diagonalizes the quadratic terms, thereby ensuring zero correlations). The vibrations of a harmonic system are in fact entirely characterized by these equations, though the averages on the left are a rather formal way of writing things in the harmonic case.

It is otherwise when the system is *non-linear*. We could well choose just these equations, which use the same fundamental characteristics of the harmonic model as are used in (13) and (14), and demand that they be (approximately) satisfied for the real vibrations :

$$\langle \partial V/\partial q \rangle = 0, \quad . \quad . \quad . \quad . \quad . \quad . \quad . \quad (19)$$

$$\langle \partial^2 V/\partial q \partial q' \rangle = \omega^2 \delta_{qq'}. \quad . \quad . \quad . \quad . \quad . \quad . \quad (20)$$

We thus again define coordinates q which should exhibit just those properties of the real vibrations that approximate to the characteristic properties of a set of normal modes. The method of approximation underlying the use of the model, as expressed in (3) and (4), may now be applied directly in evaluating (19) and (20) : we work out the averages approximately using the model Hamiltonian, so that (19), (20) go over into the previous eqns. (15), (16).

Within the limits of the approximation we have achieved the same results as previously ; in particular, the approximate eqn. (19) is compatible with (13), as we must insist if the reference configuration X^0 is to have a proper physical meaning. The advantage of this approach is to show very directly how the method depends on the use of the model. The single assumption is that the operator $H-h-\epsilon$ can be made for all practical purposes very small.

Acknowledgment

The author is much indebted to Dr. B. Szigeti for some very helpful discussions.

References

Born, M., 1951, *Fest. d. Akad. Wiss. Göttingen.*
Hooton, D. J., 1955 a, *Phil. Mag.*, **46**, 422, 433 ; 1955 b, *Z. Phys.*, **142**, 42.
Skyrme, T. H. R., 1957, *Proc. roy. Soc.* A, **239**, 399.

Time Variations of the Cosmic Ray Intensity in Jamaica†

By J. C. Barton‡ and J. H. Stockhausen§
University College of the West Indies, Jamaica

[Received September 16, 1957]

Abstract

A three-fold counter telescope has been used to study the radiation penetrating 10 cm of lead at a latitude of 18° N. A barometric coefficient of $-0{\cdot}14 \pm 0{\cdot}02\%$ per millibar was deduced from the semi-diurnal variation. The average counting rate decreased on days of high geomagnetic activity and at the same time there was a large increase in the diurnal variation.

§ 1. Introduction

Although it is obviously desirable to obtain data on any geophysical problem from as many different parts of the world as possible there is an additional advantage to be gained from studying cosmic rays in the tropics. In temperate latitudes the variations of pressure, and other atmospheric variables, are large and irregular, whereas in the tropics the most noticeable feature of the pressure records is a semi-diurnal variation superimposed on a relatively steady background. There is therefore much less uncertainty in applying corrections to the observed intensities in order to determine variations in the primary cosmic ray intensity. The experiment described here was a relatively simple one but was sufficient to show the value of working at this site.

§ 2. Apparatus

The three-fold counter telescope shown in fig. 1 had a coincidence rate of about 13 000 per hour. Recordings were taken every half hour, although only the hourly totals were used for most of the analysis. The design of the equipment followed current practice in this field and particular attention was paid to stabilizing the power supplies. Unfortunately the electricity supply was liable to interruptions caused by thunderstorms ; these were particularly prevalent during the summer months.

This apparatus was operated under a light roof at an altitude of 180 metres above sea level. Recordings were taken between September 1955 and August 1956 but those for a number of days each month had to be discarded through electrical supply failures, apparatus faults or routine checking.

† Communicated by the Authors.
‡ Now at Birkbeck College, London.
§ Now at University of Western Ontario, Canada.

The geographic latitude of the recording site is 18 0′ N and the longitude 76° 44′ W. Sea level meteorological data were obtained from the Palisadoes airport a few miles away. No upper air soundings are taken in Jamaica. Magnetic data were supplied by the San Juan Observatory in Puerto Rico.

Fig. 1

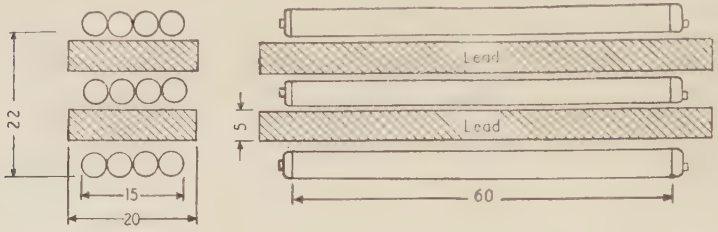

Diagram of counter telescope. All measurements are in centimetres.

§ 3. Results

3.1. *Analysis of Daily Totals*

A regression analysis between the total number of counts each day and the daily average of atmospheric pressure gave a barometric coefficient of $-0{\cdot}228 \pm 0{\cdot}032\%$ per millibar. The statistical error here is large because the changes of pressure were always small : the standard deviation of the daily averages was only 1·3 millibars.

After correcting the daily totals for the pressure changes, using the above coefficient, the remaining variations were still much larger than the inherent statistical ones. These variations might partly be accounted for by other meteorological factors. Data for these were not available but, in view of the general regularity of tropical weather, it seems unlikely that their influence could be sufficient to explain the variations.

Examination of the records suggested that the cosmic ray intensity was affected by the prevailing magnetic activity. This was first established by a partial regression analysis using the barometric pressure and the daily sums of the three hourly K indices as the independent variables. The barometric coefficient obtained in this way had the same value as before and therefore it is permissible to correct the daily totals for the pressure variations and then plot the resulting daily averages against the K numbers. Figure 2 shows that the intensity decreases with increasing magnetic activity and that the dependence on the K number is not a linear one.

3.2. *Non-periodic Variations*

The 60% increase in intensity during the solar flare of 23rd February 1956 has already been reported (Barton and Stockhausen 1956). During the period for which observations were made it was not possible to distinguish any 'Forbush' type decreases of intensity. In order to

examine more carefully whether the magnetic phenomenon of sudden commencements influenced the cosmic ray intensity the times of these events were obtained from the San Juan Observatory and the cosmic ray readings superimposed for a number of events. Figure 3 (*a*) shows the values for two-hourly periods, after correcting for pressure variations, for a total of nineteen events. In eight cases, for which there was no second event interfering and for which the records were sufficiently complete, it was possible to study this behaviour over a longer period, as shown in fig. 3 (*b*). It is apparent that, on the average, a sudden

Fig. 2

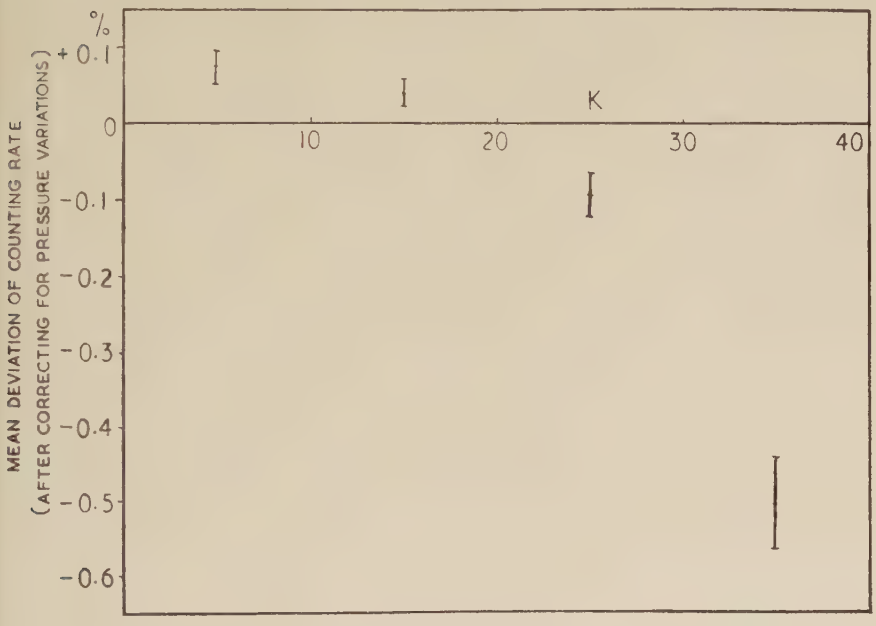

Dependence of mean counting rate on magnetic activity.

commencement leads to a small drop in intensity which continues for several days ; it is regarded as fortuitous that the decrease is larger for the particular events selected for fig. 3 (*b*). Since the days following sudden commencements are aften ones with high K numbers this result is essentially equivalent to that reported in § 3.1, although there is also an indication that the intensity may be slightly above its normal value immediately prior to a sudden commencement.

3.3. *Daily Variation*

The hourly totals for the number of cosmic rays were first grouped for each calendar month and then analysed for the diurnal and semi-diurnal components. The results for the different months were more variable than would be expected statistically but did not show any systematic

variation. A second analysis was therefore carried out in which the readings were grouped according to their K numbers. The results of this latter calculation are shown on two harmonic dials in fig. 4. Also plotted on these dials are the vectors for the daily variation of barometric pressure ; these are average values computed from the meteorological records for the same period.

Fig. 3

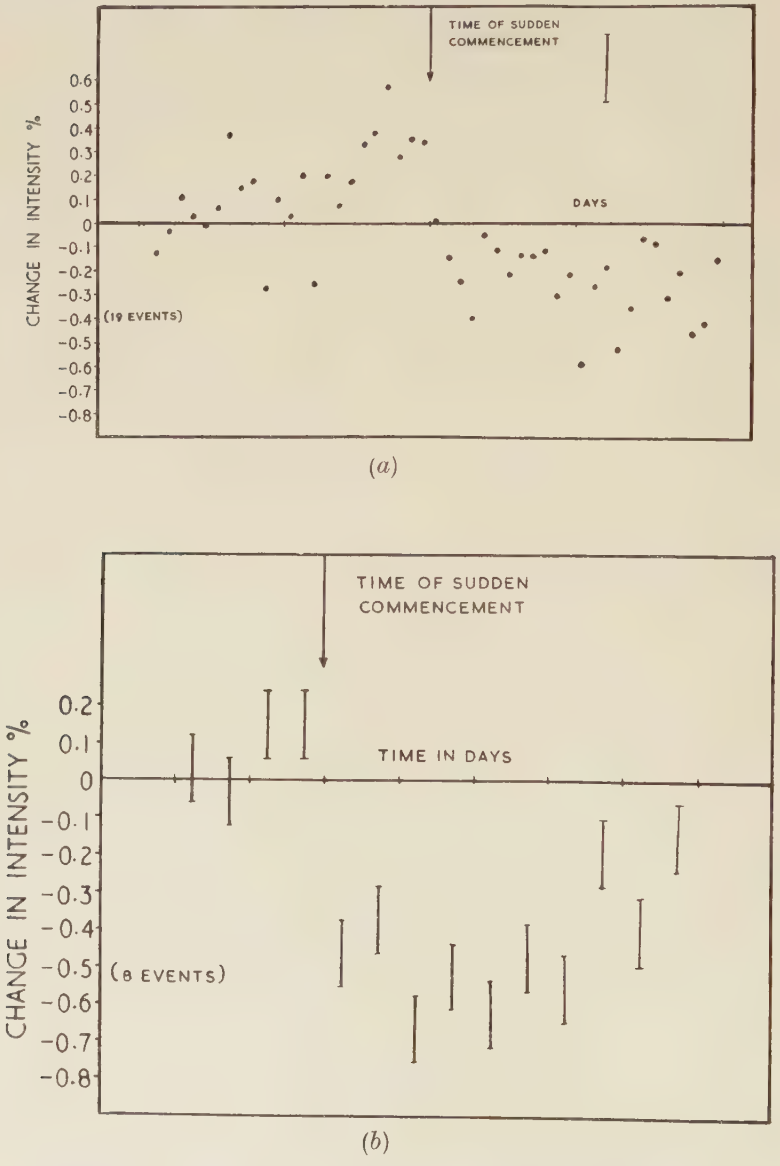

Averaged cosmic ray intensity at times of sudden commencements.

Fig. 4

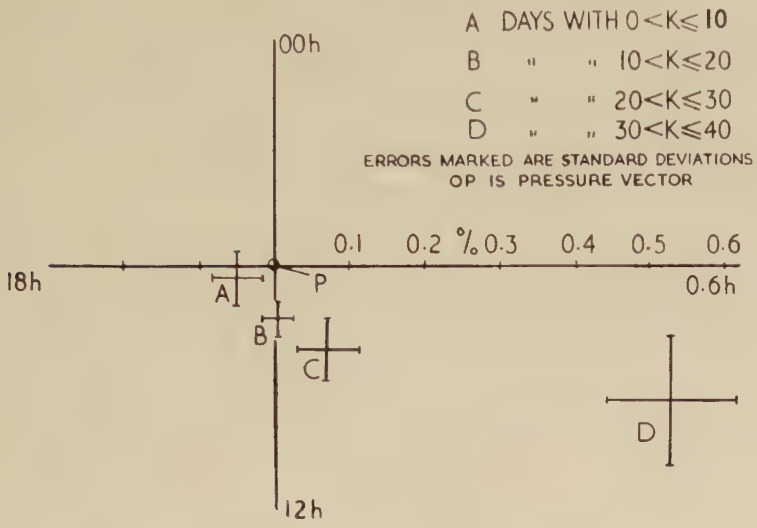

(*a*)

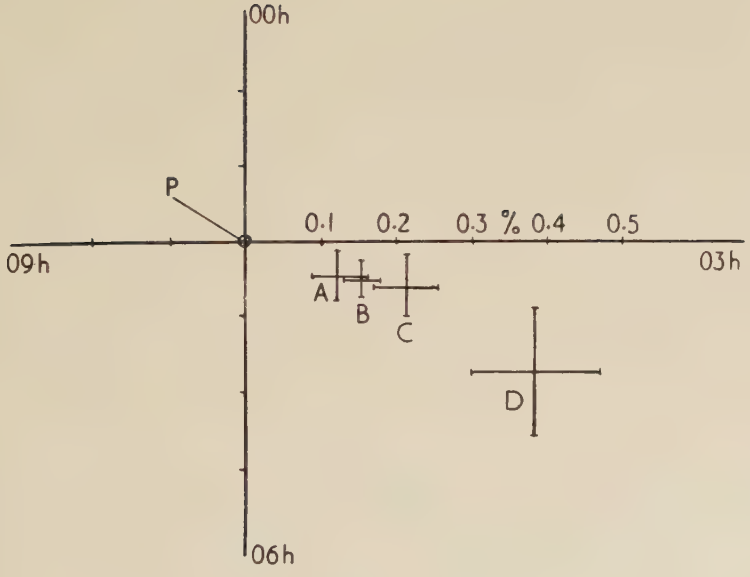

(*b*)

Harmonic dials of pressure and cosmic ray intensity variations.

For days which are relatively quiet magnetically it is seen that the semi diurnal variation is the more important one. For the average of all days with $K \leq 20$ the amplitude of this harmonic is $0{\cdot}15 \pm 0{\cdot}02\%$ and its maximum is at 4.00 hr. It is almost opposite in phase to the second harmonic of the pressure variation and is presumably caused by this. The necessary barometric coefficient would be $-0{\cdot}14 \pm 0{\cdot}02\%$ per millibar.

The diurnal variation is very small for magnetically quiet days. For days with $K \leq 10$ its phase is opposite to that of the pressure variation but the errors are too large for this result to be significant. All that can be said is that any residual diurnal variation, after correcting for pressure, must have an amplitude of less than 0·1%.

With increasing magnetic disturbance both diurnal and semi-diurnal components increase. This is particularly striking for the diurnal component which, after correcting for the pressure variation, has an amplitude of $0{\cdot}60 \pm 0{\cdot}08\%$ on the most disturbed days.

§ 4. Discussion

4.1. *Barometric Coefficient*

The value for this found from the semi-diurnal variation agrees closely with that found by Sarabhai, Desai and Kane (1953) from low altitude readings at geomagnetic latitude 13° N. The semi-diurnal pressure variation is generally believed to be explicable in terms of an atmospheric solar tide. According to the calculation of Weekes and Wilkes (1947) the relative amplitude and phase of the pressure variation are substantially constant from sea level up to a height of 25 km. Since this covers most of the region which is important for the production and decay of mesons the theory of Jánossy (1948) for the pressure coefficient should be adequate. Putting in values obtained from Rossi's (1948) curve for the absorption of the hard component near the equator this theory predicts a coefficient of $-0{\cdot}17\%$ per millibar.

The value obtained from the day to day changes of counting rate appears to be slightly larger than that deduced from the semi-diurnal variation. Although this is not yet established with certainty it is possible that temperature effects may lead to a real difference. Comparable differences between coefficients determined by using daily and monthly averages have been reported by Dolbear and Elliot (1951).

4.2. *Geomagnetic Effects*

The harmonic dials of fig. 4 show that the degree of magnetic activity plays a dominating role in the daily variation. On magnetically quiet days the results can be interpreted directly in terms of radiation which is incident isotropically, within 0·1%, and modulated solely by atmospheric effects. With increasing magnetic activity the daily variation increases very markedly. The diurnal component exhibits the more striking increase and at the same time shifts in phase to a value almost opposite to that prevailing on quiet days. (The results plotted in fig. 4

are average ones : there is some indication that individual days show appreciably different behaviour.) Combining this result with the decrease of average counting rate on disturbed days, which has about the same magnitude as the amplitude of the diurnal variation, it seems natural to conclude that the physical process is one in which a proportion of the cosmic ray beam is removed. This effect reaches its maximum in the early evening. It is not possible to state definitely that the cosmic ray intensity never exceeds its mean value at any time throughout the day but the results certainly show that reductions in the intensity are predominant.

The great influence of magnetic activity on the form of the daily variation was pointed out by Sekido and Yoshida (1950) and Elliot and Dolbear (1951). The former authors found that the amplitude of the diurnal component at stations in Japan was 0·35% during intense magnetic storms. Sekido and Kodama (1952) also noted that the phase of this component advanced as it became larger, in agreement with the behaviour shown in fig. 4.

Unfortunately most analyses of the daily variation have been made without distinguishing between days of different magnetic activity. However, Ehmert and Sittkus (1951) have given results for days influenced by strong magnetic storms : for a counter apparatus operating at 48° N they found that there was a reduction in the intensity during the latter part of the day. The magnitude of this reduction was 0·74%, which would be equivalent to a diurnal component of amplitude not greater than half of this figure. Firor *et al.* (1954), using neutron counters at high altitude, found a peak-to-peak amplitude of 1·0% at the equator and 1·4% at 48° N for days with a mean K value of 33·8. Comparison between results obtained under different conditions may be misleading but it does appear that the magnitude of the additional daily variation is not greatly dependent on the mean energy of the primary cosmic rays involved. It is also important to note that the minimum intensity is always recorded in the evening when using *local* time.

Failure to separate days of different magnetic activity may well account for some of the anomalous results which have been reported. Thus Possener and van Heerden (1956) reported a reversal of the phase of the diurnal component during certain months. Although they studied the intensity at a time of minimum solar activity it is quite possible that there were sufficient disturbed days to mask completely the true character of the variation for undisturbed days. Similarly the change of the diurnal variation which Thambyahpillai and Elliot (1953), and Sarabhai and Kane (1953) found to be associated with the solar cycle may merely be a consequence of the varying proportion of magnetically disturbed days.

The explanation of the enhanced daily variation is not known. Firor *et al.* have shown that it is very difficult to explain the results by means of the direct effect of the earth's field on the cosmic radiation. A similar conclusion has been reached from studies of the 27-day variation by Simpson (1954) and van Heerden and Thambyahpillai (1955). On the

other hand, Elliot and Rothwell (1956), by analysing the variation observed in inclined directions, concluded that the variation is due to modulation of isotropically incident primaries by fields close to the earth rather than to an anisotropic primary distribution. These views are not necessarily at variance since the arguments of Firor *et al.* do not exclude an effect due to the earth's field of about 0·1%. Just as the behaviour of the earth's field on quiet days is qualitatively different from its behaviour on disturbed days so it is possible that variations in the earth's field are sufficient to explain Elliot and Rothwell's results but are less significant for the effects which predominate on disturbed days. The assumption made here is that on the disturbed days both the earth's field and the distribution of cosmic rays are influenced by some third factor, such as turbulent magnetic fields ejected from the sun and extending over much of the solar system. There is little direct evidence for such a picture but at least it is not contradicted by the results yet available.

§ 5. Conclusions

1. The barometer coefficient for the hard component of the cosmic radiation in Jamaica is $-0{\cdot}14\pm0{\cdot}02\%$ when determined from the semi-diurnal effect and $-0{\cdot}23\pm0{\cdot}03\%$ when determined from day to day variations.

2. On magnetically quiet days the diurnal and semi-diurnal components of the daily variation can be explained solely in terms of pressure changes.

3. On magnetically disturbed days the mean intensity falls and there is a great increase in the daily variation.

Acknowledgments

We are indebted to Mr. Harker, of the Caribbean Meteorological Service, for the records of barometric pressure, and to Dr. Paul Ledig, of San Juan Observatory, for the magnetic data ; also to Dr. H. Elliot for his comments on the results.

References

Barton, J. C., and Stockhausen, J. H., 1956, *J. Atm. & Terr. Phys.*, **9,** 161.
Dolbear, D. W. N., and Elliot, H., 1951, *J. Atm. & Terr. Phys.*, **1,** 215.
Ehmert, A., and Sittkus, A., 1951, *Z. Naturf.*, 6a, 618.
Elliot, H., and Dolbear, D. W. N., 1951, *J. Atm. & Terr. Phys.*, **1,** 205.
Elliot, H., and Rothwell, P., 1956, *Phil. Mag.*, **1,** 669.
Firor, J. W., Fonger, W. H., and Simpson, J. A., 1954, *Phys. Rev.*, **94,** 1031.
van Heerden, I. J., and Thambyahpillai, T., 1955, *Phil. Mag.*, **46,** 1238.
Jánossy, L., 1948, *Cosmic Rays* (Oxford : University Press).
Possener, M., and van Heerden, I. J., 1956, *Phil. Mag.*, **1,** 253.
Rossi, B., 1948, *Rev. mod. Phys.*, **20,** 537.
Sarabhai, V., Desai, U. D., and Kane, R. P., 1953, *Nature, Lond.*, **171,** 122.
Sarabhai, V., and Kane, R. P., 1953, *Phys. Rev.*, **90,** 204.
Sekido, Y., and Yoshida, S., 1950, *Rep. Ionosphere Res. Japan*, **4,** 37.
Sekido, Y., and Kodama, M., 1952, *Rep. Ionosphere Res. Japan*, **6,** 111.
Simpson, J. A., 1954, *Phys. Rev.*, **94,** 426.
Thambyahpillai, T., and Elliot, H., 1953, *Nature, Lond.*, **171,** 918.
Weekes, K., and Wilkes, M. V., 1947, *Proc. roy. Soc.* A, **192,** 80.

Etching Patterns in High-Purity Zinc†

By I. S. Servi
Metals Research Laboratories, Electro Metallurgical Company,
Niagara Falls, New York

[Received September 16, 1957]

A single crystal of zinc having a predetermined orientation was prepared from 99·999+% grade material by the Bridgeman technique and subsequently etched in a solution containing 200 g CrO_3, 15 g Na_2SO_4, 50 cm^3 of concentrated HNO_3, and water to make 1000 cm^3 (Vinaver and Dreulle 1955).

On a face nearly parallel to the basal plane, several complex spirals were observed after etching for one hour. A typical example is given in fig. 1 (*a*), Pl. 1. These spirals were both left- and right-handed, and were surrounded by more finely etched areas.

The pattern of fig. 1 (*b*), Pl. 1 was observed only in one location, in an area which was otherwise free from any 'structure'. Interferometric observations revealed that the background was levelled, and that the 'loops' stood about 0·15 micron above this background. The typical pattern is similar in aspect to an operative Frank–Read source (Frank and Read 1950). However, some of the detailed features, namely, the two 'dots' near the centre of the pattern and the central 'dip' of the innermost line, are unexpected.

An explanation for this peculiar and heretofore unreported etching behaviour is suggested, assuming that regions around the dislocation lines are saturated with respect to a solute element much more noble than zinc, present at a very low overall concentration. A galvanic action would, therefore, occur, the material surrounding the dislocation lines dissolving at a lower rate than the rest. It should be emphasized, moreover, that the etching reagent was always found very discriminative with respect to structural features when the solution was not agitated, whereas it appeared to be an excellent levelling and polishing reagent when continuously agitated.

Interpreting the pattern as a Frank–Read source, the length L can be measured (2×10^5 Å), and the stress required to place the source in operation can be computed, based on Mott's formula (Mott 1952)

$$\text{stress}=Gb/L.$$

Assuming $4{\cdot}9\times10^6$ p.s.i. for G (Smithells 1955) and of 2·659 Å for b, the stress appears to be about 65 p.s.i., which is a reasonable value.

References

Frank, F. C., and Read, W. T., 1950, *Phys. Rev.*, **79**, 722.
Mott, N. F., 1952, *Phil. Mag.*, **43**, 1151.
Smithells, C. J., 1955, *Metals Reference Book* (London: Butterworths), p. 571.
Vinaver, W., and Dreulle, P., 1955, *Rev. Métall.*, **52**, 613.

† Communicated by the Author.

Deformation Processes in Polyethylene Interpreted in terms of Crystal Plasticity†

By F. C. Frank, A. Keller and A. O'Connor
H. H. Wills Physics Laboratory, University of Bristol

[Received October 29, 1957]

Abstract

The rolling texture of drawn polythene is interpreted in terms of slip and twinning processes characteristic of ordinary crystal plasticity in combination with the rubbery elasticity characteristic of macromolecular amorphous substances. The principal crystal plasticity elements operative are (100) [010] slip and (310) [1$\bar{3}$0] and/or (110) [1$\bar{1}$0] twinning. The observations appear to indicate that (110) [1$\bar{1}$0] slip is a less easy mode of deformation than these, at least initially. Under more general deformation conditions, it appears that these modes predominate at small strain, tending to a texture with [010] aligned to the axis of extension, giving place to [001] slip processes, which align [001] and the molecular chains along the axis of extension when the strain is large. Under certain conditions a second crystalline phase also appears which in terms of general crystal plasticity would correspond to a martensitic type transformation and might arise through a regular sequence of stacking faults on {110} planes.

§ 1. Experimental

The material of our experiments was melt pressed polythene film, Alkathene grade 2, about 0·1–0·15 mm thick. Strips of this film were passed between rollers, the spacing between the rollers being adjusted as required. In another type of preparation strips of the film were first drawn by hand past the stage of necking to an elongation of 450%. Subsequently these drawn strips were passed between rollers, the direction of advance being along the length of the strip. Relaxation experiments were carried out by placing the drawn, or drawn and rolled strips on a temperature gradient bar at the required temperature.

When a strip was mildly rolled the first sign of orientation was of the type where (100) was parallel to the plane of the film and [001] was parallel to the direction of advance, the orientation itself being only poorly defined. On increasing rolling this orientation became better defined but in addition to it a second type of orientation with (110) parallel to the film also appeared (fig. 1, Pl. 2). In the sample of fig. 1, Pl. 2, the length of the film increased by 11%, the width by 4%; and thicknesses decreased by 14%. The second type of orientation with (110) parallel to the film became more pronounced with stronger rolling, and predominantly this

† Communicated by the Authors.

orientation was produced when the drawn specimen was rolled (fig. 2, Pl. 2). (The effect of drawing was to orient [001] first.) The dimensional changes in the case of fig. 2, Pl. 2, were: increase in length 13·5%, increase in width 12·7%, reduction in thickness 25%. On mild rolling of the drawn samples there were faint signs of the (100) plane orientation besides the strong (110) orientation. Summing up, these results indicate that mild rolling produces preferentially (100), strong rolling (110) orientation, the relative proportion of the two orientations varying according to whether the sample was previously drawn or not. These observations agree essentially with those of Point (1953).

Drawn and rolled specimens which were only slightly relaxed by an anneal at ~100°C changed from the original (110) to (100) plane orientation, [001] staying parallel to the direction of original draw (fig. 3, Pl. 3). The effect of stronger annealing will not be discussed here. It will only be recalled that on annealing of a drawn sample [001] gradually tilts away from the original draw direction while the position of [010] stays unaltered, until [100] becomes parallel to the direction of original draw (e.g. Keller 1955, Pl. Ic). Redrawing of such a sample has been examined by one of us earlier (Keller 1955) and it was reported that the crystals first turn around [001] prior to [001] alignment. On re-examining this effect we now find that this rotation around [001] is not continuous but results immediately in the orientation shown by fig. 4, Pl. 3.

A further feature which became apparent is a new reflection at 4·59 Å (also reported by others in somewhat different connection; see later). As seen this reflection is present in figs. 1 and 2, Pl. 2, but is absent in figs. 3 and 4, Pl. 3. Its intensity relative to the others varied from sample to sample.

§ 2. Discussion

2.1. *Introductory*

'Drawing' chain-macromolecular substances, i.e. subjecting them to permanent extension of the order of unity or greater, whether they are crystalline or amorphous, produces a texture with preferred orientation of the molecular chains along the axis of extension. Crystalline polymers show different and rather complex orientation phenomena for smaller strains: we defer consideration of these till later in the paper. If the predrawn crystalline polymer is subjected to transverse compression, inducing only transverse displacement of the molecules, one may anticipate that the behaviour should be more nearly similar to that of non-macromolecular substances, governed by familiar principles of crystal plasticity: except that, since in any attainable condition of the majority of polymers, the chains are neither completely aligned nor fully extended, some restoring stresses of rubbery nature will be present. Since rubbery elastic moduli are relatively weak, these latter stresses should have little effect until the strain is fairly large.

In the light of these considerations we approach the interpretation of the rolling texture of drawn polythene, regarding rolling as sufficiently nearly the same as transverse compression. In those of our experiments where the polymer was not pre-drawn to begin with, conditions will not be very different. Here drawing took place during rolling, consequently at some stage compression will act on the material which is already drawn. The crystal structure (Bunn 1939) corresponds to the orthorhombic form of long chain paraffins (Müller 1928) illustrated in figs. 5 and 6.

Fig. 5

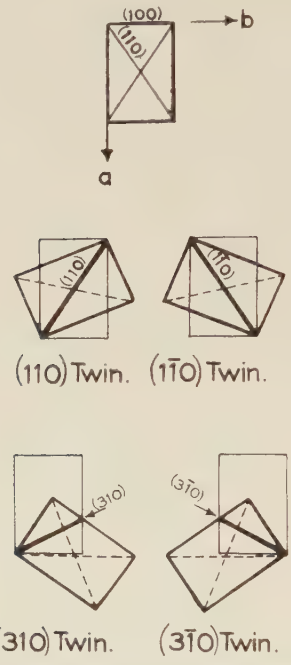

Illustration of the effect of twinning on the orientation of the unit cell when viewed in the *c* projection.

2.2. *Expected Modes of Deformation*

The expected modes of crystal plasticity involving displacements transverse to the chain axes may be simply derived by inspection of the crystal structure. The shortest lattice translation (other than that along the *c*-axis) is *b* [010]. We therefore expect a slip-mode involving dislocations with this as Burgers vector. Gliding dislocations should not be able to cut across the covalently bonded chain axes, so that the only possible slip plane for this dislocation is (100). The next largest translation is *a* [100], with (010) as its necessary slip plane. As it is a considerably longer displacement, we should expect this dislocation to be less mobile. Since it is orthogonal to the [010] (100) slip system, it is always subject to the same driving stresses, and we should generally

expect the [010] (100) slip to relieve these stresses before |100| dislocations move. $[a\ b\ 0]$ dislocations would be expected to dissociate into pairs of partial dislocations with Burgers vector $|\frac{1}{2}a, \frac{1}{2}b, \gamma|$ and $|\frac{1}{2}a, \frac{1}{2}b, -\gamma|$, γ being an unknown quantity, each having a slightly shorter Burgers vector than b [010] if γ is zero. These pairs would glide on (110). This is a reasonable slip system, but may not be observed because it is in competition with the twinning modes.

Expected twinning modes are most simply deduced from Mallard's law (cf. Frank 1953). The structure is orthorhombic pseudohexagonal. Hexagonal symmetry planes lost in the reduction of symmetry to orthorhombic are, in orthorhombic indices, (110), (1$\bar{1}$0), (310) and (3$\bar{1}$0). We anticipate these as twinning modes of the first kind : i.e. such that twin and matrix are reflections of each other in these planes as interfaces. These four modes make two conjugate pairs (310) with (110), (3$\bar{1}$0) with (1$\bar{1}$0), being pairs of planes orthogonal to each other in the related structure of higher symmetry. Hence no further modes are predicted from these considerations. In full, the corresponding twinning elements are :

Composition plane	Conjugate plane	Shear direction	Conjugate axis	Semi-angle	Shear $S=$
K_1	K_2	η_1	η_2	ϕ	$2 \cot 2\phi$
(110)	(3$\bar{1}$0)	[1$\bar{1}$0]	[130]	41° 27′	0·249
(310)	(1$\bar{1}$0)	[1$\bar{3}$0]	[110]	41° 27′	0·249

The values of ϕ and S are calculated from the lattice parameters of Bunn (1939), $a=7{\cdot}40$, $b=4{\cdot}96$.

Figure 5 shows the unit cell in c projection when twinned according to these two twin laws. Figure 6 shows the structure in the case of (310) twinning. As seen a rearrangement of the planes of the carbon zigzags is also required.

These expectations are in accordance with the observations of Koolvoort (1938) who observed (110) and (310) twinning in the normal paraffin $C_{24}H_{50}$, both as a result of deformation in the orthorhombic modification, and as a result of transformation to this form from the hexagonal modification which exists near the melting point. Incidentally, his observations are remarkably similar to those which may be made on corresponding metal systems.

The appropriate stresses to operate any of these modes are rather similar, namely compressive stresses in a range of directions near to [010] or tensile stresses in a range near to [100], with a preference for one or other of the conjugate pairs according as the axis of principal stress deviates to right or left from these directions. Whether (310) or (110) twinning will operate more easily cannot be certainly decided on *a priori* evidence, but on weak empirical grounds (cf. Frank 1953) one could expect

the system of higher indices, i.e. (310), to be preferred. This appears to be supported by the present observations, but the (110) twinning may occur as well: since it produces about the same lattice orientation, it is neither easy to distinguish by x-ray diffraction nor of great importance for the plastic behaviour, whether both or only one of these modes occurs.

Fig. 6

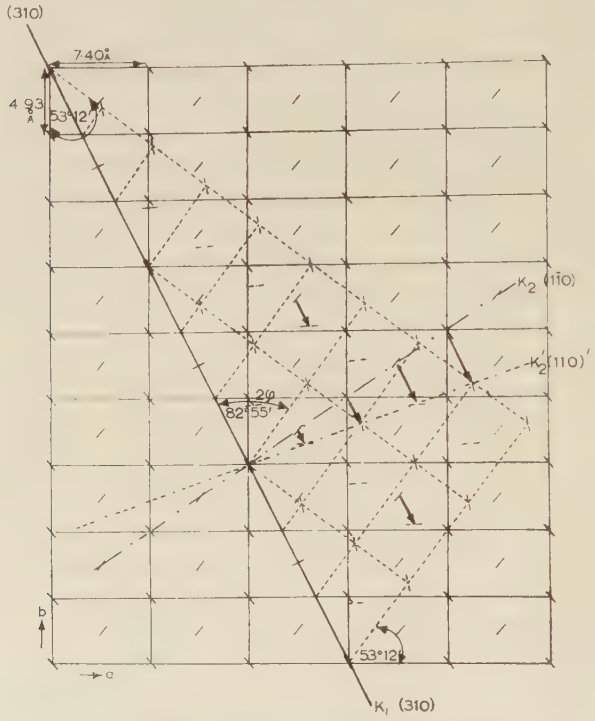

(310) twinning in terms of the structure, in c projection. The full lines show the parent, the dotted lines the twinned lattice. K_1 is the twinning plane common to both, K_2 and K_2' are the conjugate planes, which remain unaltered during twinning, in the parent and the twinned lattice respectively. Arrows show displacements of molecules in the twinning shear. It is assumed that molecules lying on the composition plane K_1 take up the symmetrical position parallel and perpendicular to the plane indicated in the drawing.

2.3. *Consequent Deformation Behaviour*

On this basis we expect the following behaviour:

Crystallites with (100) and (010) planes near to 45° to the axis of compression will deform by (100) [010] slip, undergoing a rotation which brings (100) more nearly normal to the compression axis.

Crystallites with (010) planes near to being normal to the compression axis will twin, say on (310). This makes a moderate deformation (25% shear)

accompanied by a large change of orientation, by which the planes (100), (010), (110), (110), (310) and (310) undergo small rotations (zero for (310), of course) and transform into (110), (310), (100), (110), (310) and (010) respectively.

The transformations of planes are the same for (110) twinning : only the associated small rotations are different. This is now a suitable orientation for further slip on (100) bringing that plane nearer to the plane of compression.

When this orientation is closely approached, (100) slip should cease. No twinning is possible. The only likely mode of deformation in slip on (110). If the flow stress for this mode is larger than that for (100) slip, there will be no large departure from (100) orientation before (100) slip starts again.

The outcome, for crystallites of any initial orientation, is a two component texture with (100) poles on either side of the pole or the rolling plane. If the flow stress for (110) slip is large, these (100) poles will be close together. In any case, allowing for the broad arcs of indefinite orientation usually found with polymers, including ordinary polythenes, this would appear as a single arced (100) texture. This agrees with observation.

We have remarked however that with larger amounts of deformation we must expect consequences from the fact that we are dealing with long chain molecules, imperfectly aligned and not fully extended. This refers both to molecules which may lie wholly or partly in an amorphous phase, and to molecules which may lie in folded configurations in the crystalline phase. The presence of such molecules must generate restoring stresses of a broadly rubber-like nature : that is, of low modulus, but persisting and increasing up to very large strains. These rubber-like stresses remain after the roller-pressure is removed, being equivalent to sideway compression or traction normal to the rolling plane. Their effect on the oriented crystallites should be to induce twinning, whereby the (100) planes, parallel to the rolling plane, rotate slightly and transform into (110) planes. This will produce exactly the two-component texture, both components having (110) planes preferentially parallel to the rolling plane, that is observed. This can be seen directly from fig. 5 if the plane of rolling is taken to be parallel to the (100) planes in the untwinned crystal.

In this texture, in which various crystallites, or parts of a crystallite, have twinned in alternative ways, elastically stored energy persists around the edges of every twin, balanced against a reduction in the energy associated with the rubber-like stresses. With a gentle anneal, insufficient to melt the crystals, the latter stresses can relax by molecular migration, as is regularly observed for rubber-like stresses in a non-crosslinked polymer. The crystallites can then assume a state of lower energy by twinning back again, so that the texture reverts to the single, or nearly single, (100) texture, as observed.

According to the foregoing, compression along [010] would produce twinning. Consequently the same is expected for tension along the perpendicular direction [100]. This in fact is observed in the case of specimens which were drawn, relaxed and subsequently redrawn (fig. 4).

The two possible modes of twinning can only be distinguished by small differences in the x-ray pattern. The arcs being broad it is difficult to locate them with sufficient accuracy. However it was possible to reach a conclusion by comparing the angular positions of the 200 and 110 along their respective circles. It can be deduced (see fig. 5) that the 200 reflection should be nearer to the equator in the case of (110) than in that of (310) twinning. Accordingly we appear to have (310) twinning in fig. 2 and (110) twinning in fig. 4. These modes of twinning were found to be characteristic of the two types of samples. When reaching these conclusions it was assumed that before twinning the texture was closely single (100). If the initial texture was imperfectly aligned, then crystallites in orientations deviating in opposite directions would exhibit preference in twinning between (110) and $(1\bar{1}0)$ modes, or between (310) and $(3\bar{1}0)$ modes, in either case displacing the (200) poles further from the meridian. There is evidence of such displacements by selection, the observed angles from meridian to the mid-points of (200) arcs being 59° for the first type of specimen compared with $53\frac{1}{2}°$ calculated for (310) twinning from the ideal orientation, and 68° for the second type of specimen compared with $66\frac{1}{2}°$ calculated for (110) twinning from the ideal orientation.

The assumption, involved in the foregoing interpretation, of a comparatively high critical stress for slip on $\{110\}$, is not one which could be made with confidence *a priori*. The energy of the stacking fault between two partial dislocations for slip on $\{110\}$ is an unknown quantity. If it is sufficiently low, the critical stress for this slip mode could be about the same as, or even less than that for slip on (100); and no theoretical basis exists for predicting the relative magnitude of critical stresses for slip and twinning processes. However, the alternative assumption of relatively easy $\{110\}$ slip does not appear capable of explaining the observations. If this process occurred in preference to one of the twinning processes under the stress which favours these, i.e. compression along an axis in the neighbourhood of [010], it would produce a strong component in the texture having (010) normal to the compression axis. This would be a stable orientation by reason of alternate slip on (110) and $(1\bar{1}0)$, the compression axis lying in the obtuse-angled sector between these two planes This is in disagreement with the observations. We infer that twinning does occur in preference to $\{110\}$ slip.

For a compression axis near to [100] the twinning processes do not enter into consideration. The (100) orientation (which is observed to occur as a texture component) would be unstable, the compression axis now lying in the acute-angled sector between (110) and $(1\bar{1}0)$. There should be two other stable orientations, one lying between (100) and (110),

the other between (100) and (110), in the obtuse sector in each case. We assumed above that (100) slip was easier than {110} slip, so that these two stable orientations are close to (100) and can be identified together as the observed (100) component of texture. Assuming, alternatively, that {110} slip is much easier, these two stable orientations would be close to (110) and (110). This could be identified with the {110} texture observed after strong compression but we should be left without an interpretation of the reversion to (100) texture on annealing or for the (100) component appearing after light rolling.

A more complex possibility which cannot be rejected on the evidence is that, while (100) slip has a lower critical stress than {110} slip, it has a higher rate of work-hardening, so that the (100) texture develops first, and then changes to the {110} texture when this becomes the easier slip mode. The reversion to (100) texture on annealing remains unexplained in this case but might be attributed to an oriented recrystallization.

§ 3. Extra Reflections and Stress Induced Phase Transformation

In the course of our work on polyethylene we have noticed reflections which cannot be indexed on the basis of the orthorhombic unit cell. In the rolled or pressed specimens in particular a strong reflection appeared corresponding to a spacing of 4·59 Å, the corresponding lattice planes being parallel to the plane of rolling or pressing. The relative intensity of this reflection was variable which indicates the presence of a second crystalline phase. We also found that associated with this there are other reflections with correspondingly varying intensity which are less evident because of blending with other principal reflections. Such observations are not new. The reflection at about 4·5 Å has been reported previously (e.g. Pierce *et al.* 1952) and a number of other new reflections have also been frequently quoted. Quite recently a new unit cell has been suggested by Teare and Holmes (1957) which would be a triclinic polymorph of the usual orthorhombic cell in analogy with similar polymorphism in paraffins (e.g. V. Sydow 1956). We concur with the principles of the interpretation of Teare and Holmes, but on the basis of our data we cannot accept their proposed unit cell. Our findings will be published separately once the work still in progress is complete. At this place only one aspect of this polymorphism will be discussed.

It is a common feature of all observations that the strong reflection at about 4·5 Å appears in specimens which were severely deformed. It appears, therefore, that we are probably dealing with a stress-induced phase transformation to an otherwise unstable crystal modification. Two important distinctions must be drawn in classifying stress-induced crystal transformations. Firstly, the stress may change the relative thermodynamic stabilities of two phases, or merely provide the ' activation ' for a transformation to a stabler phase. Secondly, the mechanism of transformation may be incoherent, in which case hydrostatic pressure can be the only part of the stress relevant to the change in relative stability,

and change in volume the only thermodynamically relevant characteristic of the transformation itself; or alternatively, it may be coherent, proceeding like a mechanical twinning process, in which case shear stresses will also contribute to the change in relative stability. Coherent 'shear transformations' are familiar in metals, and are called 'martensitic' after the classical example occurring in steel. The polymorphism of the normal paraffins and their derivatives, in crystal structures which essentially differ only by shears and by molecular rotations about the chain axes, suggests that they should be particularly apt for martensitic transformation. The thermodynamic requirement for such a transformation to a normally unstable phase is that the product of strain in transformation and corresponding stress should exceed the difference in free energies per unit volume of the two unstressed phases. Since, in polymers, the difference in free energy between alternative crystal structures is governed only by van der Waals forces, whereas covalent bonds contribute to the ultimate strength, which limits the applicable shear stresses, there is a relatively high *a priori* likelihood that this condition may exist, compared with the case of metals in which the same kind of interatomic forces govern both quantities. The geometric requirement is that one of the three principal strains in the transformation be zero, while the other two are of opposite sign. If there is no volume change, this means simply that the deformation is a shear. There then exist necessarily two planes, both in general irrational, which are subject to no deformation, and either of which may serve as the planar interface across which the transformation takes place. Qualitatively, such a transformation closely resembles mechanical twinning.

A particular hypothetical mechanism for a stress-induced phase-transformation would be the dissociation of pairs of partial dislocations on the {110} planes. In the first instance this produces single stacking faults on these planes. With a screw dislocation intersecting the plane it may produce a regular sequence of stacking faults constituting either a twinned crystal or a new phase. Alternatively, however, an irregular sequence of stacking faults of sufficiently high density might be responsible for the anomalous reflections. Unfortunately, though it is a very reasonable presumption that stacking faults of this kind can exist, the available degrees of freedom in molecular rotation about, and translation along, the *c*-axis prevent any reliable presumption of their detailed structure. All we are able to say is that a mechanism of this kind is reasonably likely, and would cause this sort of transformation to accompany extensive slip on {110} planes.

§ 4. Deformation under more General Conditions

General empirical experience regarding crystal plasticity leads one to expect easiest slip along the directions of shortest lattice translation. This is reasonable, because the corresponding dislocations have the smallest Burgers vectors. The square of the Burgers vector enters into

the expression for dislocation energy, and energy barriers for dislocation motion are expected to be broadly proportional to their self-energy. By this rule, the easiest modes of slip in polythene should have the slip direction [001], for which the lattice translation $c = 2{\cdot}5$ A, compared with $a = 7{\cdot}4$ A. At first sight, this agrees with the broad experience that 'drawing' polythene aligns the c-axes to the draw-axis. We ought, however, to be cautious, because we are dealing with elastically very anisotropic crystals. Stretching along the c-axis is opposed by covalent bonds : transverse stretching only by Van der Waals forces. This must raise the energy of the dislocations with Burgers vectors not in the a b plane. Compression along the c-axis, of the magnitude associated with dislocations, is liable to be taken up by chain folding, which may allow the energy to be lower, but is likely to increase the energy barrier for motion, besides making it difficult to estimate. Thus we have the alternative theoretical possibility that slip along the b-axis, [010], may be easiest. The consequence would be that for moderate strains the b-axis would approach the principal tensile axis. This would make an orientation stable against twinning under that stress, and crystallites initially far from that orientation could make a substantial discontinuous approach to it by twinning. A fibre texture with axial b, and transverse a would develop. The deforming crystallites would also tend to acquire transverse c-orientation, but crystallites with near-axial c-orientation will not deform except by secondary processes, so that a less complete preferred orientation of c-poles should be produced. At a later stage, the chain continuity should enforce a new preferred orientation with axial c. A variety of observations are in agreement with this picture. For example :

4.1. *Drawing Behaviour*

Drawing produces [001] orientation ; the c-axes, the direction of the molecular chains, align in the draw direction. This chain alignment, however, is not gradual. In the initial stages of slow drawing at first the [010] poles congregate in belts more or less near to the draw axis (e.g. Keller 1955). The exact position of this accumulation of [010] poles varies with the conditions of drawing and with the type of specimen. The alignment of [001] starts only after this stage. In any interpretation of the drawing behaviour the spherulitic texture of the material would have to be considered (Keller 1955). This is beyond the scope of the present paper. It is apparent, however, that the presence of a [010] slip will contribute to the initial tendency of the b axes to move towards the draw axis.

4.2. *Relaxation Behaviour*

In highly drawn materials, [001] poles are approximately axial, [100] and [010] poles approximately equatorial. Heating produces a large longitudinal contraction, during which [010] poles retain their equatorial position, while [100] poles approach the axial, and [001] poles the equatorial position (e.g. Keller 1955). We do not completely understand this

process. It is simple enough if we regard the material as crystallites embedded in a rubbery matrix, without intertransformation between crystalline and amorphous phases. We do not know to what extent the latter occurs, nor, if it does not occur, what prevents it. If it occurred freely, we should expect the material to crystallize in the drawn configuration, with axial [001] and even an elongation instead of a contraction. However, accepting the fact of contraction, equivalent to axial compression, and supposing that crystallites largely preserve their identity during the relaxation, the stability of the equatorial position of (010) poles will follow from the supposed ease of [010] slip, and the orientation to which crystallites should tend is that with the slip plane (100) normal to the axis of compression. This is in accordance with the observations.

4.3. *Redrawing of Relaxed Specimens*

If the material relaxed to the state in which [100] is substantially axial is redrawn, (100) poles are displaced from the meridional position by about 67° without assuming intermediate positions (fig. 4). As discussed above this is what we should expect, since all crystallites are favourably oriented for twinning. [001] alignment sets in progressively after this stage.

4.4. *Orientation within the Spherulites*

The crystallites on any radius of a spherulite have [010] parallel to this radius. This suggests what may be a profitable approach to the unsolved problem of how the spherulitic texture in polythene (and other polymers) originates. The foregoing considerations suggest that we may generally regard an axis of [010] textural orientation as indicative of the direction of a moderate extension. If this is applicable to the genesis of the spherulites it implies that crystallization is *followed* by contraction in towards a centre. It is not suggested that this will account in full for morphology of the spherulites.

References

Bunn, C. W., 1939, *Trans. Faraday Soc.*, **35**, 482.
Frank, F. C., 1953, *Acta Metall.*, **1**, 71.
Keller, A., 1955, *J. Polym. Sci.*, **15**, 31.
Kolvoort, E. C. H., 1938, *J. Instn Petrol. Tech.*, **24**, 338.
Müller, A., 1938, *Proc. roy. Soc.* A, **120**, 437.
Pierce, R. H., Tordella, J. P., and Bryant, W. M. D., 1952, *J. Amer. chem. Soc.*, **74**, 282.
Point, J. J., 1953, *J. Chim. phys.*, p. 76.
Sydow, E. v., 1956, *Ark. Kemi*, **9**, 231.
Teare, P. W., and Holmes, D. R., 1957, *J. Polym. Sci.*, **24**, 496.

Charged Dislocations and the Strength of Ionic Crystals†

By J. D. Eshelby, C. W. A. Newey and P. L. Pratt
Department of Physical Metallurgy, University of Birmingham

and A. B. Lidiard
Department of Physics, University of Reading

[Received November 13, 1957]

Abstract

If the energies required to form positive and negative ion vacancies in an ionic crystal are unequal, then in thermal equilibrium dislocations in the crystal will be electrically charged and surrounded by a Debye–Hückel cloud of vacancies. If the vacancy cloud is immobile a finite force is required to separate the dislocation from the cloud, and so the crystal will possess a yield stress below which plastic flow will not occur. The presence of divalent impurities modifies the magnitude of the charge on a dislocation, and may even reverse it. If precipitation of the impurity or association of impurity atoms and vacancies can occur, the concentration of impurities may be a complicated function of temperature. The yield stress of the crystal may then exhibit maxima and minima when plotted as a function of temperature. Experimental results showing this behaviour are presented and tentatively compared with the theory.

§ 1. Introduction

The number of Schottky defects (vacant anion and cation sites) in an ionic crystal is normally calculated by minimizing the free energy of the system subject to the condition that the crystal be electrically neutral throughout. However, as Lehovec (1953) has pointed out, the actual state of affairs is more complicated when we suppose that vacancies can only be formed at the surface of the crystal. (Compare also Frenkel 1946, Grimley and Mott 1947 and Grimley 1950.) For definiteness we consider the case of sodium chloride. Here sodium-ion vacancies are more easily formed than are chlorine-ion vacancies. Hence when the temperature is raised from the absolute zero an excess of sodium-ion vacancies is emitted from the surface into the crystal, leaving a net positive charge on the surface. The resulting space-charge discourages the emission of further sodium vacancies and encourages the emission of chlorine vacancies. Calculation shows that in equilibrium the bulk of the crystal is electrically neutral, but that there is a positive charge on the surface, balanced by an equal and opposite negative charge cloud penetrating some distance into the crystal. Because of the presence of

† Communicated by the Authors.

this double layer there is a potential difference between the surface and interior of the crystal.

It is generally admitted that vacancies can be formed at dislocations as well as at the surface of a crystal. Thus we should expect (Pratt 1957) dislocations in an ionic crystal to be charged (by having an excess of jogs of one sign), and to be surrounded by a sheath of vacancies of predominantly the opposite sign. Clearly a grain boundary or mosaic boundary should also be charged and surrounded by a balancing layer of charge, whether we regard the boundary as essentially a junction between two separate blocks of crystal, or as an array of dislocations.

We have pictured the charges on surfaces and dislocations as arising from the emission of an excess of vacancies of one sign. This is not necessary: any initial distribution of defects would re-arrange itself to give the same final equilibrium configuration. There should be similar

Fig. 1

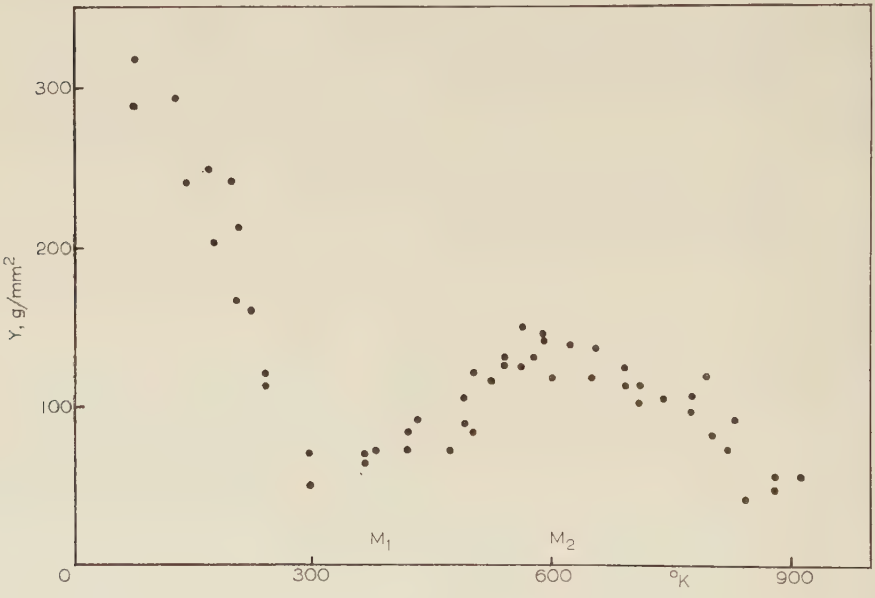

Yield stresses of rock salt specimens at various temperatures.

effects where Frenkel (interstitial plus vacancy) defects predominate, even though there is no difficulty in imagining their formation and disappearance in the body of the lattice as well as at surfaces and dislocations.

Suppose that the temperature is low enough for the charge cloud around a dislocation to be immobile. The electrostatic field of the vacancies is such as to pull the charged dislocation back to the axis of the cloud if it is displaced, and so a certain minimum mechanical stress will be required to pull the dislocations away from their clouds and cause plastic flow.

Thus we have a mechanism which may in part determine the yield point of an ionic crystal.

If a sodium chloride crystal contains divalent impurities mobile enough to play their part in forming the ion atmospheres the above account must be modified. At high temperatures there is qualitatively no modification, but at low temperatures the impurities cause the sign of the charge on a dislocation (or surface) to reverse. At one particular intermediate temperature the dislocations are uncharged, and at this temperature the yield strength of the crystal should drop to zero if the present mechanism were the only one determining it. Again, at low temperatures some of the impurity may precipitate out in a new phase, and thus reduce the concentration of impurity which take part in ion-cloud formation. If this is so the yield stress can have a succession of maxima and minima when plotted as a function of temperature. The measured points in fig. 1 do indeed show this sort of behaviour.

The strength of ionic crystals will not, of course, be determined entirely by the mechanism discussed here. The factors commonly considered in connection with the strength of metals will also be operative, for example the elastic interactions between point defects and dislocations. We have thought it best, however, to present a preliminary account of the theory of charged dislocations ignoring these complications. Bassani and Thomson (1956) have dealt with the same topic, though from a different point of view. They showed that in NaCl a positive-ion vacancy is attracted into that part of the core of a (110) dislocation where the lattice is compressed, with a binding energy of about 0·4 ev relative to normal lattice positions. Divalent impurity ions were found to be little attracted into dislocation cores. From a knowledge of the binding energy of a point defect and a dislocation it is not possible to calculate a yield stress without introducing additional assumptions. Our approach, on the other hand, emphasizes the role of the charge cloud around a dislocation, and so we are able to obtain a yield stress by a purely electrostatic calculation. We may note that Bassani and Thomson's model of a set of sites along a dislocation at which vacancies may be trapped with a certain binding energy is formally included in our 'vacancy source' model so long as the predicted charge on the dislocation does not require these sites to be completely emptied. Evidently the connection between the two models needs further examination.

§ 2. The Charge on a Crystal Surface

We give first a brief sketch of the generalization of Lehovec's results to the case where mobile divalent impurities are present. (A more detailed account will appear elsewhere.)

Let N be the number of cation (or anion) sites and cN the mean number of impurity atoms per unit volume. Let n_+, n_-, n_i be the numbers per unit volume of cation vacancies, anion vacancies and impurity atoms at a

point where the electrostatic potential is v. (We suppose that $v=0$ at the surface of the crystal.) In what follows we assume that n_+, n_-, n_i, cN are all small compared with N. We use an affixed ∞ to denote the value of any quantity far from the surface of the crystal. T, e, k are the absolute temperature, the electronic charge and Boltzmann's constant.

If g_+, g_- are the free energies of formation of anion and cation vacancies the vacancy concentrations at a given point are

$$n_+ = N \exp\{-(g_+ - ev)/kT\}$$
$$n_- = N \exp\{-(g_- + ev)/kT\}.$$

The concentration of impurities must, according to Boltzmann's barometric formula, depend on v through a factor $\exp(-ev/kT)$. The constant corresponding to $g_\pm$, however, is indeterminate, since for the present we do not allow impurities to enter or leave the system. But at large distances from the surface n_i must approach the bulk value cN, and so

$$n_i = cN \exp\{-e(v-v_\infty)/kT\}.$$

Similarly n_+^∞ and n_-^∞ must agree with the values deduced neglecting the Lehovec effect. Thus

$$\left.\begin{aligned} n_+^\infty &= N \exp\{-(g_+ - ev_\infty)/kT\} = N\alpha \\ n_-^\infty &= N \exp\{-(g_- + ev_\infty)/kT\} \\ &= n_+^\infty - n_i^\infty = N(\alpha - c) \end{aligned}\right\} \quad . \quad . \quad . \quad . \quad (1)$$

where

$$\alpha = \tfrac{1}{2}c + \{(\tfrac{1}{2}c)^2 + \exp[-(g_+ + g_-)/kT]\}^{1/2}. \quad . \quad . \quad . \quad (2)$$

A derivation of (2) has been given by Lidiard (1957). For our purpose it is enough to note that $\alpha = \exp[-\frac{1}{2}(g_+ + g_-)/kT]$ in the region of intrinsic conductivity but that at low enough temperatures the number of positive-ion vacancies equals the number of divalent impurities, so that $\alpha = c$.

v_∞ is determined by the first equation of (1) which may be put in the form

$$ev_\infty/kT = \ln\alpha + g_+/kT. \quad . \quad . \quad . \quad . \quad . \quad . \quad (3)$$

Thus

$$n_+ = N\alpha \exp p$$
$$n_- = N(\alpha - c) \exp(-p)$$
$$n_i = Nc \exp(-p)$$

where

$$p = e(v - v_\infty)/kT.$$

The charge per unit volume,

$$\rho = -e(n_+ - n_- - n_i) = 2N\alpha \sinh p$$

is related to the potential by Poisson's equation $\nabla^2 v = -4\pi\rho/\epsilon$ where ϵ is the static dielectric constant of the material, and so

$$\nabla^2 p = \kappa^2 \sinh p \quad . \quad . \quad . \quad . \quad . \quad . \quad . \quad (4)$$

where

$$\kappa^2=8\pi e^2 N\alpha/\epsilon kT. \qquad (5)$$

The solution of (4) for the plane boundary has been given by Lehovec (1953). (It occurs also in the theory of colloids : see for example Verwey and Overbeek 1948.) The potential has effectively risen from 0 to v_∞ at a depth κ^{-1} below the surface. (Our κ and Lehovec's characteristic length λ are related by $\kappa\lambda=\sqrt{2}$.) The charge Q on the surface and the field E just inside the crystal are given by

$$Q=-\frac{\epsilon}{4\pi}E=-\frac{2\epsilon\kappa kT}{4\pi e}\sinh\frac{ev_\infty}{2kT}. \qquad (6)$$

The solution for an internal surface is clearly obtained by putting two surface solutions back-to-back. The charge on the internal surface is

$$Q_{\text{int}}=2Q. \qquad (7)$$

§ 3. The Force Required to Move a Charged Dislocation

We consider next the field about a dislocation. We should have to solve (4) in cylindrical coordinates. Unfortunately it is not possible to solve this non-linear equation exactly. If p is small enough for us to replace $\sinh p$ by p the solution is

$$p=AK_0(\kappa r)+BI_0(\kappa r) \qquad (8)$$

where K_0, I_0 are the modified Bessel functions normally so denoted (Watson 1945) ; the equation may also be solved if p is large enough for $\sinh p$ to be replaced by $\frac{1}{2}\exp p$. In any case it is not quite clear what boundary conditions we should impose at the dislocation line, and so we shall use the following argument to find the charge on a dislocation.

Consider a mosaic boundary made up of edge dislocations spaced a distance $h\ll\kappa^{-1}$ apart. Macroscopically the charge per unit area is $2Q$. Microscopically, however, the charge is not uniformly spread, but resides on the dislocations. Thus the charge per unit length of dislocation is

$$\sigma=2Qh. \qquad (9)$$

Let h increase. At first σ increases linearly with h. But when h passes through the value κ^{-1} the charge clouds of the dislocations will no longer overlap and the dislocations are effectively independent. Thus it seems reasonable to suppose that the charge on an isolated dislocation is given by (9) with h set equal to κ^{-1} times a numerical constant near to unity. If we take this constant to be unity the charge on an isolated dislocation is

$$\sigma=2Q/\kappa. \qquad (10)$$

For lack of the precise solution of (3) we use (8) to find the field surrounding the dislocation. If the field is to fall off with distance the term in I_0 must be rejected. The charge on the dislocation is then

$$\sigma=-\lim_{r\to 0}\frac{\epsilon}{4\pi}.2\pi r\frac{dv}{dr}=\frac{\epsilon AkT}{2e}$$

using the relations

$$K_0'(x) = -K_1(x), \quad \lim_{x \to 0} xK_1(x) = 1. \qquad (11)$$

Comparing with (8) we have

$$v - v_\infty = (2\sigma/\epsilon)K_0(\kappa r).$$

The potential due to the line-charge on the dislocation is

$$-(2\sigma/\epsilon)\ln r + \text{const.}$$

and so that due to the charge cloud surrounding it is

$$v_{\text{cloud}} = (2\sigma/\epsilon)[K_0(\kappa r) + \ln(\kappa r)] + \text{const.}$$

Fig. 2

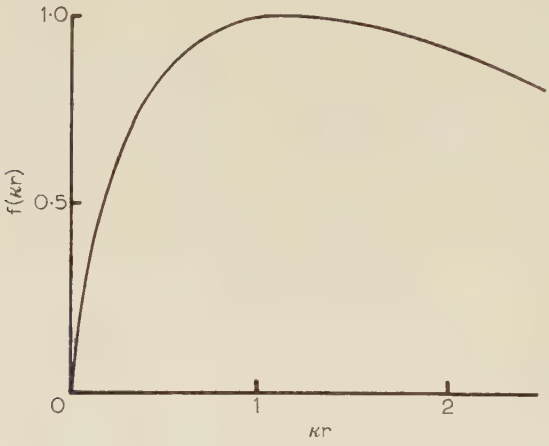

The restoring force on a charged dislocation.

If the dislocation moves a distance r from the centre of the cloud, the cloud remaining fixed, it is subject to a force

$$F = -\sigma \frac{d}{dr} v_{\text{cloud}}$$

$$= (2\sigma^2\kappa/\epsilon)[K_1(\kappa r) - (\kappa r)^{-1}]$$

by (11). If the movement is the result of the force $b\tau$ due to the resolved shear stress τ acting on a dislocation with Burgers vector b we must have $F + b\tau = 0$ in equilibrium, or

$$\tau = 0{\cdot}80(\sigma^2\kappa/\epsilon b)f(\kappa r)$$

where $f(x)$ (fig. 2) is the function $x^{\ 1} - K_1(x)$ divided by its maximum value, 0·40, which occurs when $x = 1{\cdot}02$. The shear stress required to pull the dislocation away from its cloud is thus

$$Y = \tau_{\max} = 0{\cdot}80\sigma^2\kappa/\epsilon b. \qquad (12)$$

We shall suppose that g_+ and g_- are represented adequately by the linear functions of temperature

$$\left.\begin{aligned} g_+(T)&=g_+^0-kT\ln A_+ \\ g_-(T)&=g_-^0-kT\ln A_- \end{aligned}\right\} \quad . \quad . \quad . \quad . \quad . \quad . \quad (13)$$

so that in the intrinsic conductivity range

$$\alpha=(A_+A_-)^{1/2}\exp\{-\tfrac{1}{2}(g_+^0+g_-^0)/kT\}.$$

It is convenient to introduce in addition the quantity

$$\alpha'=\exp(-g_+/kT)=A_+\exp(-g_+^0/kT). \quad . \quad . \quad . \quad (14)$$

Evidently α' is the concentration of positive-ion vacancies which we should infer if we neglected the presence of impurities and also the requirement of bulk neutrality. We may call it the ' naive ' concentration.

Figure 3 (*a*) illustrates how v_∞ varies with temperature. As a function of $1/kT$ the curve $\ln\alpha'$ is of uniform slope $-g_+^0$. The curve $\ln\alpha$ has the constant value $\ln c$ in the impurity conduction range, and changes over to a line of slope $-\frac{1}{2}(g_+^0+g_-^0)$ in the intrinsic range. According to (3) ev_∞/kT is numerically equal to the vertical distance between the $\ln\alpha'$ and $\ln\alpha$ curves, and is positive where $\ln\alpha'$ is uppermost. At a certain temperature T_a the two curves intersect and v_∞ is zero. Following the usage in colloid theory we shall call such a temperature an isoelectric temperature. At T_a the charge on a surface or dislocation (eqns. (6) and (10)) is zero and, according to (12), the yield stress Y vanishes as shown schematically in the lower part of fig. 3 (*a*). In fact at an isoelectric point the naive and true vacancy concentrations coincide and the neglect of electrostatic effects is justified. If T_a lies in the impurity conduction range its value is

$$T_a=g_+/k\ln(c^{-1}).$$

Even in the absence of vacancies the two curves may intersect at high temperatures provided $g_+^0<g_-^0$ and $A_+<A_-$. At such an ' intrinsic ' isoelectric point $g_+=g_-$ (eqn. (13)), that is, the naive concentration of negative vacancies has just caught up with the naive concentration of positive vacancies. The position of the intrinsic isolectric point will be altered by the presence of impurities since α approaches

$$\tfrac{1}{2}c+\{(\tfrac{1}{2}c)^2+A_+A_-\}^{1/2}$$

rather than $(A_+A_-)^{1/2}$ at infinite temperature.

We have supposed above that the impurity concentration c remains constant throughout the impurity range. In fact, if the heat of solution of the impurity is positive it will precipitate out in a new phase at low temperatures (provided equilibrium is attained) and we shall have

$$c=A\exp(-B/kT) \quad . \quad . \quad . \quad . \quad . \quad . \quad (15)$$

with nearly constant A and B. As the temperature rises (15) will reach

a value $c=c_0$ at which all the precipitate is re-dissolved and at higher temperatures c will remain at the value c_0. Thus in the impurity range, at low temperatures, the $\ln \alpha$ curve will have a sharp knee and will intersect or fail to intersect the $\ln \alpha'$ curve in one of the ways indicated in fig. 3 (*b*) according to the particular values of g_+, B, A_+, A. Two of

Fig. 3

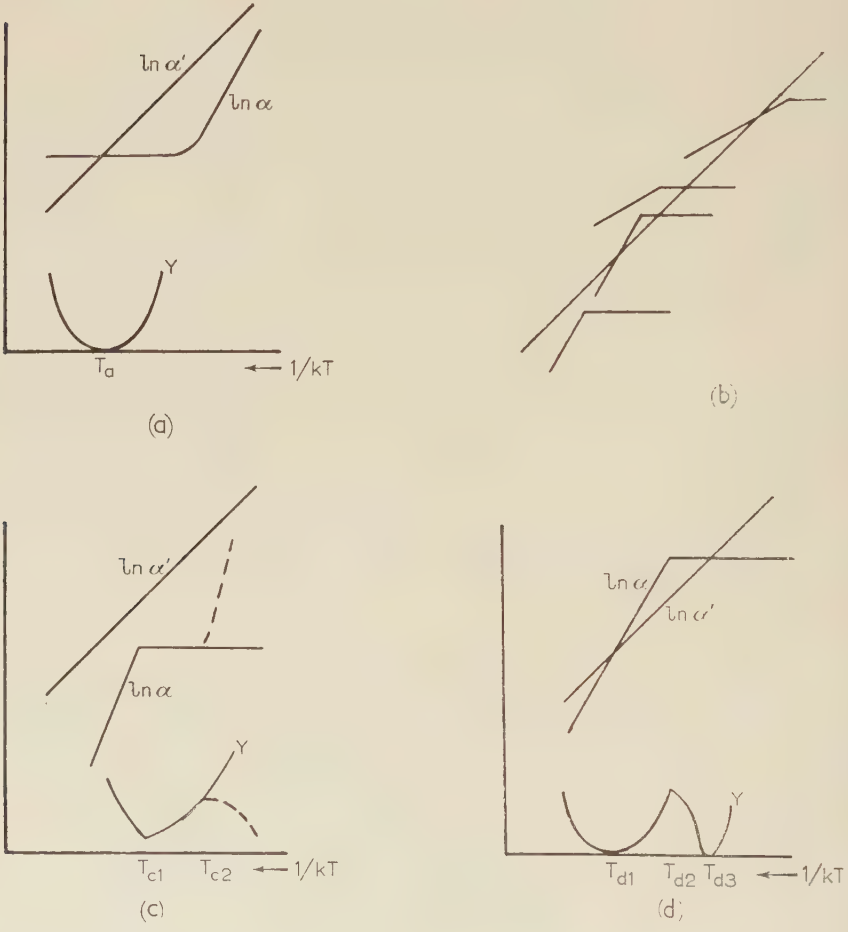

these possibilities are shown in greater detail in fig. 3 (*c*), (*d*) together with qualitative sketches of the behaviour of the yield stress. In fig. 3 (*d*) there are two isoelectric points T_{d1} and T_{d3} and a maximum in Y at T_{d2}. (Since (12) is dominated by the behaviour of the hyperbolic sine the maxima of $| ev_\infty/kT |$ and Y will very nearly coincide.) In fig. 3 (*c*) there is a minimum in the yield stress at T_{c1}. (We ignore the dotted

curves for the present.) The values

$$T_{d1}=(B-g_+)/k \ln A$$

$$T_{d3}=g_+/k \ln (c_0^{-1})$$

$$T_{d2}=T_{c1}=B/k \ln (A/c_0)$$

are easily verified : the position of the maximum or minimum is independent of g_+. If there were a number of impurities with different values of A, B, c_0 the $\ln \alpha$ curve could in principle have a complicated zigzag shape and give rise to a succession of isoelectric points and maxima and minima.

There is also the possibility that vacancies and impurities may associate at low temperatures (Lidiard 1954). As in the case of precipitation this will lead to a fall in the $\ln \alpha$ curve below a certain temperature, but the knee at T_{c1} or T_{d2} will be smooth instead of abrupt, and the change of slope small.

§ 4. The Values of g_+ and g_-

In most problems relating to Schottky defects in ionic crystals (conductivity, diffusion) it is sufficient to know only the sum g_++g_- of the free energies of formation, since it is this sum which determines the bulk concentration of defects. However, in order to predict yield stresses from eqn. (12) it is necessary to know the values of g_+ and g_- individually. Moreover, we have implicitly assumed that the values of g_+ and g_- for the formation of vacancies at a surface are still appropriate when the vacancies are formed at a dislocation, and this assumption evidently needs examination.

It is clear that if dislocations are supposed to be in thermal equilibrium in a crystal g_++g_- for a dislocation must be equal to g_++g_- for a surface, since otherwise Schottky defects would distil over from one to the other. We can establish the equality more directly with the help of an imaginary experiment. Consider a crystal containing, say, a single edge dislocation. We have to show that no work is required to transfer an Na–Cl pair from a jog on the dislocation to a kink in a step on the external surface. Cleave the crystal in two along a plane containing the dislocation line. This will require the expenditure of a certain amount of work. If the plane is suitably chosen one of the new surfaces formed will be flat, and the other will be flat except for a single step representing the termination of the extra half-plane of Na–Cl pairs associated with the dislocation. Transfer an Na–Cl pair from a kink in this step (formerly a jog on the dislocation) to a kink in a step on the external surface. This requires no work. If the halves of the crystal are now joined together again the work expended in cleaving is recovered.

This argument cannot be applied to the transfer of a single ion, since the transfer is not a ' repeatable step ' which leaves the physical state of the crystal unchanged. Thus we cannot infer that g_+ for the dislocation

is the same as g_+ for the surface. Strictly speaking even the transfer of a neutral pair shifts the position of a jog and alters the form of the dislocation and its relation to the free surface, so that the energies of cleaving and re-assembling do not exactly balance. The difference, negligible in the present context, provides a driving force which tends to make the dislocation climb out of the crystal.

Etzel and Maurer's (1950) experiments give the value

$$\alpha = 5{\cdot}2 \exp\{-1{\cdot}01 \text{ ev}/kT\} \quad . \quad . \quad . \quad . \quad (16)$$

for the concentration of Schottky defects in the intrinsic range. Thus (cf. eqn. (13))

$$g_+^0 + g_-^0 = 2{\cdot}02 \text{ ev}$$

and $A_+A_- = (5{\cdot}2)^2$. It is reasonable to suppose that the frequency of vibration of an ion bordering a vacancy is reduced whether the vacancy is positive or negative. In this case both A_+ and A_- are greater than unity and

$$1 < A_+ = 5{\cdot}2/A_- < 5{\cdot}2. \quad . \quad . \quad . \quad . \quad . \quad (17)$$

This means that $g_\pm$ at room temperature can differ from $g_\pm = g_\pm^0$ at 0°K by a tenth of an electron-volt or so (compare (13)).

The calculations of Mott and Littleton (1938) and their later modifications are mainly aimed at finding the sum $g_+^0 + g_-^0$ which determines the bulk concentration of defects. The separate energies, g_+', g_-' say, required to remove a positive or a negative ion from the bulk of the crystal are found during the course of the calculation. When a positive–negative pair is replaced on the surface of the crystal or a dislocation an amount of energy L, the lattice energy per ion pair, is recovered, and so $g_+^0 + g_-^0 = g_+' + g_-' - L$.

In order to find g_+^0 and g_-^0 individually we have to decide what fraction of L is recovered when a positive ion alone or a negative ion alone is replaced on a surface kink or dislocation jog. At first glance we might think that this fraction would be the same for a positive ion as for a negative ion if only Coulomb forces and nearest-neighbour anion–cation repulsive forces were operative. This would give $g_+^0 = g_+' - \frac{1}{2}L$, $g_-^0 = g_-' - \frac{1}{2}L$. This is Lehovec's assumption. In this case it seems more reasonable to use the results of Mott and Littleton or of Brauer (1952), who neglect next-nearest neighbour interactions, rather than those of Bassani and Fumi (1954) who do not. Mott and Littleton's figures give $g_+^0 = 0{\cdot}65$ ev, $g_-^0 = 1{\cdot}21$ ev, Brauer's $g_+^0 = 0{\cdot}70$ ev, $g_-^0 = 1{\cdot}41$ ev. However, the assumption that L is split equally in this way ignores the fact that on adding, say, a positive ion the ionic displacements in the vicinity of the kink or jog change from those appropriate to a negative kink or jog to those for a positive kink or jog : and conversely on addition of a negative ion. This means that the energy gained on adding a positive ion from infinity will be different from that gained on adding a negative ion, in the same way that the different displacements around

positive and negative vacancies make g_+' and g_-' different. Indeed it is possible that this difference is comparable with or even equal to the difference between g_1' and g_2'. In the extreme case g_+^0 and g_-^0 will each be equal to one half the energy of formation of a Schottky pair. Lehovec's assumption corresponds to the opposite extreme where the displacements round a kink or jog are primarily determined by other factors and are not sensitive to the sign of the kink or jog. Evidently without detailed calculations all we can say is that probably g_+^0 lies between 0·6 and 1·0 ev and that the values for surface and dislocation need not be identical.

§ 5. Discussion

As it stands the theory is unlikely to give good numerical results even with the correct values of g_+ and g_-. The replacement of $\sinh p$ by p in (4) is not justified unless

$$|ev_\infty/kT| < 1 \quad . \quad . \quad . \quad . \quad . \quad . \quad . \quad (18)$$

in the case of the plane solution. A similar or more severe restriction will apply to the cylindrical solution. With any reasonable values of the constants (18) is only obeyed within a few tens of degrees on either side of an isoelectric point. Even if the mathematical approximation were adequate outside these regions the high defect concentration which it predicts near a dislocation would require the physical assumptions to be refined. Moreover, in just those regions where the theory is at its best (near an isoelectric point) other hardening mechanisms, masked elsewhere, will prevent the yield stress falling to zero. However, we may hope that the experimental maxima and minima in the yield stress will coincide with the maxima and minima of $|ev_\infty/kT|$. In the present paper we therefore limit ourselves to a tentative comparison of the critical temperatures in figs. 1 and 3.

The points in fig. 1 show the yield stresses of a series of rock-salt specimens measured at various temperatures. The experimental details will be given elsewhere. Briefly, all specimens were cleaved from one large melt-grown single crystal, annealed for half an hour at 650°C, furnace-cooled to room temperature, and finally re-heated and held at the testing temperature for fifteen minutes before measuring the stress–strain curve. The divalent impurity content of the material is unknown, but it is estimated to be one part in 10^6. For brevity we give the labels $\mathbf{M_2}$, $\mathbf{M_1}$ to the maximum and minimum in fig. 1.

If g_+ is less than g_- than $\ln \alpha'$ must be above $\ln \alpha$ at high temperatures. The transition from intrinsic to impurity controlled conduction must then be associated with a maximum in $|ev_\infty/kT|$ (compare the dotted curves in fig. 3 (*c*)). This could perhaps be identified with $\mathrm{M_2}$ if allowance is made for experimental scatter and the uncertainty in the impurity content. Identification of the minimum $\mathrm{M_1}$ with any of the possibilities of fig. 3 enables one to write

$$g_+ = kT_{\mathrm{M_1}} \ln (1/c),$$

c being the free impurity concentration at M_1. We then find that g_+ is less than 0·6 ev unless (locating M_1 at 320 °K) c is less than about 10^{-9}. Even if some of the impurity is precipitated or associated with vacancies such a value would seem unreasonably low. (Compare Haven's (1955) measurements of the solubilities of Ca, Cd and Mn in NaCl.) This line of interpretation therefore leads us to a value of g_+ considerably less than g_-, and which is probably about 0·4 ev. It is interesting to note the agreement with Bassani and Thomson's (1956) value for the binding energy between a dislocation and a positive ion vacancy.

An interpretation based on the alternative starting point that g_+ is greater than g_- cannot be sustained. For we should then have to suppose that the maximum M_2 was associated with the onset of precipitation and that the minimum M_1 represented a crossing of the $\ln \alpha$ and $\ln \alpha'$ lines. For this to occur the heat of solution of the impurities would have to be greater than g_+, i.e. greater than 1 ev, which would be quite inconsistent with the conductivity results.

Thus we may say that comparison of our theory with experimental results on NaCl suggests that g_+ is considerably smaller than g_-, perhaps only a quarter of it. It suggests that the maximum M_2 is associated with the change from impurity-controlled conduction to intrinsic conduction, and that the minimum M_1 is associated with the onset of precipitation of the principal impurities. It would obviously be very interesting to have experimental results for crystals containing known amounts of deliberately added impurities. We should expect a reduction of strength at high temperatures (associated with the increased $\ln \alpha$) with the removal of the maximum to higher temperatures (associated with a higher temperature for the ' knee ' in the $\ln \alpha$ curve) and possibly the appearance of a new minimum at intermediate temperatures.

It is possible, however, that the fall in yield stress above M_2 has another explanation, namely that the charge cloud surrounding a dislocation is mobile enough to move with it at high temperatures. Electrical phenomena on deforming rock salt at various temperatures gives some support to this idea.

If a dislocation moves away from its charge cloud an electric polarization is produced, proportional to the product of charge and distance moved. The movement of charged dislocations should thus give rise to a potential between opposite faces of a crystal, or to a flow of charge between electrodes connected by a low-resistance circuit (Pratt 1957). Plastic deformation is proportional to the distance moved by the dislocations, and so we might at first sight expect proportionality of voltage (or charge) and plastic deformation. However, though the dislocations are all of the same sign electrically, they can have opposite signs mechanically, in the sense that for a dislocation with a given Burgers vector we can always find another with an equal and opposite Burgers vector. Uniform deformation will involve the movement of nearly equal numbers of dislocations with opposite Burgers vectors in opposite directions, and

there will be no large net electrical polarization. In inhomogeneous deformation, on the other hand, a net flow of dislocations of one mechanical sign in the same direction can occur. Marked electrical effects of this type were indeed observed by Fischbach and Nowick (1955) under such conditions.

Caffyn and Goodfellow (1955) observed smaller electrical effects in homogeneously deformed rock salt, and they found, moreover, that the effects decreased with temperature, disappearing altogether above 600°K. This suggests that at high temperatures the cloud follows the dislocation, so that no separation of charge is possible. In a temperature range where defects impeding a dislocation can only just keep up with its motion we may expect to observe a serrated stress-strain curve (compare Cottrell 1953). It is interesting to note that Classen-Nekludowa (1929) observed jerky flow in rock salt at 500°K and above.

We conclude by mentioning some phenomena which might be associated with charged dislocations. Though we have been considering Schottky defects there should be similar effects when Frenkel defects predominate.

By plastic bending it is possible to introduce an excess of dislocations of one mechanical sign into a crystal. A crystal treated in this way should give large charge displacements or voltages when deformed homogeneously. In such a crystal it would also in principle be possible to observe the converse effect, plastic deformation by the ' electrophoretic ' movement of dislocations in an applied electric field.

The movement of a dislocation under stress modifies the elastic constants of a material and, in an alternating stress field, there is a contribution to the mechanical damping. A charged dislocation should make analogous contributions to the dielectric constant and dielectric loss when it moves under the influence of an applied electric field. However, the restoring force which binds a dislocation to the centre of its charge cloud is proportional to $r \ln (1/\kappa r)$ rather than to r when it is given a small displacement r (compare fig. 2). Thus for a charged dislocation these effects, if observable, should be markedly non-linear.

A dislocation is repelled by the charge on a crystal surface or internal mosaic boundary made up of dislocations with spacing less than κ^{-1}. According to (6) and (10) the repulsive force near the wall is $\pi/0{\cdot}80$ or about four times the force necessary to tear a dislocation from its charge cloud. Thus when a dislocation has been pulled away from its charge cloud it may be held up by internal boundaries or the surface of the crystal until the stress is raised somewhat. This only applies when the dislocations in the boundary are closely spaced in comparison with κ^{-1}. If κ^{-1} is small compared with the spacing each dislocation is surrounded by an individual ion cloud which completely screens its charge and electrostatically the boundary offers almost no hindrance to the passage of a dislocation through it. In a crystal with divalent impurities the screening length κ^{-1} drops sharply as we pass from the impurity to the intrinsic conductivity range. According to this model a mosaic boundary

behaves like a Venetian blind, closed to dislocations at low temperatures, but open at high temperatures.

Again, two charged dislocations screened by their charge clouds exert a short-range repulsion on one another. If the dislocations are, say, a distance $r = \frac{1}{2}\kappa^{-1}$ apart the electrostatic force between them is 80% of its unscreened value $2\sigma^2/\epsilon r$. Their elastic fields give rise to a force of the order of $\mu b^2/2\pi r$, where μ is a suitable elastic constant and b is the Burgers vector. These two forces are approximately equal if σ is of the order of one electronic charge per atom plane. Consider, for example, a regular array of edge dislocations forming a vertical tilt boundary. If one dislocation, together with its ion cloud, is displaced out of the plane of the boundary the elastic fields of its neighbours tend to pull it back, but their electric fields tend to repel it further. In some circumstances an energetically reasonable compromise might be for successive dislocations to lie alternately to left and right of the mean plane of the boundary. Such an arrangement has been observed in ionic crystals (Mitchell 1956).

Lehovec (1953) has shown that in a pure NaCl crystal there should be an extra conductivity proportional to the surface area, since in the ion cloud near the surface the concentration of cation vacancies (which carry most of the electrolytic current) is greater than it is in the body of the crystal. His analysis is easily extended to the case where there are mobile divalent impurities. Evidently the concentration of positive-ion vacancies near a surface exceeds or falls short of its bulk value according as v_α is negative or positive. Thus a surface increases the conductivity for temperatures where $\ln \alpha'$ is above $\ln \alpha$ in fig. 3, but decreases it where $\ln \alpha$ is above $\ln \alpha'$. According to the argument leading to (7) and (9), one square centimetre of an internal boundary made up of dislocations spaced more closely than κ^{-1} should affect the conductivity in the same way as two square centimetres of external surface, while an isolated dislocation should be equivalent to a strip of external surface of width $2\kappa^{-1}$.

A number of crystallographic points need further discussion. Charge cannot form on pure screw dislocations. It may be energetically advantageous for a screw dislocation to turn towards edge orientation so that it may build up a charge with its balancing cloud. Again, if a charged segment of dislocation forming a Frank Read source of length l expands into a large loop its original charge will not be spread uniformly over the loop. A simple argument suggests that only a segment of length l will be charged, and that the line joining its centre to the centre of the unexpended Frank–Read source will be parallel to the Burgers vector. Subsequent dislocations from this source will be initially uncharged.

References

Bassani, F., and Fumi, F. G., 1954, *Nuovo Cim.*, **11**, 274.
Bassani, F., and Thomson, R., 1956, *Phys. Rev.*, **102**, 1264.
Brauer, P., 1952, *Z. Naturforsch.*, **7a**, 372.
Caffyn, J. E., and Goodfellow, T. L., 1955, *Nature, Lond.*, **176**, 878.
Classen-Nekludowa, M., 1929, *Z. Phys.*, **55**, 555.

Cottrell, A. H., 1953, *Phil. Mag.*, **44,** 829.
Etzel, H. W., and Maurer, R. J., 1950, *J. chem. Phys.*, **18,** 1003.
Fischbach, D. B., and Nowick, A. S., 1955, *Phys. Rev.*, **98,** 1543.
Frenkel, J., 1946, *Kinetic Theory of Liquids* (Oxford : Clarendon Press), p. 37.
Grimley, T., 1950, *Proc. roy. Soc.* A, **201,** 40.
Grimley, T., and Mott, N. F., 1947, *Disc. Faraday Soc.*, **1,** 3.
Haven, Y., 1955, *Rep. Conf. on Defects in Crystalline Solids* (London : The Physical Society), p. 261.
Lehovec, K., 1953, *J. chem. Phys.*, **21,** 1123.
Lidiard, A. B., 1954, *Phys. Rev.*, **94,** 29.
Lidiard, A. B., 1957, *Handbuch der Physik*, XX (Berlin : Springer-Verlag), p. 245.
Mitchell, J. E., 1956, *Lake Placid Conference*, to appear.
Mott, N. F., and Littleton, M. J., 1938, *Trans. Faraday Soc.*, **34,** 485.
Pratt, P. L., 1957, *Inst. Metals Monograph and Report Series*, **23,** 99.
Verwey, E. J. W., and Overbeek, J. Th. Q., 1948, *The Theory of Lyophobic Colloids* (Amsterdam : Elsevier).
Watson, G. N., 1945, *Bessel Functions* (Cambridge : University Press), p. 77.

The Decay of Long-Lived Holmium 166†

By M. A. Grace, R. T. Taylor‡ and P. B. Treacy
The Clarendon Laboratory, Oxford

[Received October 11, 1957]

Abstract

The decay of long-lived ^{166}Ho is discussed and results are given which suggest that the 817 and 718 kev γ-rays are each in competition with separate cascade pairs of energies 537 + 280 kev and 438 + 280 kev respectively. A level scheme is proposed consistent with the existence of a low lying rotational spectrum in the product nucleus ^{166}Er.

§ 1. Introduction

Irradiation of holmium in the pile leads to the formation of two holmium activities attributed to the ground state and an isomeric state of ^{166}Ho. The short-lived state of 27 hr half-life decays by β emission with the excitation of a number of states in ^{166}Er including the first excited state at 80 kev: an exhaustive study of this mode of decay of ^{166}Ho has been made by Graham, Wolfson and Clark (1955) and the state of 80 kev in ^{166}Er has been identified as 2^+. The decay of the state of ^{166}Ho with a half-life greater than 30 years has been studied by Milton *et al.* (1955) who showed that the β decay was accompanied by γ-rays of energies 845, 725, 282, 184 and 80 kev. Coincidence measurements suggested that these were emitted in a single cascade.

The work described in the present paper was started as part of a programme of experiments on the alignment of the rare-earth nuclei, with a view to determining the magnetic moment of long-lived ^{166}Ho and also to gaining further information on its decay scheme. In order to interpret such an experiment unambiguously, it is necessary first to know the decay scheme of the nucleus involved, including, if possible, the spins of the levels and the multipolarities of the γ-rays (see for instance Blin-Stoyle and Grace 1957). A preliminary study of this isotope confirmed the presence of the five γ-rays found by Milton *et al.* but led us to believe that the decay scheme differed significantly from that proposed by them. It was decided to use scintillation counters to investigate the γ-ray spectra in coincidence and to extend the previous

† Communicated by the Authors.

‡ Now at the Randall Laboratory of Physics, University of Michigan, Ann Arbor, Michigan, U.S.A.

work to include a study of summation peaks and of angular correlations so as to obtain an unambiguous decay scheme and if possible to limit the possible spin assignments of the levels.

§ 2. Gamma-Ray Spectra

A specimen of 200 mg of ' Specpure ' Ho_2O_3 was irradiated for 12 days in the A.E.R.E. pile at a neutron flux of $1{\cdot}4\times10^{12}$ neutrons/cm^2/sec. When the short-lived activity had been allowed to decay out a source of approximately one microcurie of ^{166}Ho was obtained : such a yield is concordant with that obtained by Milton *et al.* A spectrum of γ-rays from this source in ' good ' geometry is shown in fig. 1. This was obtained

Fig. 1

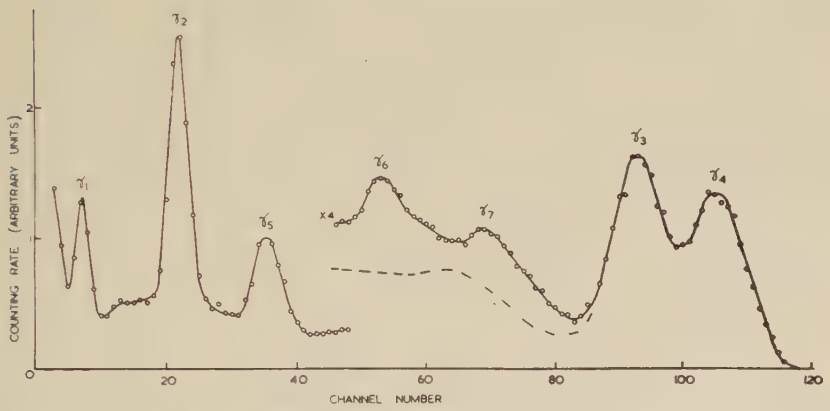

Spectrum of γ-rays from ^{166}Ho recorded with a 2 in.$\times$2 in. NaI (Tl) crystal. For meaning of symbols γ_1, etc. see fig. 4.

with the source 12 in. from a 2 in. diameter$\times$2 in. high NaI (Tl) crystal (Harshaw) fitted to an E.M.I. type 6097 F photomultiplier. This instrument gives a resolution of about 8% for γ-rays of 840 kev. The spectrum was recorded on a 120-channel kicksorter of the Scarrott–Hutchinson type. The γ-ray spectrum remained sensibly unaltered over the period of a year and therefore if any contamination was present it must have been of half-life long compared with this. Although no chemical purification of the source was carried out the close resemblance between our spectrum and that of Milton *et al.* (who did carry out a chemical separation) leads us to believe that our source was effectively pure.

The energies of the γ-ray peaks (γ_1 etc.) are shown in the table and include the five γ-rays already known. These energies were determined using standard sources of ^{54}Mn, ^{137}Cs and ^{203}Hg of energies assumed to be 840, 662 and 283 kev respectively. Also shown are the relative intensities which were estimated using calculated absorption coefficients

for NaI and graphical estimates of observed ' peak-to-total ' values for these three sources.

These results show clearly that the 280 kev γ-ray is weaker than the other four. It should also be pointed out that the weak peaks revealed at 438 and 537 kev cannot be attributed entirely to Compton effect: the broken curve shown under them represents an attempt to estimate the latter, using the data from the calibration sources.

Because of the difficulty in interpreting the 280 kev γ-ray as part of the main cascade, it was thought desirable to study the formation of ' sum ' peaks to determine the total energy liberated in the decay chain.

Gamma Rays from the Decay of ^{166}Ho

Label	Our value of γ-ray energy (kev)	Milton *et al.*'s value of γ-ray energy (kev)	Adopted value of γ-ray energy (kev)	Relative intensity of γ-ray peaks		
				Ungated	Gated on γ_4	Gated on γ_3
γ_1	80 ± 3	$80{\cdot}3\pm2$ †	$80{\cdot}3\pm2$	1·1	—	—
γ_2	183 ± 5	184 ± 1 †	184 ± 1	1·0	1·0	1·0
γ_3	718 ± 10	725 ± 20	718 ± 10	1·0	0·8	—
γ_4	817 ± 10	845 ± 20	817 ± 10	1·0	—	0·8
γ_5	277 ± 5	282 ± 4	280 ± 3	0·3 ‡	0·15 ‡	0·15 ‡
γ_6	410 ± 15	—	438	(0·1)	(0·2)	—
γ_7	528 ± 15	—	537	(0·1)	—	(0·1)

† From β-spectrometer measurements by Graham and Clark (1955).
‡ Not corrected for internal conversion of γ_5.

The spectrum due to a 0·01 μc source in contact with a 4 in $\times$ 4 in. crystal is shown in fig. 2. Sum peaks are seen corresponding to the main γ-rays but there is no evidence for one corresponding to the simultaneous capture of the 817, 718, 280 and 184 kev γ-rays (the 80 kev γ-ray contribution is expected to be difficult to observe because of its low energy and internal conversion). The intensity of this total energy peak is less than 2% of that predicted. Since both the ' gated ' spectrum described in § 3 and the sum peak measurements were made with approximately the same resolving time (2 μsec) a finite lifetime to one of these states could not account for the absence of a sum peak. We therefore conclude that the decay scheme cannot consist merely of a single cascade chain. On the other hand it is clear that the 817, 718 and 184 kev γ-rays are in cascade.

Using the 4 in $\times$ 4 in. crystal in ' good ' geometry, an attempt was made to detect γ-rays of energies greater than 817 kev. No peaks corresponding to cross-over transitions were observed with an intensity greater than 1% of the 817 kev γ-rays.

Fig. 2

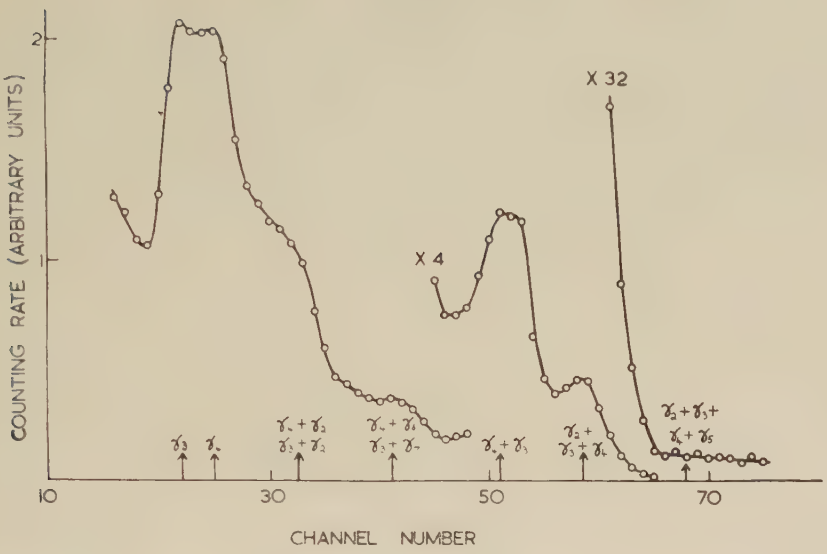

Spectrum of γ-rays from ^{166}Ho showing sum peaks under conditions of poor geometry, recorded with a 4 in. $\times$ 4 in. NaI (Tl) crystal.

Fig. 3

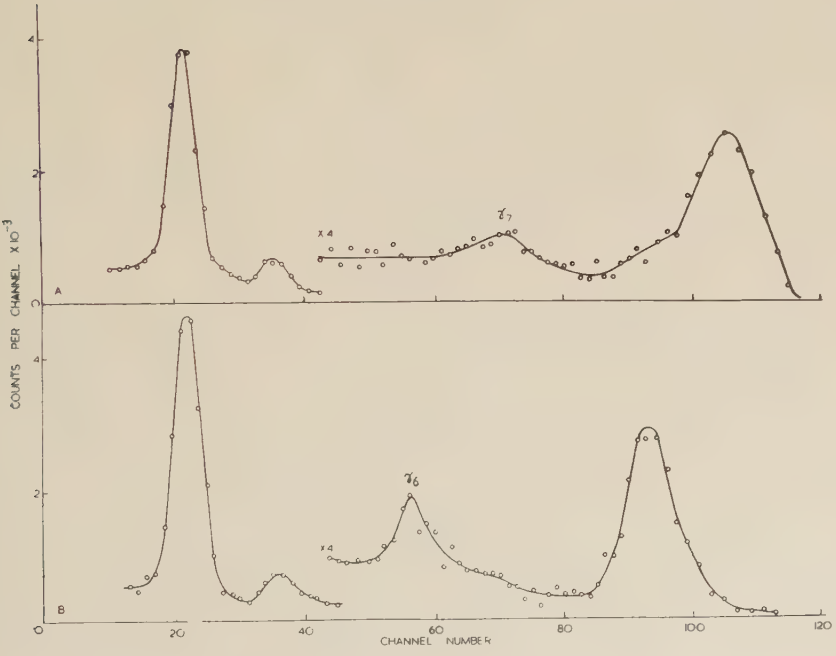

Spectrum of γ-rays in coincidence with (A) γ_3, and (B) γ_4.

§ 3. Coincidence Experiments

The coincidence measurements were made with a pair of scintillation counters fitted with 2 in. crystals at a distance of 3 in. from the source. The output from one was fed through a single channel pulse height analyser, the output of which was used to gate a multichannel instrument which recorded the spectrum from the second counter. The results of spectra gated on the 718 and 817 kev peaks are shown in fig. 3 : the intensities of the peaks are given in the table. Again it is evident that the 817 and 718 and 184 kev γ-rays are in coincidence and that there is in each gated spectrum a γ-ray of energy about 280 kev with about half the intensity of that in the ungated spectrum. Such a behaviour has been noted by Milton *et al.* (private communication). In our gated spectra there is no significant difference between the energies of the two ' 280 kev ' γ-rays observed. However, the fact that peaks at 438 and 537 kev appear in coincidence with those at 817 and 718 kev respectively suggests that the 280+438 kev and 280+537 kev groups are associated with the corresponding cross-over γ-rays of 718 and 817 kev.

Angular correlation measurements showed that the 718–817 and the 718–184 cascades were isotropic to within 1% and 5% respectively. For the 817–184 pair, measurements were made at 90°, 135°, 180°, 225° and 270° and the angular correlation can be fitted by the function:

$$W(\theta)=1+A_2P_2(\cos\theta)+A_4P_4(\cos\theta),$$

with $A_2=-0{\cdot}19\pm0{\cdot}06$ and $A_4=0{\cdot}01\pm0{\cdot}06$. Such an angular correlation is not unique and does not permit an unambiguous assignment of spins to the levels involved.

§ 4. Discussion

The decay scheme of fig. 4 incorporates the idea of a pair of cascade transitions by-passing the 718 and 817 kev γ-rays and appears to offer the simplest explanation to the observed discrepancies in the hypothesis of a straight cascade, namely :

(i) The absence of a sum peak of a total energy of 2000 kev, although a strong peak of 1720 kev exists.

(ii) The existence of γ-rays at 438 and 537 kev whose total intensity approximates to that of the 280 kev γ-ray.

(iii) The apparent reduction in intensity of the 280 kev γ-ray in the ' ungated ' as compared with the ' gated ' spectrum.

The present evidence is insufficient to determine the sequence of the 718 and 817 kev γ-rays, and similarly ambiguity exists as regards the intermediate level positions for the cascade transitions. Other possible explanations for these observations have been considered but the present scheme seems to offer the most straightforward key to the disintegration scheme.

If it is assumed that the transitions involve no higher multipoles than quadrupole then some limitations can be put on the level spins. From the angular correlation measurements of Milton *et al.*, I_2 must be 4 and the energies of the γ-rays strongly suggest that I_3 is the third member of the rotational sequence built up on this ground state with spin 6^+. Since none of the angular correlations we have observed is of the type $(J+4 \rightarrow J+2 \rightarrow J)$ we know that I_4 cannot be 6. In view of the transitions to the two members of the rotational sequence I_2, I_3 and not to

Fig. 4

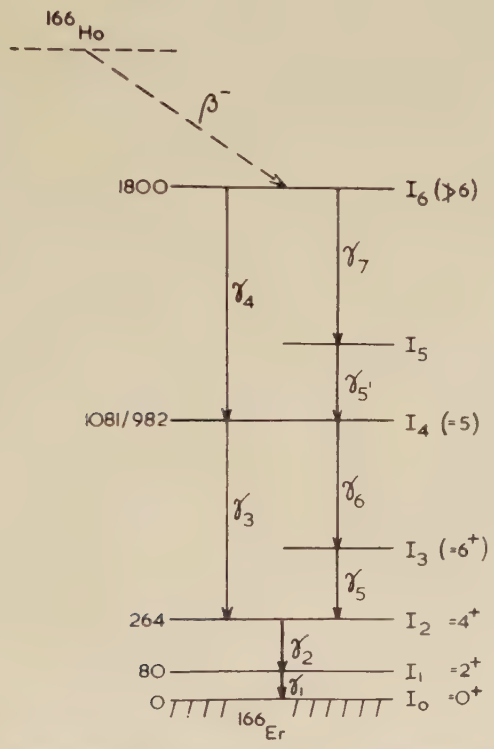

Proposed decay scheme for ^{166}Ho $(\beta^-)^{166}$Er. Energies shown are in kev.

I_1 it seems probable that I_4 is 5. By admixing a small quadrupole constituent in the principally dipole transition, agreement can be obtained with either of the observed correlations with γ_2. Again, allowing a possible small quadruple admixture in γ_3, the observed correlation γ_2–γ_4 is not consistent with the unique result which must occur were I_6 greater than 6. Approximate equality in the excitation of the different states I_2, I_4, I_6 shows that the majority of the transitions proceed through the state I_6. In order to account for this, it is suggested that both ^{166}Ho and the level I_6 possess odd parity and that the parity of the lower states in ^{166}Er are all even.

Acknowledgments

It is a pleasure to acknowledge the generous way in which the Chalk River Laboratory Group and especially Dr. J. C. D. Milton have sent us the results and discussion of their work prior to publication.

This work was supported financially for two of us by the Department of Scientific and Industrial Research (R. T. T.) and the Australian National University (P. B. T.).

References

Blin-Stoyle, R. J., and Grace, M. A., 1957, *Handbuch der Physik*, Volume 42 (Berlin : Springer-Verlag).

Graham, R. L., and Clark, M. A., 1955, *Phys. Rev.*, **98**, 1173.

Graham, R. L., Wolfson, J. L., and Clark, M. A., 1955 (quoted by J. C. D. Milton, personal communication).

Milton, J. C. D., Fraser, J. S., and Milton, G. M., 1955, *Phys. Rev.*, **98**, 1173.

The Observation of Vacancy Sources in Metals†

By R. S. Barnes, G. B. Redding and A. H. Cottrell
Atomic Energy Research Establishment, Harwell

[Received September 30, 1957]

Abstract

Helium atoms have been injected into copper by alpha-particle bombardment in a cyclotron. On subsequent heating, the helium precipitates out as small gas bubbles in those parts of the metal where the helium atoms receive vacancies from nearby sources. From the distribution of the gas bubbles it is concluded that grain boundaries are effective sources of vacancies, but twin boundaries are not. Isolated sources of vacancies exist within the crystals, but there is no evidence that the dislocation network generates appreciable numbers of vacancies.

§ 1. Introduction

When the temperature of a crystalline solid is increased the equilibrium number of vacancies in it increases steeply. In most metals these vacancies cannot originate by vacancy-interstitial pair creation in the perfect lattice because the energy of formation of an interstitial is much higher than that of a vacancy. The vacancies must enter good regions of the crystal from various sources, for example, grain boundaries, subgrain boundaries, dislocations, and free surfaces, where it is not necessary to form interstitials with vacancies. Evidence for such sources has previously been indirect, depending for example on observations of voids formed during the interdiffusion of two metals (Balluffi and Alexander 1952, Barnes 1952, Bückle and Blin 1952, Seith and Kottmann 1952).

In the experiment described below we have developed a method for locating vacancy sources in a metal and for observing, on a microscopic but not atomic scale, these sources in operation. Helium atoms are first injected into the metal by bombardment with alpha-particles. On subsequent heating, these atoms attempt to precipitate within the metal in the form of gas bubbles, and to acquire the extra space necessary for this they capture large numbers of vacancies. Thus a blanket of bubbles forms in the regions of the metal immediately accessible to vacancies from the sources, but until these bubbles have become sated with vacancies, no bubbles are formed in the remaining regions, which they blanket.

† Communicated by the Authors.

§ 2. Method and Results

Johnson–Matthey spectroscopically standardized copper was bombarded with 30 MeV (approximately) alpha-particles from the Birmingham cyclotron until 2·5 kw hr had been dissipated in it. This is estimated to have deposited helium to a concentration of 1 atm% in a band of metal about 0·003 cm thick lying at a depth of 0·12 cm below the bombarded face of the specimen. Being brazed to a water-cooled copper target holder, the specimen did not heat above 200°C during the irradiation. After allowing the radioactivity to decay, pieces were cut from the specimen and individually heat-treated. Each piece was then polished, mechanically and electrolytically, and examined microscopically.

Those pieces not heated after bombardment showed no bubbles. Only after heating to 650°C for 1 hour did bubbles first appear, and then only in localized regions. Figure 1, Pl. 4 shows a section cut perpendicularly through the band of helium, taken from a specimen heated at 750°C for 1 hour *in vacuo*. The gas bubbles are localized in regions which appear dark and which occur (*a*) where grain boundaries cross the band, (*b*) on the periphery of the band, and (*c*) as small circular islands within the band. Electron micrographs of two-stage carbon replicas taken from the surface show that individual bubbles are less than 2×10^{-5} cm across. Figure 2, Pl. 4 gives an example showing several islands of bubbles. It will be seen that the bubbles appear to be crystallographic in shape, but it is not yet clear whether this is their natural shape or is a consequence of the electropolishing treatment.

Prolonged heating, particularly at high temperatures, causes the bubbled zones to spread farther out from the vacancy sources until eventually the whole band is uniformly filled with bubbles. This uniformity of the final distribution shows that the process does not occur by the migration of helium atoms to the sources of vacancies. The rate of advance of the bubbled zones is greatest near the periphery of the band, where the concentration of helium is lowest, and least in the centre of the band, where most of the helium is deposited. This is to be expected since, for a given rate of generation of vacancies from a source, the width of the bubbled zone fed by that source should increase at a rate inversely proportional to the concentration of helium present.

These various effects have been observed repeatedly in copper specimens. Preliminary experiments have shown closely similar effects to exist also in beryllium.

Figure 3, Pl. 5, taken from a copper specimen heated to 700°C for 2 hours, is a section almost parallel to the plane of the band. Such a taper section magnifies the width of the band and is more informative. Many coherent twin boundaries are visible and it will be seen that they do not assist the precipitation of the helium atoms. Non-coherent twin boundaries are also visible, particularly in the central grain of the photograph, and it will be seen that these also, when not connected to grain boundaries, do not assist the creation of bubbles. Some single-ended sources of vacancies attached

to grain boundaries are also visible. It is thought from these, and from similar examples seen in other specimens, that they are non-coherent twin boundaries attached to grain boundaries ; and thus that these non-coherent boundaries can accelerate the transport of vacancies but not create them, whereas coherent boundares do not accelerate the transport of vacancies.

§ 3. Discussion

The conclusion that the bubbles grow by the capture of vacancies is based on the peculiar distribution of the bubbled regions in incompletely annealed specimens. Particularly striking is the observation that bubbles form along the edge of the helium band before they form in the centre, despite the concentration of helium being highest in the centre. There is no hindrance to the formation of bubbles along the edge, since these outlying regions of the band are accessible to vacancies arriving from all sources outside the band.

Only two major sources of vacancies within the metal have been positively identified in these experiments ; grain boundaries, and certain sources within the grains which, because they produce bubbled zones that are practically circular in all sections taken through the band, appear to be point sources. The nature of the latter is not clear. They may be small cavities, present in the specimen before heating, which lose vacancies and close up during heating. Or they may be points, such as dislocation nodes, that can emit vacancies provided these vacancies can reach them along suitable channels connecting them to grain boundaries. Certainly, dislocation networks in the crystal, if acting at all as vacancy sources, are not doing so to a significant extent along most of their length.

Acknowledgments

We wish to thank Professor W. E. Burcham and the Birmingham University Cyclotron Group who supervised the bombardment of the specimens, Miss B. C. Woolley of A.E.R.E., Harwell, who took the electron micrograph, and Mr. D. J. Mazey of A.E.R.E., Harwell, who helped with the experimental work.

References

Balluffi, R. W., and Alexander, B. H., 1952, *J. appl. Phys.*, **23**, 953.
Barnes, R. S., 1952, *Proc. phys. Soc. Lond.* B, **65**, 512.
Bückle, H., and Blin, J., 1952, *J. Inst. Metals*, **80**, 385.
Seith, W., and Kottmann, A., 1952, *Z. angew. Chem.*, **64**, 379.

A Note on Stress Pulses in Visco-Elastic Rods†

By D. S. Berry
Research Association of British Rubber Manufacturers,
Shawbury, Shrewsbury

[Received September 24, 1957]

Abstract

This note gives a brief mathematical treatment of the relationship between the transient stress in a semi-infinite visco-elastic rod and the attenuation coefficient and phase velocity as functions of steady state frequency. Except in the case of a delta function stress input, the expression obtained disagrees with Kolsky's result (1956). The reason for the failure of the latter is pointed out.

Under certain conditions, which are usually satisfied, the general solution for the passage of a stress pulse along a semi-infinite visco-elastic rod can be related to the steady state solution. We use the result obtained by Berry and Hunter (1956) by means of Laplace transform methods that the stress at time t at a point distant x from the origin is

$$\sigma(x, t)=\frac{1}{2\pi i}\int_{\gamma-i\infty}^{\gamma+i\infty}\bar{\sigma}(0, s)\exp\left[-\mu(s)x+st\right]ds, \quad x\geqslant 0, \quad t>0, \qquad (1)$$

where

$$\bar{\sigma}(0, s)=\int_0^\infty \sigma(0, t)\exp\left(-st\right)dt$$

and $\mu(s)$ is determined from the equation

$$\mu^2=\rho s^3\int_0^\infty g(t)\exp\left(-st\right)dt \quad . \quad . \quad . \quad . \quad . \quad . \quad (2)$$

so that it is positive when s is real and positive. In this expression ρ is the density of the rod and $g(t)$ is the strain per unit stress at time t after the application of a constant stress. We suppose that the rate of creep at constant stress tends to zero as $t\to\infty$ so that $g(t)$ can be represented by the expression

$$g(t)=a+\int_0^\infty G(\tau)[1-\exp\left(-t/\tau\right]d\tau \quad . \quad . \quad . \quad . \quad . \quad (3)$$

where $G(\tau)$ is an unnormalized distribution function of retardation times of creep (Gross 1953). Substituting this form of $g(t)$ into eqn. (2) we find that

$$\mu^2=\rho s^2\left[a+\int_0^\infty\frac{G(\tau)\,d\tau}{1+s\tau}\right] \quad . \quad . \quad . \quad . \quad . \quad . \quad (4)$$

and it follows that $\mu(s)$ is regular in the half-plane $\Re(s)\geqslant 0$.

---

† Communicated by I. N. Sneddon.

We limit the class of stress pulses applied at the origin to δ-function pulses and finite pulses of finite duration, t_1, say. In the first case $\bar{\sigma}(0, s)$ is a constant, while in the second it is of the form

$$\bar{\sigma}(0, s)=\int_0^{t_1} f(t) \exp(-st)\, dt \quad . \quad . \quad . \quad . \quad . \quad . \quad (5)$$

and is thus regular in $\Re(s)\geqslant 0$. We may then put

$$\bar{\sigma}(0, i\omega)=A(\omega)-iB(\omega) \quad . \quad . \quad . \quad . \quad . \quad . \quad . \quad (6)$$

where $$A(\omega)=\int_0^{t_1} f(t)\cos\omega t\, dt, \quad B(\omega)=\int_0^{t_1} f(t)\sin\omega t\, dt \quad . \quad . \quad (7)$$

$A(\omega)$ and $B(\omega)$ being even and odd functions respectively (constant and zero for a δ-function).

Under the above restrictions the integrand in eqn. (1) is regular in $\Re(s)\geqslant 0$ and γ may be taken as zero. It can be shown from eqn. (4) that the functions $\alpha(\omega)$, $c(\omega)$ defined by

$$\alpha(\omega)=\Re[\mu(i\omega)], \quad c(\omega)=\omega/\Im[\mu(i\omega)] \quad . \quad . \quad . \quad . \quad . \quad (8)$$

are both even, positive functions of ω. Then, introducing the functions (7) and (8) and making a change of variable, the integral (1) may be reduced to the real integral

$$\sigma(x, t)=\frac{1}{\pi}\int_0^{\infty} [A(\omega)\cos\omega(t-x/c)+B(\omega)\sin\omega(t-x/c)]\exp(-\alpha x)\, d\omega. \quad (9)$$

To show that $\alpha(\omega)$ and $c(\omega)$ are the attenuation coefficient and phase velocity, respectively, we consider the stress in the rod due to the imposition of the sinusoidal stress

$$\sigma(0, t)=\sigma_0 \exp(i\omega t)$$

at the origin. Then

$$\bar{\sigma}(0, s)=\sigma_0/(s-i\omega)$$

and, from eqn. (1), we have the result

$$\sigma(x, t)=\frac{\sigma_0}{2\pi i}\int_{\gamma-i\infty}^{\gamma+i\infty}\frac{\exp(-\mu x+st)}{s-i\omega}\, ds. \quad . \quad . \quad . \quad (10)$$

When $\mu(s)$ is defined by eqn. (4), it is not difficult to show, by means of the residue theorem, that as $t\to\infty$ the stress given by eqn. (10) tends to the steady state value

$$\sigma_s(x, t)=\sigma_0 \exp(-\alpha x)\exp[i\omega(t-x/c)]. \quad . \quad . \quad . \quad (11)$$

Kolsky (1956, eqn. (5)) has given an expression for a stress pulse in a visco-elastic rod which consists of twice the first term in the integral (9). Representation of the stress input by a cosine integral alone is not valid since it is then, in effect, an even function of t and a second pulse is implied, originating in a negative interval of time. In eqn. (9), however, half of the applied stress is represented by a sine integral which, being an odd function of t, makes the sum of the two terms zero for $t<0$. When there is a δ-function stress at the origin the two expressions agree so long as the δ-function is defined symmetrically when it is subjected to the Fourier cosine transform and unsymmetrically for the Laplace transform (Sneddon 1955).

It should be noted that the phase velocity $c(\omega)$ is a function of both the real and imaginary parts of the complex modulus $E^*(i\omega)$ (Gross 1953). It is a consequence of eqn. (2) that

$$E^*(i\omega)=E_1(\omega)+iE_2(\omega)=-\frac{\rho\omega^2}{[\mu(i\omega)]^2}, \quad . \quad . \quad . \quad . \quad (12)$$

and it follows by means of eqn. (8) that

$$c^2=\frac{2(E_1{}^2+E_2{}^2)}{\rho[E_1+\sqrt{(E_1{}^2+E_2{}^2)}]}. \quad . \quad . \quad . \quad . \quad . \quad (13)$$

The velocity of propagation of the wave-front, c_1, is readily obtained by considering the integral (1), which is zero if

$$\mathfrak{R}(st-\mu x)\to-\infty \text{ as } |s|\to\infty \text{ in } |\arg s|<\tfrac{1}{2}\pi.$$

We find, using eqn. (4), that

$$1/c_1=\lim_{|s|\to\infty}\mathfrak{R}\,(\mu/s)=\sqrt{(\rho a)}$$

or, from eqns. (8) and (12)

$$c_1=c(\infty)=\sqrt{\frac{E_1(\infty)}{\rho}}. \quad . \quad . \quad . \quad . \quad . \quad . \quad (14)$$

Acknowledgment

The author is indebted to the Council of the Research Association of British Rubber Manufacturers for permission to publish this note.

References

Berry, D. S., and Hunter, S. C., 1956, *J. Mech. Phys. Solids*, **4**, 72.
Gross, B., 1953, *Mathematical Structure of the Theories of Viscoelasticity* (Paris: Hermann).
Kolsky, H., 1956, *Phil. Mag.*, **1**, 693.
Sneddon, I. N., 1955, *Handb. der Physik, Bd. II* (Berlin: Springer), pp. 198–348.

CORRESPONDENCE

Propagation of Dislocations in Electron Irradiated Lithium Fluoride

By A. D. Whapham
Metallurgy Division, A.E.R.E., Harwell, Berks.

[Received October 14, 1957]

A study of the properties of dislocations in irradiated materials is fundamental to an understanding of the effect of irradiation on mechanical properties. The development in recent years of etching techniques which produce etch pits sited at the point of emergence of dislocation lines at the surface of a crystal has provided a useful method of observing dislocations. The 50% hydrofluoric acid, 50% acetic acid and ferric fluoride etch for lithium fluoride, developed by Gilman and Johnston (1956) and used as a tool in the present investigation, is particularly good since it reveals all dislocations, does not seem to depend on impurity atoms and does not require any annealing of the specimen.

Dislocations have been produced in a Harshaw lithium fluoride (100) cleavage face by micro-hardness indentations both before and after irradiation by 1 Mev electrons at a flux of $3\,\mu$ A cm^{-2} for 1 hour. Differences in dislocation behaviour were revealed by subsequent etching and the appearance of the cleavage face after treatment is shown in the figure (Pl. 6). The etching technique worked reliably on the irradiated material. Identations 1 to 4, made before irradiation with a load of about 2 g on the Vickers diamond indenter, produced star patterns of dislocations with arms radiating along the ⟨100⟩ (screw dislocations) and ⟨110⟩ axes (edge dislocations). (These star patterns are essentially the same as those etched before irradiation (not illustrated) showing that no appreciable movement of these dislocations has occurred during the irradiation.) The edge dislocations have been propagated by the stress field to about 4·5 diameters and the screw dislocations to about 3 diameters of the central impression. In the case of indentations 5 to 10 made after irradiation (5, 6, and 7 with 2 g load and 8, 9 and 10 with 10 g) the edge dislocations have only been propagated to about 1 diameter from the centre of the impression while the motion of screw dislocations has been so restricted that no evidence of propagation is seen on the photograph.

It is known that irradiation produces hardening in most materials. In the case of alkali halide crystals this has been shown by Podachewsky (1935) for irradiation with ultra-violet light and x-rays and confirmed in the case of x-irradiation by Pratt (1951). It has been shown also

for fast proton irradiation (Vaughan *et al.* 1953) and for x-irradiation and 1 MEV electron irradiation (Westervelt 1953). In metals neutron irradiation increases the tensile strength and hardness (cf. McReynolds *et al.* (1954) in the case of aluminium, Gieb and Grace (1952) for molybdenum, Kunz and Holden (1954) iron, zinc, Meyer (1954) mild steel and Billington and Siegel (1950) for stainless steels). This hardening can be due either to difficulty of generation or of propagation of dislocations.

In the present work indentation has generated dislocations in the irradiated material (large numbers of dislocations closely clustered around identations 8, 9 and 10 can be clearly seen), but no information about the generation stress is given by the experiment. The experiment proves, however, that the stress for propagation of the dislocations is raised by irradiation since the dislocations produced in irradiated crystal do not glide away from the indentation as readily as those produced before irradiation. Hence irradiation produces lattice friction. The origin of this friction is not known but it may be due to isolated defects or aggregates distributed in the crystal lattice.

It is understood that Gilman (1956) has made a similar study of the propagation of dislocations in neutron irradiated lithium fluoride but, as pointed out by Lomer (1956), complications arise in the interpretation of the results since nuclear disintegration of the lithium occurs when it is bombarded with neutrons. (No such reaction can occur with 1 MEV electrons.)

At present, work is in progress to determine the magnitude of the stress necessary to generate and propagate dislocations in lithium fluoride subjected to various amounts of electron irradiation.

ACKNOWLEDGMENT

The author would like to thank Dr. A. H. Cottrell and Dr. M. J. Makin for helpful discussions of this work.

REFERENCES

BILLINGTON, D. S., and SIEGEL, S., 1950, *Metal Progr.*, **58**, 847.
GEIB, I. G., and GRACE, R. E., 1952, *Phys. Rev.*, **86**, 643.
GILMAN, J. J., 1956, *Discussion*, Lake Placid Conference (A. H. Cottrell, private communication).
GILMAN, J. J., and JOHNSTON, W. G., 1956, *J. appl Phys.*, **27**, 1018.
KUNZ, F. W., and HOLDEN, A. N., 1954, *Acta Metallurgica*, **2**, 816.
LOMER, W. M., 1956, *Discussion*, Lake Placid Conference (A. H. Cottrell, private communication).
MCREYNOLDS, A. W., AUGUSTYNIAK, W., MCKEOWN, W., and ROSENBLATT, D. B., 1954, *Phys. Rev.*, **94**, 1417.
MEYER, R. A., 1954, *J. appl. Phys.*, **25**, 1369.
PODACHEWSKY, M. N., 1935, *Phys. Z. Sowjet.*, **8**, 81.
PRATT, P. L., 1951, *Thesis*, Cambridge University.
VAUGHAN, W. H., LEIVO, W. J., and SMOLUCHOWSKI, R., 1953, *Phys. Rev.*, **91**, 245.
WESTERVELT, D. R., 1953, *Acta Metallurgica*, **1**, 755.

The Half-Life of Thallium 196 and the Multipolarity of the 426 keV Transition in Mercury 196

By G. Andersson, J. O. Burgman and B. Jung
The Gustaf Werner Institute for Nuclear Chemistry, Uppsala, Sweden

[Received October 4, 1957]

In a β-spectrometric investigation of neutron deficient Pb and Tl isotopes, Andersson *et al.* (1955) observed the conversion lines of a 426 kev γ-ray. This was identified as a transition in ^{196}Hg, earlier reported by Staehelin (1952), who studied the decay of ^{196}Au. Further arguments for the assignment were obtained from excitation data and from the non-appearance of the rather strong K-line in the conversion electron spectrum of an electromagnetically separated mass 197 sample. From a number of successive automatically recorded spectra the half-life, which should thus be characteristic of ^{196}Tl, was very preliminary estimated as $\approx$4 hr.

Later the growth and decay of the K-line was more accurately measured (Andersson *et al.* 1957). From a straight line over several half-lives the longer-lived component was determined as $(2{\cdot}4\pm0{\cdot}2)$ hr. Its growth indicated a 35 min parent, which was also consistent with the mass assignment 196, as ^{196}Pb had independently been assigned a 37 min period. Knight and Baker (1955), who used enriched Hg targets to produce Tl-activities, report $\approx$3 hr half-life for ^{196}Tl in acceptable agreement with the value quoted above.

According to Staehelin (1952) the 426 kev transition de-excites the lowest excitation level of ^{196}Hg. It should thus be of pure E2 character, which was supported by the measured conversion coefficients. The K L conversion ratio obtained by Andersson *et al.* (1957), however, indicated a considerable M1 admixture.

We have now reinvestigated the pertinent conversion lines at about $0{\cdot}3\%$ resolution in a double-focusing beta spectrometer (Arbman and Svartholm 1956) using mass separated sources (cf. Andersson 1957). The half-life of the K-line in $A=196$ was measured as $(1{\cdot}8\pm0{\cdot}1)$ hr and the K/L ratio as $2{\cdot}75\pm0{\cdot}28$ in good agreement with the value 2·86 obtained for electric quadrupole radiation by interpolation from Rose's tables (1954–1956).

The cause of the earlier discrepancy was found to be an M1 γ -ray in the decay of 2·7 hr ^{197}Tl, coinciding energetically with the ^{196}Hg transition within the resolving power of the beta spectrometer. In the above-mentioned measurement on $A=197$ (Andersson *et al.* 1955) the sample must have been just weak enough for the K-line not to appear. It should be especially pointed out that ^{197}Tl grows from 42 min ^{197m}Pb, that is, with about the same parent half-life as ^{196}Tl, which explains the result reported by Andersson *et al.* (1957).

The present investigation illustrates the difficulties encountered in nuclear spectroscopic work on mixtures of several nuclides and emphasizes the importance of mass separated samples.

References

Andersson, G., Arbman, E., Bergström, I., and Wapstra, A. H., 1955, *Phil. Mag.*, **46,** 70.

Andersson, G., Arbman, E., and Jung, B., 1957, *Arkiv Fysik*, **11,** 297.

Andersson, G., 1957, *Arkiv Fysik*, **12,** 331.

Arbman, E. and Svartholm, N., 1956, *Arkiv Fysik*, **10,** 1.

Knight, J. D., and Baker, E. W., 1955, *Phys. Rev.*, **100,** 1334.

Rose, M. E., Goertzel, G. H., and Swift, C., 1954–1956, privately distributed tables.

Staehelin, P., 1952, *Phys. Rev.*, **87,** 374.

REVIEWS OF BOOKS

Light Scattering by Small Particles. By H. C. van de Hulst. (London : John Wiley and Sons. Inc.) [Pp. xiii+470.] 96*s*.

Many current scientific investigations depend upon the observation and interpretation of the scattering of electromagnetic radiation by small particles. These range from particles of colloidal metal in solid and liquid suspension through spherical water particles and ice crystals in the atmosphere to the particles of planetary atmospheres and of the dust clouds of interstellar space. In all these investigations the Mie theory based on the rigorous solution of Maxwell's equations for the scattering of a plane wave by a homogeneous sphere is of primary importance. There is, however, a wide gulf between the formal solutions of the equations, which lead to complicated formulae, and practical applications : the average experimental worker has difficulty even in applying the mass of tabulated numerical data which is now available on account of the pitfalls of interpolation.

Professor Hulst gives an exhaustive treatment of the Mie theory for scattering by spheres over the whole range of sizes. The functions which are most needed for the interpretation of experimental observations on Raleigh scattering, Rayleigh–Gans scattering, scattering by large dielectric spheres and by reflecting metallic spheres are presented in graphical and in tabular numerical form. A detailed account is given of the best methods to be followed for obtaining numerical results and valuable suggestions are made for reliable interpolation in the published tables. Throughout the book emphasis is laid on the discussion of the physical significance of the mathematical results.

Although the book is mainly concerned with the Mie theory, there is an adequate account of other treatments and of light scattering by particles of non-spherical form. An interesting review of the author's own work on atmospheric phenomena including the theory of the glory or Brocken spectre is included.

Part III of the book, which will be of great value to physicists, meteorologists, astronomers and chemists, is concerned with practical applications. There is a useful discussion of the properties of particles which may be investigated by observations of light scattering, of the measurements which should be made, and of the information about the scattering particles which can be deduced from them. J. W. M.

High Energy Physics : Proceedings of the Seventh Annual Rochester Conference. Edited by R. G. Sachs. (New York : Interscience Publishers Inc.) [Pp. 482.] $4.50

The annual Rochester report is an invaluable guide to the present state of high-energy physics in the days of a literature too vast for anyone to cover. The introductory surveys to the eleven sessions take up over a third of it, and enable any nuclear physicist to understand the current problems and the work towards their solution presented by the specialists in the remainder of the report. This year's report comes when there is a pause in the flow of the subject, as last year's did not, and is thus more useful as a reference work. Electromagnetic investigations into the structure of the nucleon, the role of the dispersion relations in pion physics and the extent of their mathematical vigour, the phase-shift analysis of nucleon–nucleon scattering and our understanding of the parity puzzles can now all be summarized in a reasonably compact form. Data are also being steadily accumulated in the less familiar fields of extremely high-energy cosmic rays and reactions involving antiprotons and strange particles, particularly on the interaction between nucleons and K mesons.

A change of typewriter has improved the legibility, and photographs and more complicated diagrams can now be reproduced. D. J. C.

The Detection and Measurement of Infra-red Radiation. By R. A. Smith, F. E. Jones, and R. P. Chasmar. (Oxford University Press, 1957). [Pp. xiii+458.] 70*s*.

The major part of this book (about 250 pp.) is concerned with the detectors of infra-red radiation. Particular care has been taken to relate the actual performance of the various types of thermal and quantum detectors to ultimate limits set by fundamental physical principles. For the first time the science (as opposed to the art) of infra-red detection has been presented in book form and this is likely to remain the standard work on the subject for a considerable time.

Another main section (about 140 pp.) deals with other experimental techniques used in the infra-red region. Here the treatment is uneven. Some chapters are very good but, for example, that on the design and performance of infra-red spectrometers is rather brief. It is a pity that no theoretical account has been attempted of the performance of a spectrometer *as a whole* in the case—common in the infra-red region—of an energy limited instrument. The reader of this book could not then have been left with the impression (possibly unintended) that diffraction grating spectrometers are used only when the higher resolution is required. Many are now being produced commercially which will mostly be used to give higher intensity spectra (better signal–noise ratio) than the more usual prism instruments.

The publication of this book seems to have been rather slow for important and not very recent topics such as the indium antimonide photoconductive cell and F-centre filters are not mentioned. However, these are minor points of criticism. This book is an important addition to the infra-red literature.

N. S.

BOOK NOTICES

Solid State Physics. Advances in Research and Applications. Vol. 4. Edited by Frederick Seitz and David Turnbull. (London: Academic Books Ltd.) [Pp. xiv+540.] $12.00

The fourth volume of this useful series contains the following articles:

"Ferroelectric and Antiferroelectrics" by Werner Känzig (General Electric Research Laboratory, New York).

"Theory of Mobility of Electrons in Solids" by Frank J. Blatt (Michigan State University).

"The Orthogonalized Plane-Wave Method" by Truman O. Woodruff (General Electric Research Laboratory, New York).

"Bibliography of Atomic Wave Functions" by Robert S. Knox (University of Rochester); and

"Techniques of Zone Melting and Crystal Growing" by W. G. Pfann (Bell Telephone Laboratories).

N. F. M.

[The Editors do not hold themselves responsible for the views expressed by their correspondents.]

Fig. 1

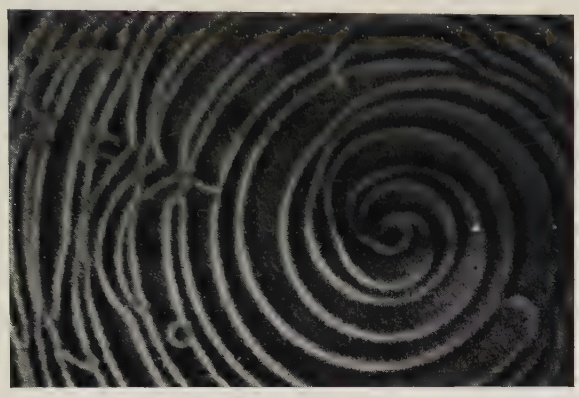

(*a*) ×500

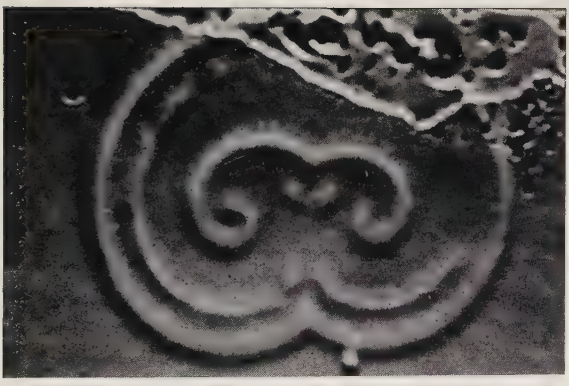

(*b*) ×1000

Etched zinc single crystal—surface parallel to basal plane.

Fig. 1

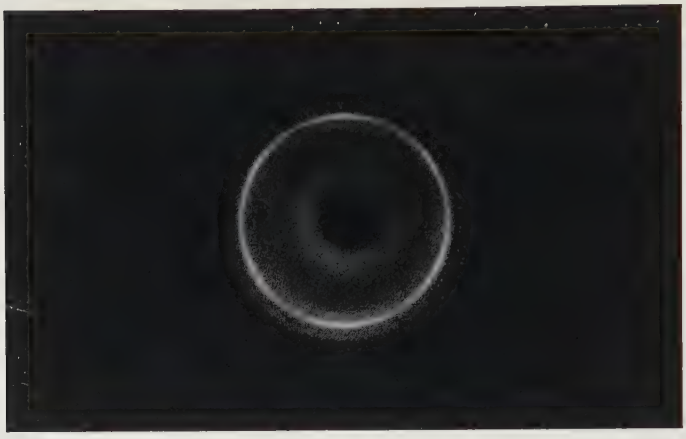

X-ray diffraction pattern of mildly rolled polyethylene film. X-ray beam parallel to direction of rolling. Plane of rolling horizontal.

Fig. 2

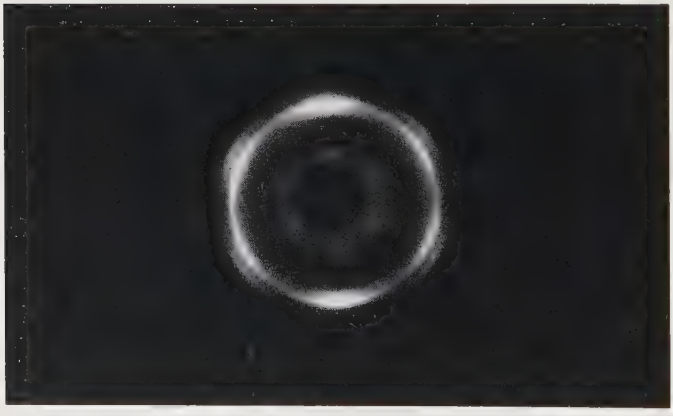

X-ray diffraction pattern of strongly rolled polyethylene film. X-ray beam parallel to direction of rolling. Plane of rolling horizontal.

Fig. 3

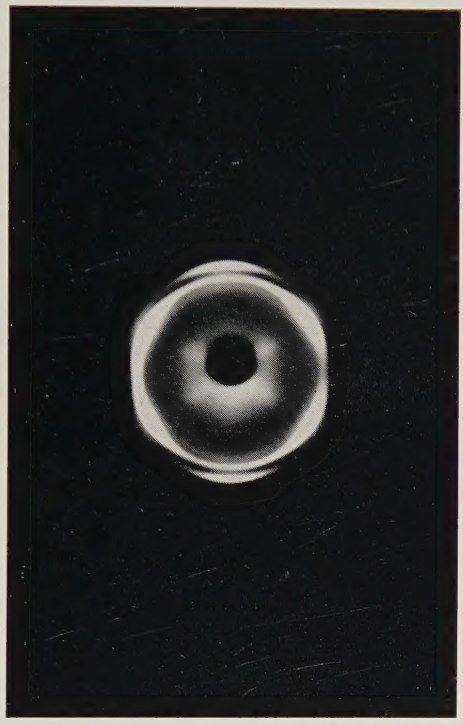

X-ray diffraction pattern of strongly rolled and subsequently lightly annealed polyethylene film. X-ray beam parallel to direction of rolling. Plane of rolling horizontal.

Fig. 4

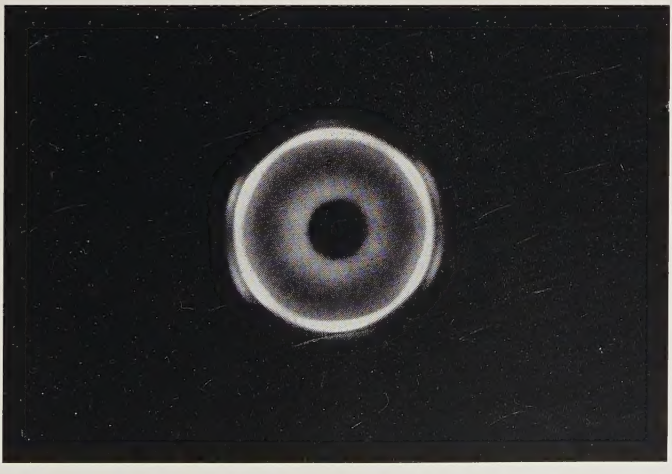

X-ray diffraction pattern given by a polyethylene strip which was first fully drawn, then annealed at 110°C and subsequently redrawn ~60%. Direction of drawing vertical.

Fig. 1

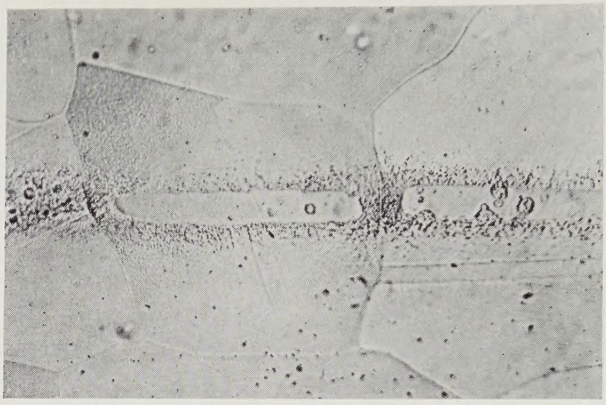

Section perpendicular to the helium band in copper after an anneal of 1 hour at 750°C. ×500.

Fig. 2

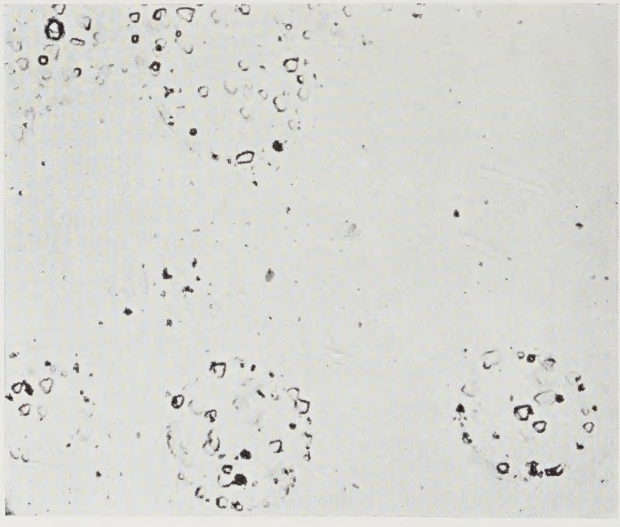

Electron micrograph of a two-stage carbon replica taken from the surface of copper containing islands of helium bubbles. ×7000.

Fig. 3

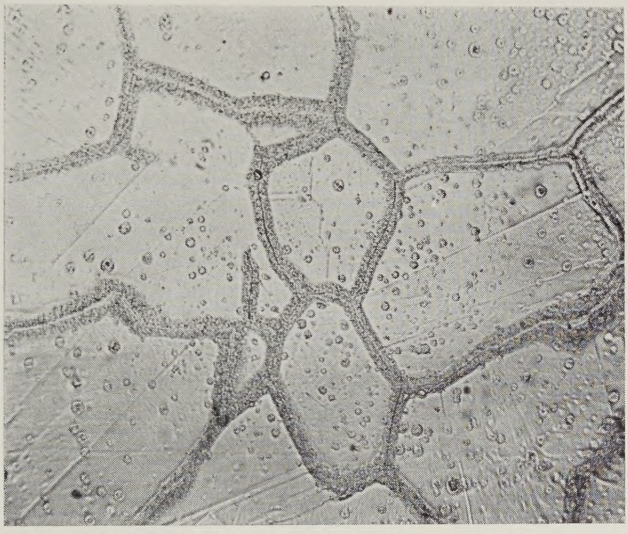

Taper section of the helium band in copper after an anneal of 2 hours at 700°c (same surface as seen in fig. 2). ×500.

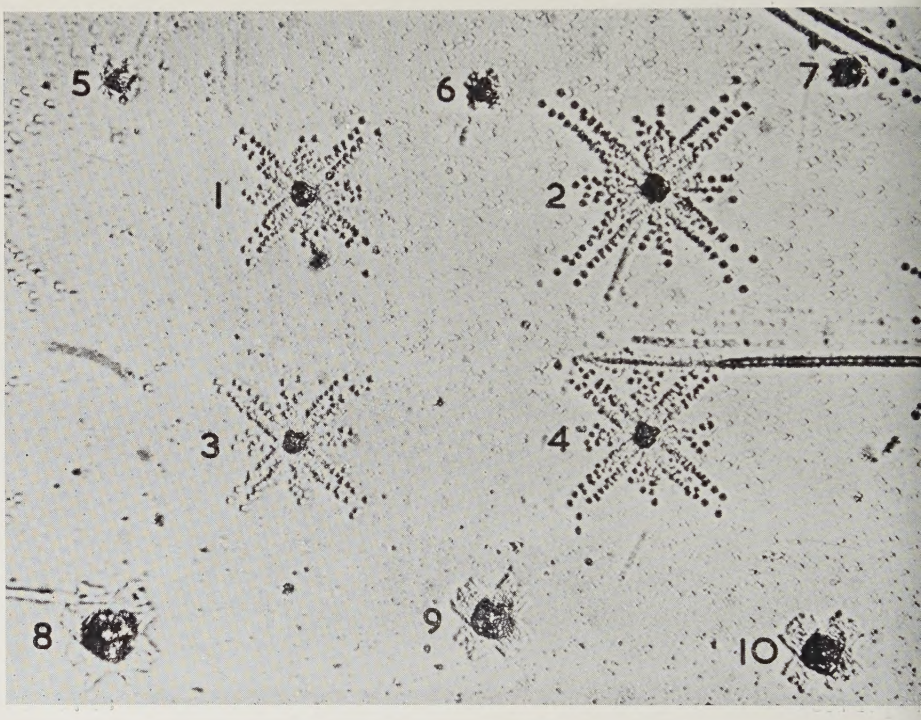

Etched (100) cleavage face of the electron irradiated lithium fluoride specimen. The cube axes are horizontal and vertical ($\times 500$).